ÉCOLE DE TECHNOLOGIE SUPÉRIEURE
UNIVERSITÉ DU QUÉBEC

MANUSCRIPT-BASED THESIS PRESENTED TO
ÉCOLE DE TECHNOLOGIE SUPÉRIEURE

IN PARTIAL FULFILLEMENT OF THE REQUIREMENTS
FOR THE DEGREE OF DOCTOR OF PHILOSOPHY
Ph. D.

BY
Yousef BABA ZADEH BEDOUSTANI

DESIGN AND CONTROL OF A CABLE-DRIVEN 6-DOF LOADING SIMULATOR

MONTREAL, MARCH 31TH, 2015

© Copyright 2014 reserved by Yousef Baba Zadeh Bedoustani

© Copyright reserved
It is forbidden to reproduce, save or share the content of this document either in whole or in parts. The reader who wishes to print or save this document on any media must first get the permission of the author.

BOARD OF EXAMINERS

THIS THESIS HAS BEEN EVALUATED

BY THE FOLLOWING BOARD OF EXAMINERS

Mr. Pascal Bigras, Thesis Supervisor
Département de génie de la production automatisée at École de technologie supérieure

Mr. Ilian A. Bonev, Thesis Co-supervisor
Département de génie de la production automatisée at École de technologie supérieure

Mr. Zhaoheng Liu, President of the Board of Examiners
Department of Mechanical Engineering at École de technologie supérieure

Mr. Vincent Duchaine, Member of the jury
Département de génie de la production automatisée at École de technologie supérieure

Mr. Mohamed Saad, External Evaluator
Department of Electrical Engineering at Université du Québec en Abitibi-Témiscamingue

THIS THESIS WAS PRENSENTED AND DEFENDED

IN THE PRESENCE OF A BOARD OF EXAMINERS AND PUBLIC

FEBRUARY 20TH, 2015

AT ÉCOLE DE TECHNOLOGIE SUPÉRIEURE

ACKNOWLEDGMENTS

I am very grateful to many special individuals for their generous support, guidance, wisdom, encouragement and inspiration throughout my doctoral studies and dissertation process. First and foremost, I would like to express my sincere gratitude to Professors Pascal Bigras and Ilian Bonev. Words could hardly express how much blessed I was to have them as my directors. The completion of this dissertation would not have been possible without their continuous and tireless support, motivation, and mentoring.

I would also like to extend my deep appreciation to my committee members for their insightful comments on my dissertation.

I also want to thank CORO lab members for their friendship and intuitive discussions specially Andy Yen, Albert Nubiola and Longfei Zhao.

Lastly and most importantly, my deepest gratitude goes to my wife and my parents. This work would not have been done without their love, patience, and support.

CONCEPTION ET COMMANDE D'UN SIMULATEUR DE CHARGE BASÉ SUR UN ROBOT À CÂBLE À 6 DEGRÉS DE LIBERTÉ

Yousef BABA ZADEH BEDOUSTANI

RÉSUMÉ

Dans ce travail, un robot à câbles destiné à la simulation de charges mécaniques (CabOLS) est conçu et construit de façon à contrôler avec précision les efforts dans un espace à 6 degrés de liberté sur une cible fixe ou se déplaçant lentement. Le CabOLS offre plusieurs avantages: la simplicité et l'efficacité de la structure mécanique et du contrôleur, la précision dans la simulation de charge ainsi qu'un faible coût de fabrication. La conception mécanique du CabOLS est novatrice par l'utilisation de ressorts linéaires de précision installés sur chacun des câbles dans le but d'estimer la tension dans les câbles afin d'éviter la nécessité d'ajouter des capteurs de force. Les ressorts servent également à compenser certains effets non-linéaires comme les jeux d'engrenages des réducteurs de vitesses, permettant ainsi de faciliter l'asservissement du mécanisme.

La structure du régulateur est conçue pour être aussi simple que possible. Afin d'exercer un contrôle de force précise sur l'objet cible, deux niveaux de contrôle respectivement dans les espaces des articulations et cartésiennes ont été considérés. La projection optimale de la tension dans les câbles ainsi que la résolution de la redondance des actionneurs en temps réel sont également étudiés dans ce travail. Il est démontré que même si l'algorithme de résolution de la redondance n'est pas linéaire, la combinaison de cette résolution avec le modèle de contrôle du CabOLS est linéaire. Cette linéarité permet de facilité la formulation du calcul des gains dans les deux niveaux de contrôle simultanément.

Cette thèse présente également l'application du CabOLS pour analyser la rigidité d'un robot industriel. Dans un processus automatisé, le CabOLS est contrôlé de façon à exercer une suite d'efforts sur l'effecteur d'un robot ABB. Pour chacun de ces efforts, un laser de poursuite mesure la déviation correspondante de l'effecteur. Ces données sont alors utilisées pour identifier la raideur des articulations du robot. Des modèles linéaire et non-linéaire de raideurs articulaires sont étudiés. Les données obtenues grâce au CabOLS permettent également de valider les paramètres de rigidité identifiés.

Ce travail propose également une formulation généralisée, compact et maniable de la dynamique des manipulateurs à câbles. Cette formulation est novatrice puisqu'elle emploie l'analyse de masse variable s'appuyant sur une approche de Lagrange pour tenir compte de l'effet d'augmentation et de diminution de la masse dû à la variation de longueur des câbles.

Mots clés: Robot parallèle actionné par câbles, simulation de chargement, la résolution de la redondance, le contrôle de la force, la rigidité du robot, formulation de Lagrange pour masses variables.

DESIGN AND CONTROL OF A CABLE-DRIVEN 6-DOF LOADING SIMULATOR

Yousef BABA ZADEH BEDOUSTANI

ABSTRACT

In this work, Cable-Driven Omnidirectional Loading Simulator (CabOLS) is designed and built to accurately control a 6-DOF wrench on a fixed or slow moving target. The CabOLS offers several important advantages: simplicity and efficiency of the mechanical structure and controller, precision in load simulation as well as the cost efficiency. The mechanical design of CabOLS is innovative in that it employs an accurate linear spring in each cable to estimate the tension in the cable instead of using a force sensor which adds complexity to the design. The spring also compensates for the nonlinear effect of backlash of the gearbox and thereby makes a simple control topology feasible.

The structure of the controller is managed to be as simple as possible without losing efficiency. In order to achieve accurate force control on the target object two levels of control in Cartesian and joint spaces were considered. Optimal projection of the tension in the cables i.e. redundancy resolution is examined in this work. It is proven that even though the redundancy resolution algorithm is nonlinear, the combination of the redundancy resolution algorithm and the model of the CabOLS is linear. Linearity makes it possible to apply robust method to simultaneously formulate the gains of the controller in both spaces. Moreover, the real-time redundancy resolution algorithm was successfully developed and utilized in closed-loop control system.

The present work also demonstrates the application of the CabOLS for stiffness analysis of industrial robots. In an automated process the CabOLS is controlled to exert the desired wrench vector on an ABB robot and a laser tracker is employed to measure the related deflection. Simultaneously, the stiffness of joints is identified by means of the incoming data. In this work nonlinear and linear modeling of the joint stiffness are also formulated. CabOLS as a dynamic load simulator, makes it feasible to identify joint stiffness using either linear or nonlinear modeling. Moreover, the CabOLS makes it possible to validate the identified stiffness parameters.

This work also formulates the generalized, compact, and tractable closed-form of dynamics of cable-driven parallel manipulators. This formulation is innovative in that it employs Lagrangian variable mass analysis to exert the effect of mass streaming caused by cable elongation.

Keywords: Cable-driven parallel manipulator, loading simulator, redundancy resolution, force control, robot stiffness, variable mass Lagrangian formulation.

TABLE OF CONTENTS

Page

LIST OF TABLES

Page

LIST OF FIGURES

Page

LIST OF ABREVIATIONS

3D	Three diminutions
CabOLS	Cable-driven omnidirectional loading simulator
CCT	Conservative Congruence Transformation
CDPM	Cable-Driven Parallel Manipulator
CoRo	Control and Robotics Laboratory
CSME	Canadian Society of Mechanical Engineer
DOF	Degree of freedom
ETS	École de technologie supérieure
KKT	Karush-Kuhn-Tucker
LAR	Large Adaptive Reflector
NIST	National Institute of Standards and Technology

LIST OF SYMBOLS

gr	gram
kg	kilogram
m	meter
mm	millimeter
N	Newton
Nm	Newton meter
Nm/rad	Newton meter per radian
rad	radian
Sec	Second

INTRODUCTION

Cable-driven parallel manipulators (CDPMs) are a unique generation of parallel robots which are becoming increasingly utilized in a variety of applications. CDPMs use cables instead of rigid links to transfer power and to perform motion or wrench on the end-effector. CDPMs offer some high-grade features including the potential of operating in workspaces ranging from large to very small, and that of simple assembly and reconfiguration. They also offer high speed as well as high acceleration, and a high load-to-weight ratio. Based on the requirements of the application, CDPMs can provide workspaces from several centimeters to hundreds of meters. In addition, the outstanding power transmission of the cables allows the manipulator to exert forces/wrenches ranging from several grams to several tons. Accordingly, applications of existing CDPMs are assigned to two categories: i) position control of the moving platform ii) force/wrench control on the target object. A lot of CDPMs have been developed for a vast number of positioning purposes. They include astronomical observation, structure building devices, assembly, rescue, service or rehabilitation, just to name a few. However, for the force control purposes only a few cable mechanisms have been developed. Even the existing ones are not 6-DOF. Furthermore, since they are not fully automated mechanisms, most of them cannot be classified as a robot. Loading simulator, an example of force control purpose, is used in various applications from biomedical and tension analysis of material to stiffness analysis of industrial robots.

The focus of the present thesis is on an application of the CDPM as a 6-DOF loading simulator. In this work, a 6DOF Cable driven omnidirectional loading simulator (CabOLS) is designed and built to precisely control the wrench on a target object, which can move slowly.

Due to complexity of the dynamic analysis of CDPMs, this work started with it using Lagrangian variable mass formulation. A shortcoming of former studies is that they have ignored the effect of mass stream resulting from the elongation of the cables entering into the system (Bedoustani, Taghirad et Aref, 2008). The present thesis is innovative in that it employs Lagrangian variable mass formulation to exert this effect in CDPMs. As a result, a

generalized, compact and tractable closed-form dynamic modeling of the CDPMs was formulated.

Following the initial studies on the dynamics of CDPMs, a 6-DOF loading simulator was designed and assembled. In the mechanical and geometric design stages, cable collision workspace as well as wrench capability were taken into consideration. In the hardware design stage the simplicity of the mechanical components, the actuators, and specifically cost efficiency were emphasized. At this stage, the greatest challenge was to measure the tension in each cable without using any sensors that would increase both the mechanical and electrical complexity as well as the cost. To this end, different approaches were examined. Finally, we came up with an innovative idea to make cables more flexible by adding a precise spring to each limb of the CDPM. The added spring made it possible to estimate the tension in each limb by calculating the elongation of the cable and spring combination. Besides, this innovative and cost-effective method has an added valuable advantage. It effectively compensates for the nonlinear effect of backlash from the actuators and gearboxes. This in turn makes it possible to develop a simple control topology without the need to model nonlinearity effects such as backlash and friction.

In the control stage, different control topologies were verified practically as well as through simulation. Our thesis sought to keep the control topology as simple and efficient as possible. To that end, in order to achieve accurate force control on the target object in Cartesian space, two levels of control, one in Cartesian space and the other in joint space, were considered. The pole placement method was utilized to formulate the gains of the controller in Cartesian and joint space simultaneously. In real-time implementation of the closed-loop control, the real-time redundancy resolution, i.e the optimal projection of positive tension in cables, is critical and presented us with a highly challenging task. This challenging task was performed in this project. Consequently, a combination of the redundancy resolution algorithm and the model of the CDPM in closed loop control were analyzed in this thesis. Because of its significance for control, we aimed at keeping the control topology simple and efficient.

As a next step, the experimental stiffness analysis of industrial robots was evaluated using CabOLS. The stiffness of industrial robots is mostly related to joint flexibility and yields significant errors in tool positioning. Joint flexibility itself is a function of the flexibility of the motor and power transmissions. Robot manufacturers do not present sufficient information on their robots' joint stiffness. Moreover, the flexibility of the joints could change during long term operation. In order to enhance and maintain the accuracy of robots, therefore, it is essential to perform an experimental stiffness analysis. Such an analysis demands three important elements; i) an automated omni-directional load simulator ii) sufficiently accurate deflection measurements and iii) proper modeling of the joints' stiffness.

The present work demonstrates the use of the CabOLS for stiffness analysis in industrial robots. The CabOLS is controlled to exert the desired wrench vector on an industrial robot in multiple configurations. Nonlinear and linear modeling of the joint stiffness are also formulated in this work, the nonlinear modeling being based on the nonlinearity of the Harmonic Drives employed in each joint of current commercial midsize robots. As a dynamic load simulator, the CabOLS makes it feasible to identify joint stiffness using either linear or nonlinear modeling. This work demonstrates the function of the CabOLS in an experimental stiffness analysis. Moreover, the CabOLS makes it possible to validate the identified stiffness parameters.

The first chapter of this dissertation includes a review of the related literature. The following three chapters present three submitted journal articles based on this work. Due to the complexity of the dynamic analysis of CDPMs, this work began by investigating the dynamic analysis of the CDPMs in general. The first paper includes the results published in The Transactions of the Canadian Society for Mechanical Engineering (CSME). The second paper focuses on the design and control of the CabOLS as a loading simulator. The results were submitted to the Journal of Dynamic Systems, Measurement, and Control. The third paper focuses on innovations to the application of the CabOLS in the stiffness analysis of industrial manipulators and submitted to the journal Robotics and Computer-Integrated Manufacturing. The closing chapter includes the conclusions and plans for future work.

CHAPTER 1

LITERATURE REVIEW

1.1 Cable-driven parallel manipulators

In recent years, much work has been done on various types of parallel manipulators. The *Stewart-Gough* mechanism is one of the most widely-used robots in this category and the properties of this class of parallel robot have been studied by *Merlet* in (Merlet, 2006). Parallel robots have low structural weight compared to serial manipulators. They are very rigid because of their mechanical closed-chain structure and also they have high accuracy in positioning. However, limited workspace is their main disadvantage. Another emerging class of parallel robots is the cable-driven parallel manipulators (CDPMs). The flexibility of their cables is the most important distinguishing difference between CDPMs and other general parallel robots. In fact, cable dynamics and restrictions play a key role in their overall dynamics. In other words CDPM inherits cable properties including cable restriction in the transmission of force in one direction.

Some advantages of cable-driven parallel manipulators are as follows (Barrette et Gosselin, 2005a):

- Workspace ranges from very small to very large areas (from several centimeters to several hundred meters) because cables take up only a little space when rolled around a pulley,
- CDPMs have low structural weight, not only due to the low weight of the cables, but also because the actuators are fixed and located away from the manipulator,
- Cables, motors, and cable wrench mechanisms combined are less expensive than other actuators such as hydraulic ones, which are widely used in parallel robots,
- Cables as links in CDPMs allow a flexible configuration,
- Redundancy in CDPMs provides an extra layer of safety in the case of link failures.

However, the end-effector (moving-platform) must be positioned without exceeding several limitations:

- The cables must always be in tension (forces must be positive),
- The cable forces must be less than the maximum tension values (cable failure),
- The moving platform must avoid regions of singularities,
- The cables must not collide with each other or with the moving platform.

A major characteristic of CDPMs needs to be remembered: cable dynamic redundancy is unavoidable. In fact, redundancy is necessary in cable robot design in order to satisfy the positive tension constraint in cables. Subsequently, redundancy in cable robots introduces complexities into the kinematic analysis, dynamic analysis, optimal force distribution (redundancy resolution) and control design. Table 1.1 briefly compares the performance of serial robots, parallel robots and CDPMs.

Table 1.1 Performance comparison of serial robots, parallel robots and CDPMs.

Properties	**Serial robot**	**Parallel robot**	**CDPMs**
Stiffness	Low	High	Medium
Workspace	Medium	Low	High
Singular points	Low	High	Medium
Load on each link	Whole of external load+ end-effector & tools+ actuators+ provirus-links	Part of external load+ end-effector & tools+ actuators	Part of external load+ end-effector & tools
Bending load on link	High	Medium	Zero
Axial load	Medium Compression/ Tension	High Compression / Tension	High Tension only
Velocity-Acceleration	Medium	High	High
Inertia of system	High	Low	Low
Fabrication of links	Medium	Hard	Easy
Accuracy	Low	High	Average
Complexity of processing	Low	High	High
Failure in one link	Loses its connectivity Fails-without safety	Normal Safe	Normal Safe
Manufacturing cost	Medium	High	Low
Performance as a loading simulator	Low	Medium	High

1.2 Applications of CDPMs

Performance specifications of CDPMs such as speed, payload and workspace can be adapted to a wide range of applications. Workspaces of several centimeters up to hundred meters can be achieved for required applications. Payloads ranging from several grams to several tons are possible due to the outstanding power transmission of the cables. Applications of existing CDPMs could potentially be assigned to two categories of positioning and loading simulators. Currently, whereas many CDPMs have been developed for positioning purposes, only a few cable mechanisms have been developed for loading simulator applications and even the existing cable mechanisms are not 6-DOF loading simulators. Moreover, most of them could not be categorized as a robot since they are not fully automated mechanisms. The following three subsections briefly present existing CDPMs in positioning applications, some robotic mechanisms and cable mechanisms as loading simulators, respectively.

1.2.1 Existing CDPMs in positioning applications

The crane is one of the primary cable mechanisms used for positioning for example see figure 1.1 . The first generation of RoboCrane was built in 1985 by *Landsberger* and *Sheridan* (Landsberger et Sheridan, 1985). Thereafter, plenty of robots have been developed for different applications based on this concept, one of the most prevalent being carrying containers in seaports (Holland et Cannon, 2004; Thompson et Campbell, 1996). The NIST RoboCrane is used to transport equipment and tools (see figure 1.2) (Bostelman, Jacoff et Bunch, 1999). However, this design, which is largely based on gravity to maintain the tension on the cables, is only suitable for a limited class of tasks. Using gravity for putting containers on board a ship is indeed suitable, but not for applications such as machining. Furthermore, this type of robot can only work at low acceleration and with absolutely minimal disturbance. Moreover, workspace is one of the most important issues when designing this robot.

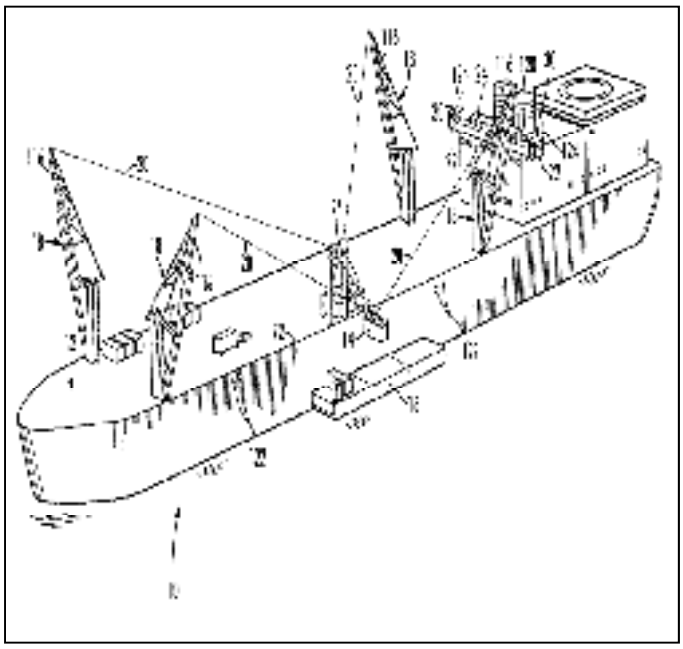

Figure 1.1 A parallel cable robot for carrying loads in ships and seaports. Picture taken from (Holland et Cannon, 2004)

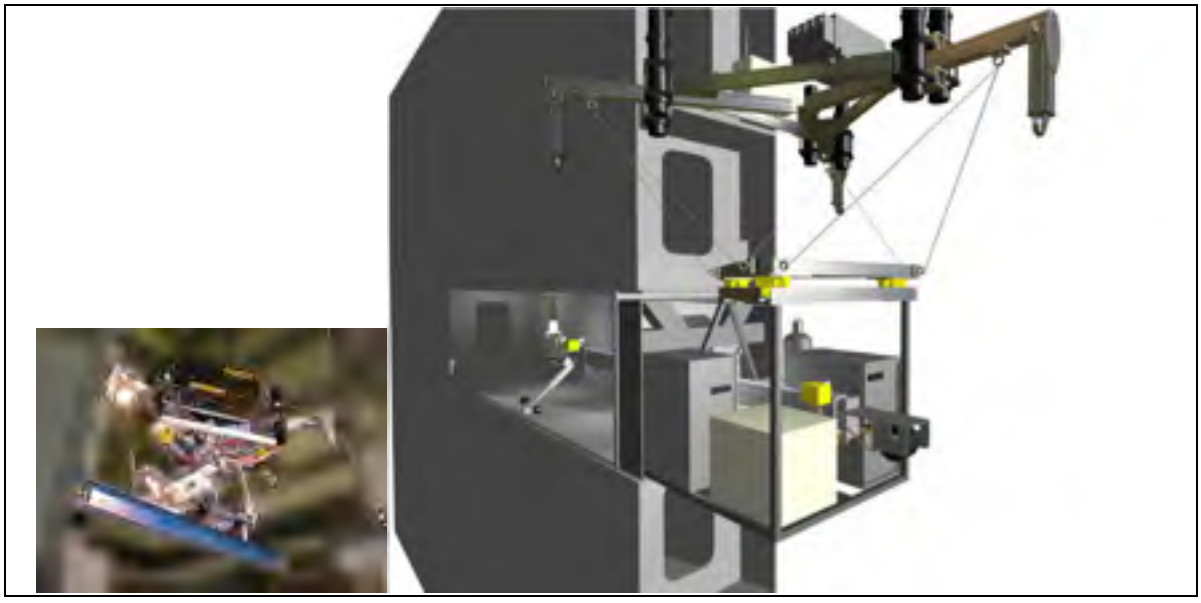

Figure 1.2 The NIST RoboCrane used to transport equipment. Taken from (Bostelman, Jacoff et Bunch, 1999)

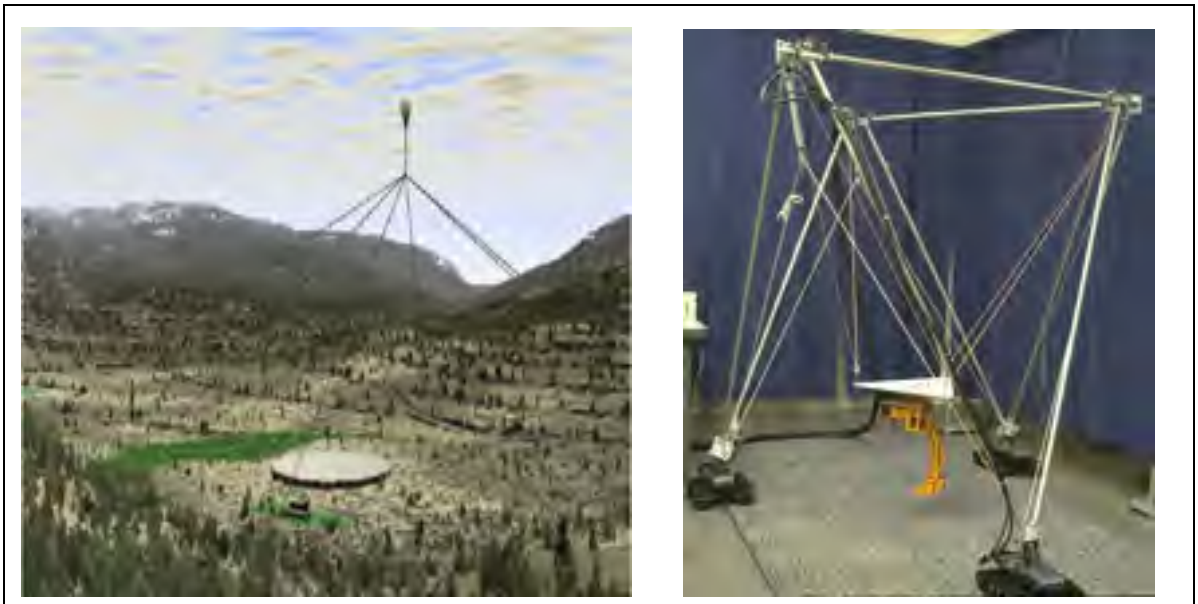

(a) (b)

Figure 1.3 (a) The LAR radio telescope (Carlson et al., 2000). (b) The RoboCrane (Bostelman, Jacoff et Bunch, 1999).

In some CDPM designs such as the LAR radio-telescope (Carlson et al., 2000) a vast workspace as well as accuracy in position are required (see figure 1.3). In the LAR radio-telescope, a hydrogen balloon is used to keep the cable in a tension state while, in the *RoboCrane* (Holland et Cannon, 2004) (Durrant-Whyte, Dissanayke et Rye, Oct.3, 2000), Earth's gravity is used for this purpose.

The SEGESTA cable robot (figure 1.4) was designed and built to implement a control algorithm specially formulated for applications that require high velocities (Fang et al., 2004). It has seven cable actuators located at the corners of the base such that it minimizes possible cable contact (Hiller et al., 2005). Obviously, it is impossible to have tension on cables at all points within the workspace. Furthermore, a dynamic analysis of the robot in the workspace is required to calculate the forces in actuator space (Bruckmann et al., 2007).

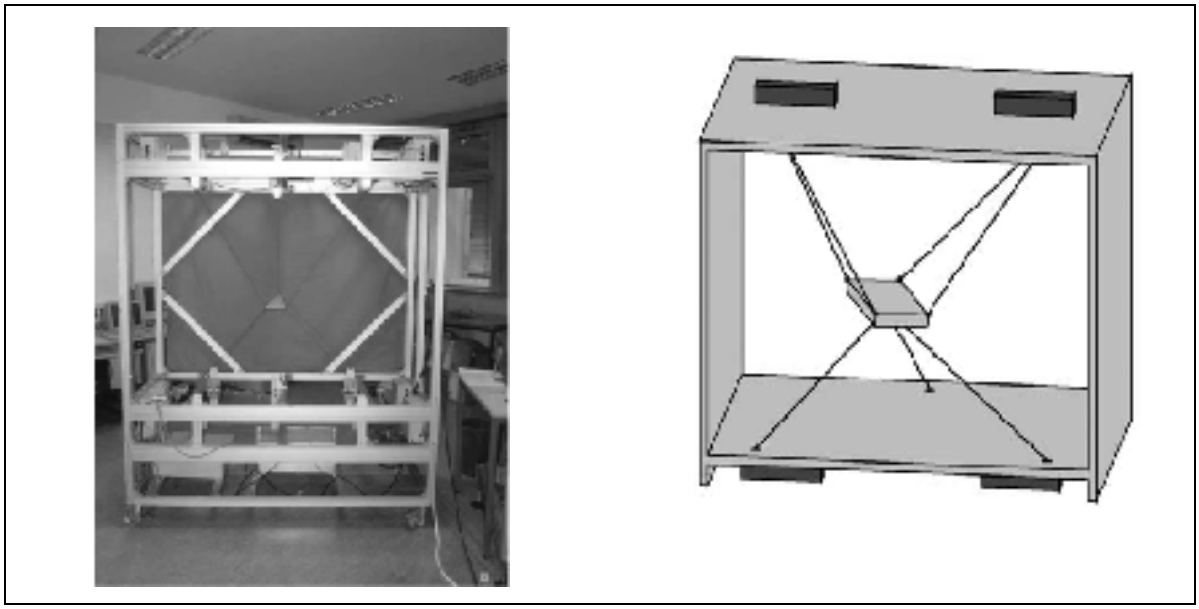

Figure 1.4 The SEGESTA cable robot (Fang et al., 2004).

In the application of virtual reality systems such as auto-pilot simulations, Tadokoro et al. replace the Stewart-Gough mechanism with a WARP cable robot (Tadokoro et al., 2001a; Tadokoro et al., 2001b). The rationale is that, although the Stewart-Gough parallel robot is one of the most widely used structures in the above mentioned applications, its architecture presents problems like (Tadokoro et al., 2001a):

- The large space needed for installation because of hydraulic cylinder actuators,
- The range of possible acceleration for a long period is limited,
- The possible magnitude and time of acceleration are restricted,
- The rotational range of motion is small,
- The necessity for spherical joints in the tow side of the prismatic hydraulic joint (complex SPS joint).

These problems, along with the restrictions of this mechanism in the workspace, lead designers to consider other structures, like the WARP cable robot (Tadokoro et al., 2001a; Tadokoro et al., 2001b). This particular mechanism is driven by multiple cable wires suspended from various directions to move a platform in 6 DOF and its architecture covers

most of the problems inherent in the Stewart-Gough structure. In order to solve the force problem, the WARP mechanism (figure 1.5) uses eight cables. This redundant architecture has advantages such as enhancing safety in case of cable failure, improving workspace, and solving redundancy problems by the optimal distribution of forces in joint space.

The potential of using cable robots for covering very large workspaces is exploited by companies like SkyCam and CableCam. The SkyCam cable robot was in fact a turning point in broadcasting and high definition live capture of sporting events. To achieve good motion control, these cable robots employ two sweeping cables in each Cartesian direction. However, each sweeping pair of cables has the same actuator (see figure 1.6). In other words, the tension force problem in cables is solved and guaranteed by the mechanical design.

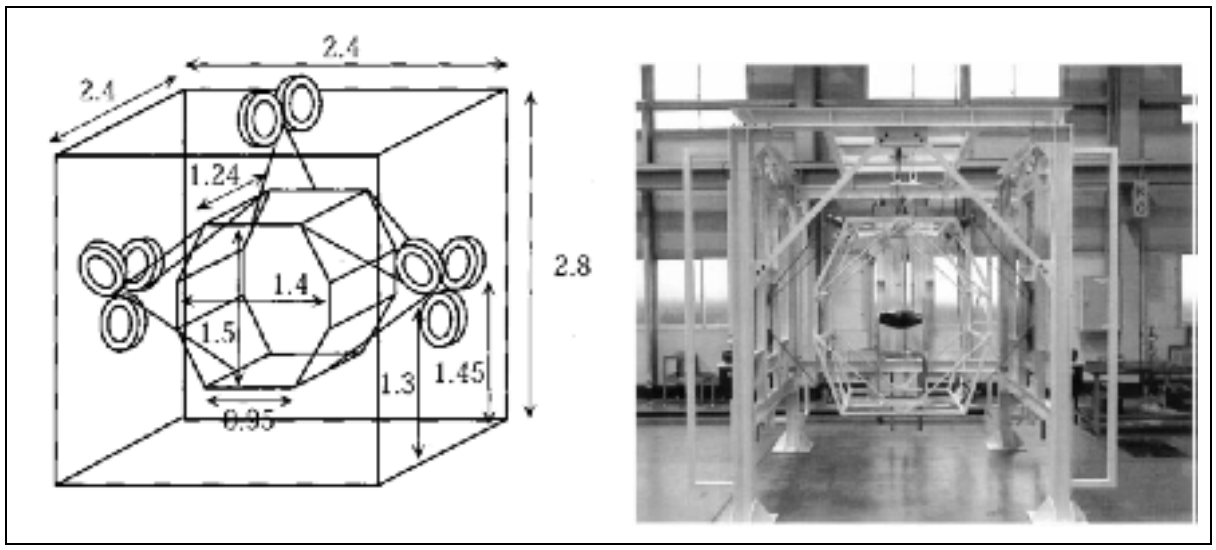

Figure 1.5 The WARP cable robot as a system for virtual reality applications (Tadokoro et al., 2001a; Tadokoro et al., 2001b).

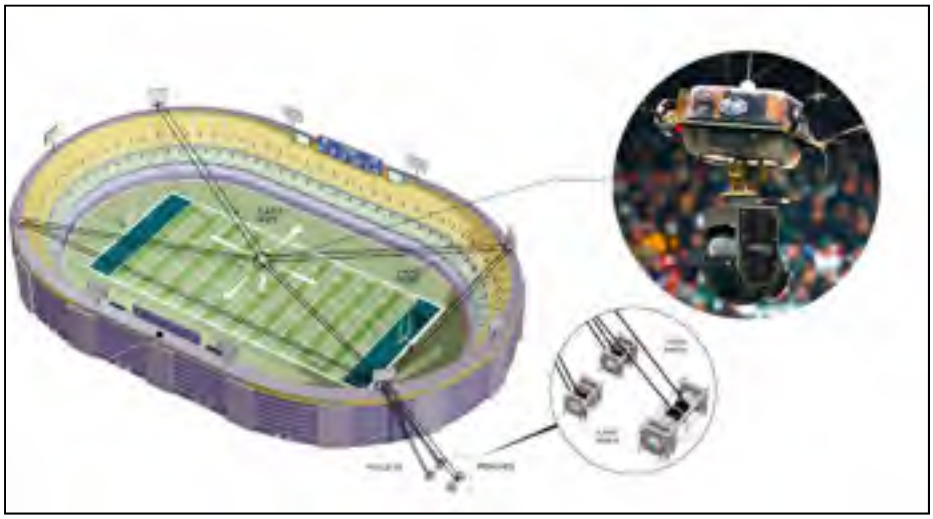

Figure 1.6 The CableCam cable robot. Picture taken from www.cablecam.com.

The CDPM demonstrator IPAnema at Fraunhofer IPA achieves performance characteristics beyond the capabilities of conventional industrial robots. One of its key features is to reach high speeds of up to 2.5 m/s. There are many more CDPMs in positioning applications. However, we selectively mention some only.

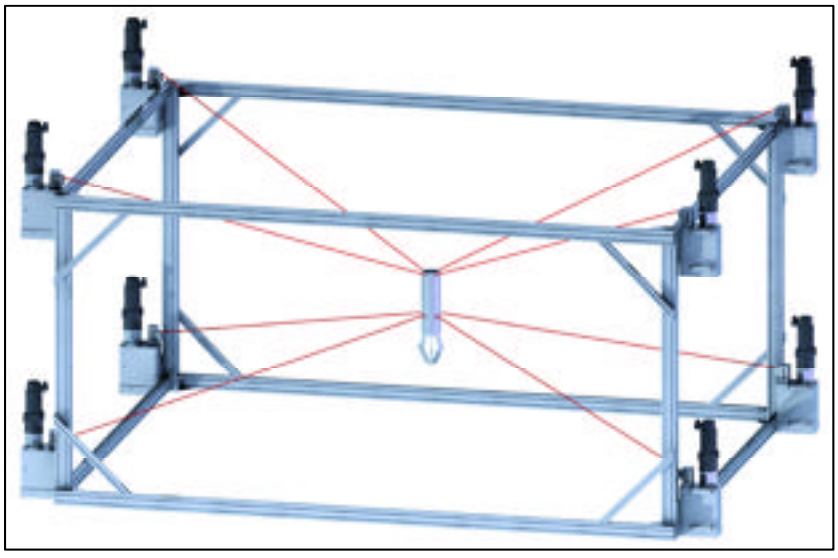

Figure 1.7 The IPAnema parallel cable robot (Miermeister et Pott, 2010).

1.3 Some loading simulator mechanisms

The Bionix Servo-hydraulic (figure 1.8) is a multipurpose test mechanism developed by the MTS Company. This compact system is designed to study the mechanical properties of biomaterials, medical devices and orthopedic constructs (Voor et al., 1998). It is also used to obtain the full spectrum of spine dynamics. This dynamic simulation is required in biomedical investigations and especially orthopedic research. The mechanism is released in only two configurations: axial and axial-tensional. The axial configuration is designed to perform accurate and repeatable fatigue studies, and also tension, bending and compression tests of biomaterials. The axial-tensional configuration is well-suited to testing durability and wear in components such as knee, hip, and spine implants. It can also be used for studying surgical techniques and conducting complex kinematic studies of joints, tissues and orthopedic constructions (Voor et al., 1998). Notwithstanding this mechanism can apply forces in one direction only and moments of inertia around one axis. In other words, it has only two DOF. Moreover, there is serious restriction in the video capture and x-ray radiography of models during tests. These disadvantages are regardless of its high price.

Figure 1.8 The MTS loading simulator. Picture taken from www.mts.com

The MTS 858.2 MiniBionix is a special spine test fixture with six degrees-of-freedom (Jirková et al., 10-12 December 2007). This system, shown in figure 1.9, allows the operator to perform a wide variety of spinal column kinematic studies. Moreover, the system makes it possible to have axial force and moment at the same time. It can also measure the bending moment, axial loads, or a combination of torsion or flexural motions. Its mechanism involves multi-channel and axial/torsion systems for analyzing both skeletal and soft tissue during surgical treatment and, due to the use of servo-hydraulic actuators, it operates in low friction and high stiffness. Therefore, it can easily simulate human spine dynamics. This simulator is, however, extremely complex. Moreover, the hydraulic actuators are difficult to control precisely. They also require a hydraulic pump.

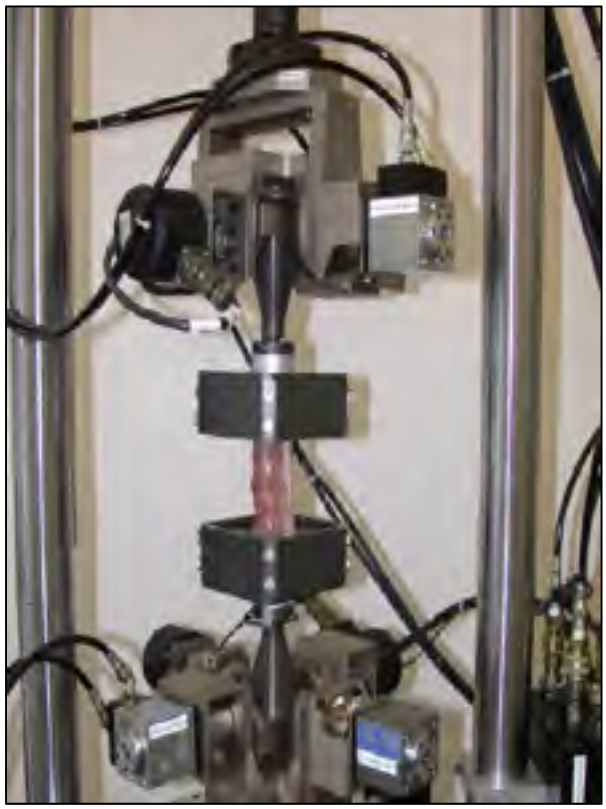

Figure 1.9 The MTS 858.2 MiniBionix spine test fixture with 6 DOF (Jirková et al., 10-12 December 2007).

Figure 1.10 shows another mechanism which has been used by Professor Dennis J. DiAngelo at University of Tennessee Health Science Center as a spinal testing device (Kim,

Cammisa et Fessler, 2006). This system consists of a two-column frame housing a servomotor connected to the controller (Chen, 1996; DiAngelo et al., 2000; Faber, DiAngelo et Foley, 1997; Jirkova et al., 2007). As shown in figure 1.11, a single-axis force sensor is attached to one end of the actuator shaft. On the other end, it is connected to fixtures containing a pinned connection and a linear bearing for attaching the machine to the cervical spine. This system has two degrees of freedom. In fact, the mounting fixtures that are added to it allow unconstrained motion and rotation in a plane. The flexion/extension axis of the spine is placed against the load axis of the actuator. Therefore, a compressive load, and a flexion/extension bending moment are applied to the upper holder. For some tests, like lateral bending tests, the spine is first rotated through 90° in the mounting fixtures, and then the base is left unconstrained in an axial rotation. As shown in figure 1.10 (A), a rotational displacement transducer is attached to the upper pinned assembly and measures the global rotation of the spine. This approach restricts the motion to two degrees of freedom.

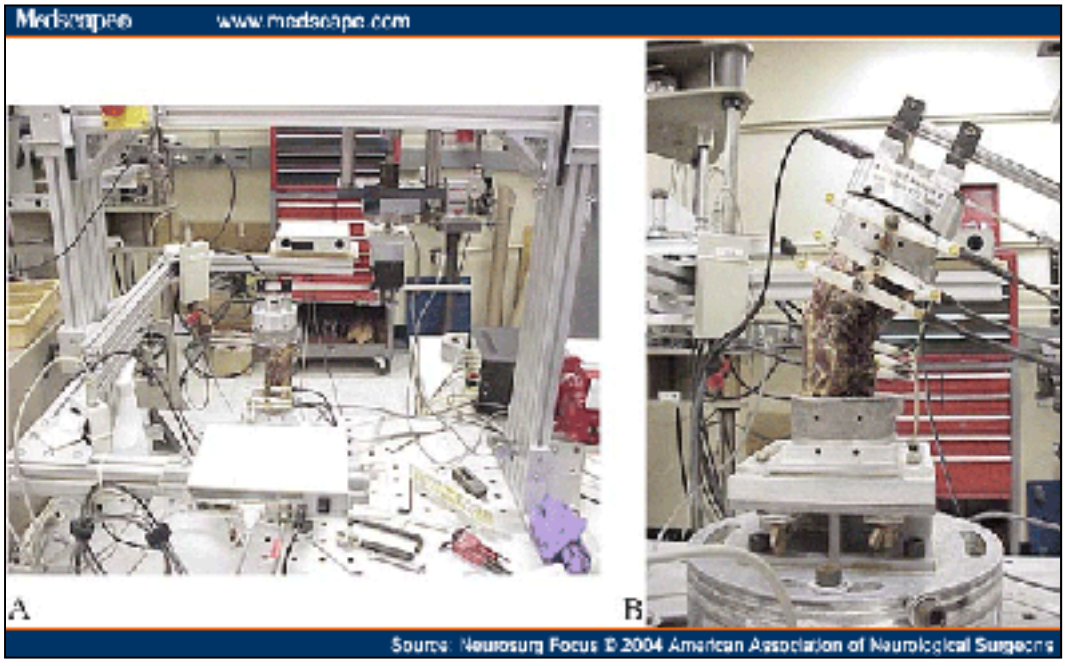

Figure 1.10 The extension testing set-up. Overview (A) and close-up (B) show pictures of the mounted spine. For flexion testing, the spine is rotated 180° in the mounting fixtures (Kim, Cammisa et Fessler, 2006).

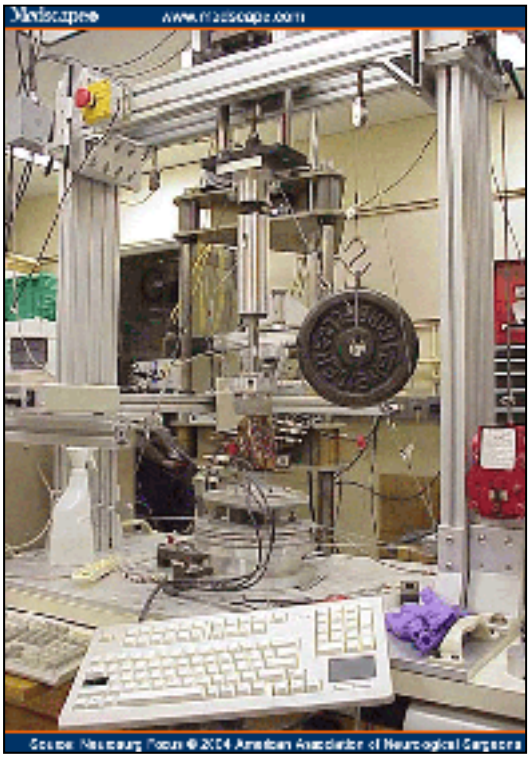

Figure 1.11 The axial rotational testing arrangement (Kim, Cammisa et Fessler, 2006).

The R- 2000 parallel manipulator from Rotopod Parallel Robotic Corporation (Hampton, NH) is another mechanism, which has been used by Prof. Gregory N. Kawchuk of Alberta University as a loading simulator spine testing applications (see figure 1.12) (Kawchuk et al., 2010). This parallel robot is based on a Stewart- Gough mechanism. The system is composed of an upper and a lower test fixture. The upper fixture is fastened to a cross-beam attached to the base of the robot. The lower fixture is mounted on the six- axis load cell which is attached to the R-2000 robot test platform (Goertzen et Kawchuk, 2009) shown in figure 1.13. Similar to other Stewart-Gough platforms, this mechanism does not allow extensive displacements. Its mechanical design is complex: it has a big structural frame and it uses hydraulic actuators, which make it expensive.

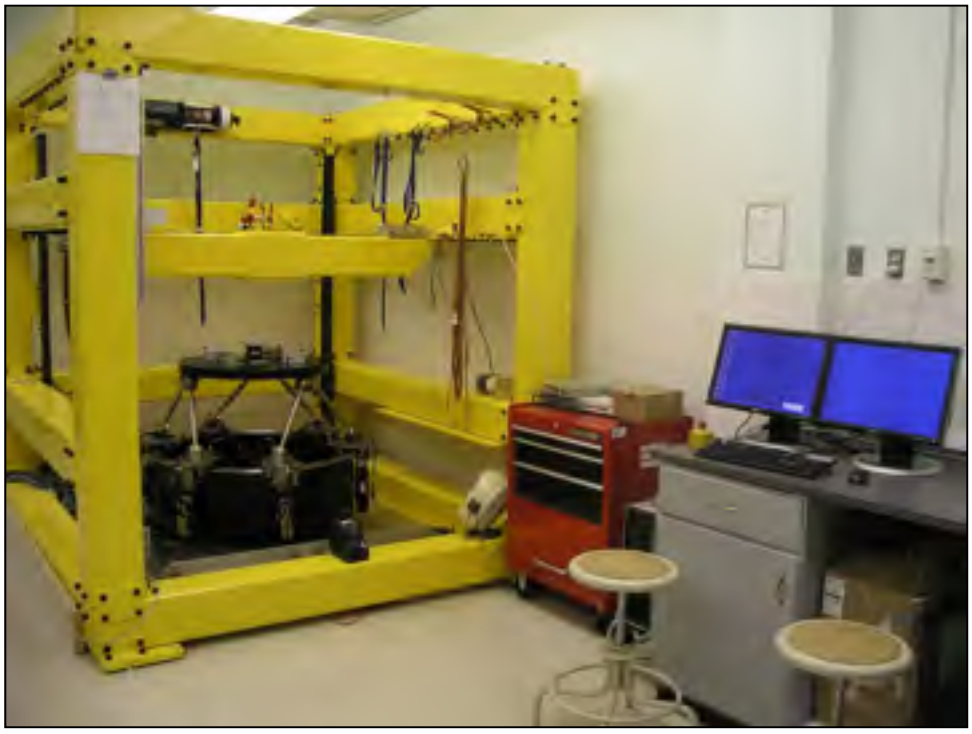

Figure 1.12 The R2000 mechanism based on Stewart- Gough mechanism (Kawchuk et al., 2010).

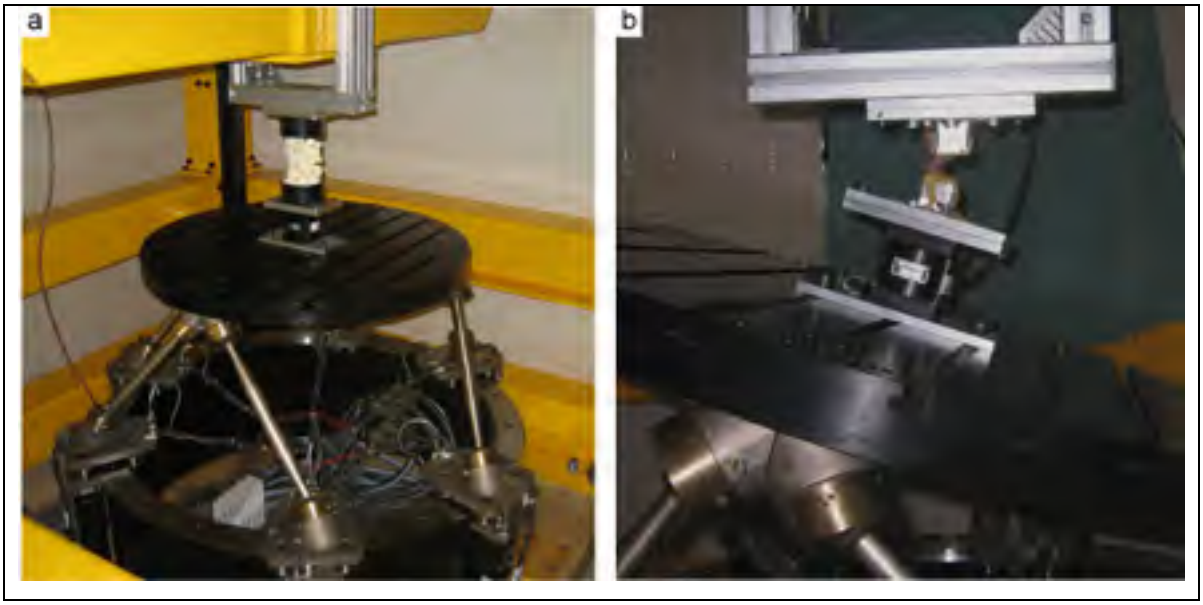

Figure 1.13 Isolated spine segments testing by R-2000 robot (Kawchuk et al., 2010).

Another mechanism, which has been used at Lutheran Hospital, Cleveland, is a serial robotic manipulator. The spine health research lab, led by Professor Lars Gilbertson, especially focuses on advancing the basis of new therapies for spine disorders. To that end, the well-known KUKA robot is employed to apply forces to the spine model (Healy et al., 2014) (see figure 1.14). However, stable and robust contact force control schemes for a rigid robot (such as KUKA) in contact with a rigid environment is very hard problem. In fact, it involves the formulation of highly nonlinear dynamics for the constrained robot, which results in very high bandwidths. Hence, the digital control requires very high sample rates. Also, it is very difficult to find robust solutions to modeling errors such as friction in the drive systems, poor knowledge of the actual robot dynamics, contact stiffness, and contact geometry (DeSchutter et al., 1997).

Figure 1.14 The KUKA robot as a spine testing system, Lutheran Hospital Cleveland clinic center, spine health research Lab (Healy et al., 2014).

The cable mechanism, designed by Crawford in (Eguizabal et al., 2010), was used by biomechanical engineers. This mechanism was designed to apply only pure moment to the

spine specimen. Figure 1.15 shows one such design whose mechanism has been optimized for the purpose of maintaining a continuous load on the spine (J.P. Dickey August 14-18, 1998).

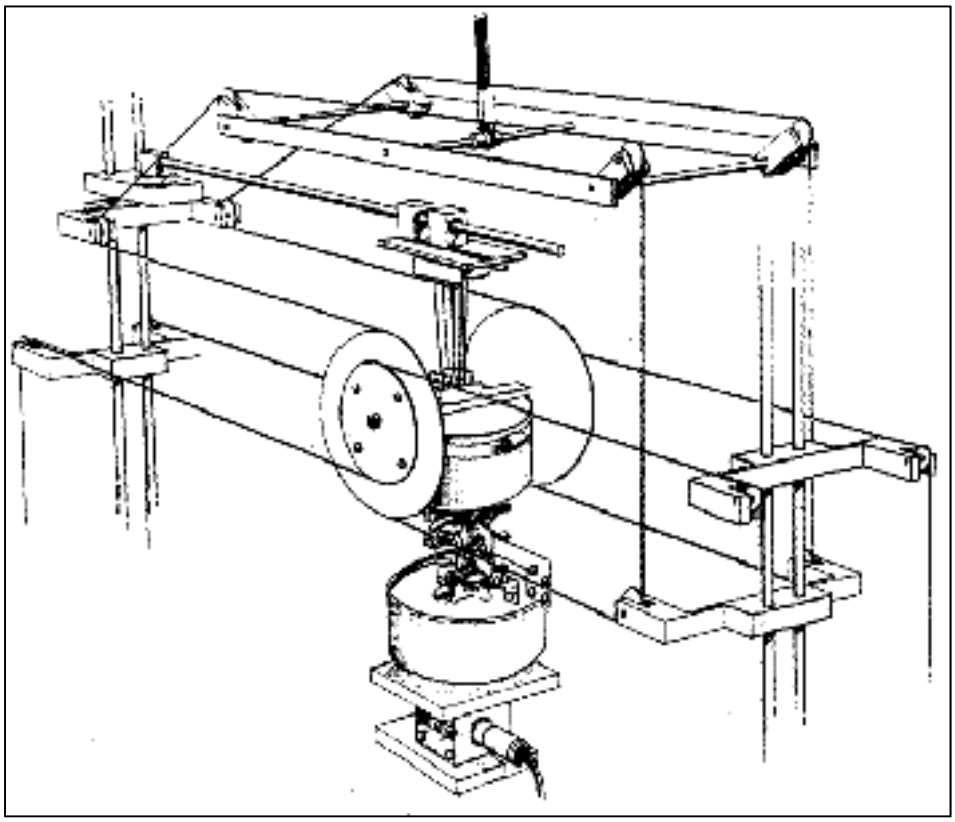

Figure 1.15 Schematic of the cable-driven pure moment mechanism (J.P. Dickey August 14-18, 1998).

The specimen is mounted in the center while the force sensor is fixed at the bottom. The load wheel then applies the loads to the top of the spine segment. The shaft, shown at the top of figure 1.15, is used to move the pulley carriage; it can also be used for applying vertical force to the counterweight mechanism (or to systems like the MTS mechanism.). The movement of the pulley carriage creates equal and opposite cable forces on the larger load wheel, causing a pure flexion moment. Also, a constant extension moment can be applied to the smaller wheels by cables acting around pulleys and hanging masses that are not shown in this figure. Figures 1.16 and 1.17 show a similar design to load apparatus for applying continuous pure

moment to multi-segment spine specimens (Lysack et al., 2000). This design allows a continuous cycling of the spine between specified flexion and extension.

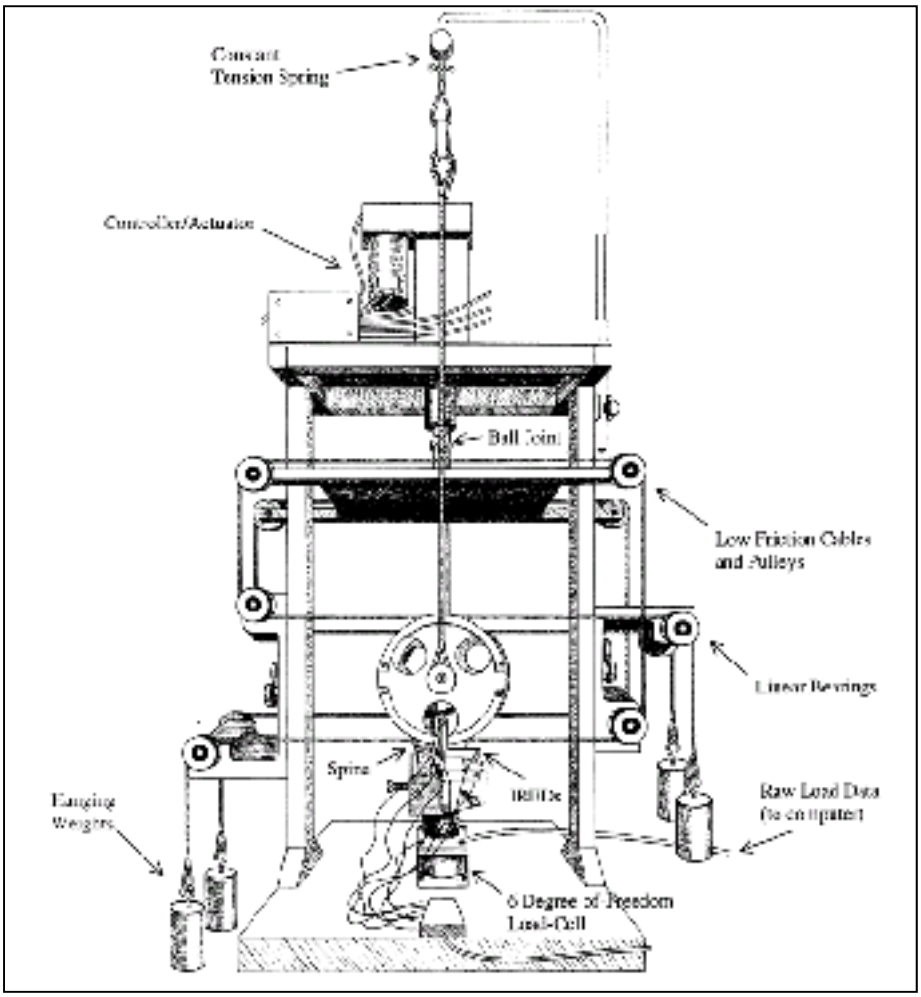

Figure 1.16 Schematic of the cable-driven pure moment mechanism (Lysack et al., 2000).

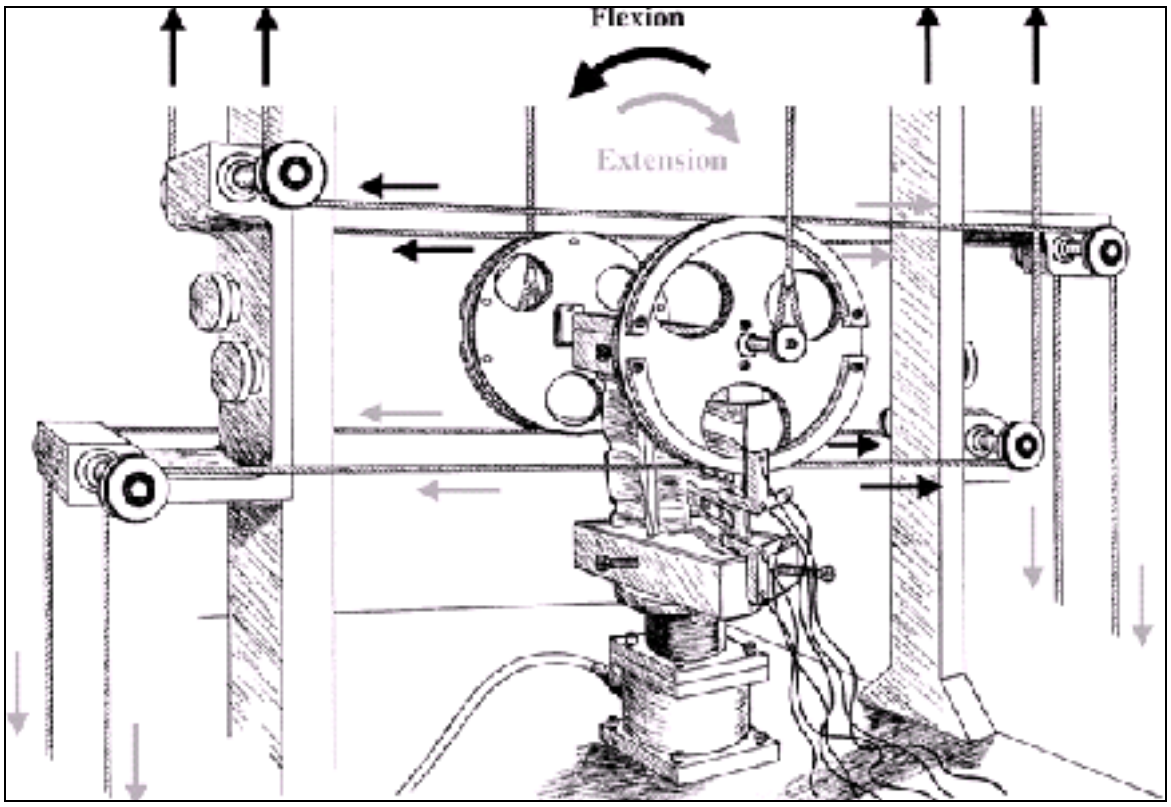

Figure 1.17 Close-up of the apparatus set for flexion and extension (Lysack et al., 2000).

The latest mechanism, shown in figures 1.18 and 1.19, is another cable-driven pure moment system, also based on the Crawford design (Eguizabal et al., 2010). This system is actuated by a MTS Servo-hydraulic test mechanism. Similar to the Crawford cable mechanism, it consists of a loading ring attached to the spine model. A Spectra cable with a 200 lb capacity is wound around the loading ring in a suitable configuration. This structure provides either flexion or extension forces on the spine specimen. The cable is then routed to the actuator via low friction pulleys fixed to the master frame. The position of the pulleys must be adjusted before starting the tests (Eguizabal et al., 2010).

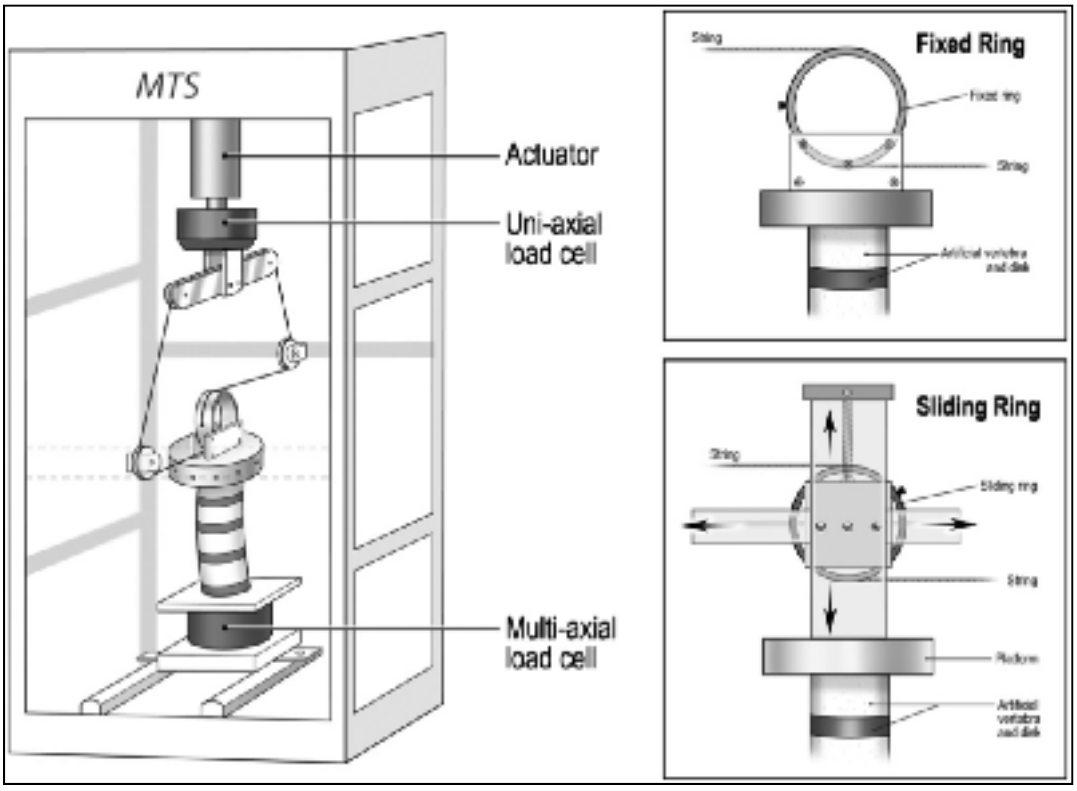

Figure 1.18 Schematic of the cable-driven pure moment system drive with a MTS servo-hydraulic mechanism (Eguizabal et al., 2010).

The cable mechanism designed by Crawford in (Eguizabal et al., 2010), is completely reliable for valid test conditions (J.P. Dickey August 14-18, 1998). However, these structures are limited in their degree of freedom. Moreover, its mechanical design is complicated. It could be even more complex to improve this mechanism in order to have more degree of freedom.

Figure 1.19 The cable-driven pure moment test mechanism with a MTS servo-hydraulic mechanism (Eguizabal et al., 2010).

1.4 Loading simulators in stiffness analysis of robots

Experimental stiffness analysis needs a setup that includes a load simulator and a device such as a laser tracker for accurate deflection measurements. The load simulator simulates external loads on the end-effector of a serial or parallel robot. The deflection caused by this load is simultaneously measured. The collected force-deflection data is used for the joint or Cartesian stiffness identification of the manipulators. The first example of an experimental loading simulator used for stiffness analysis is shown in figure 1.20 (Alici et Shirinzadeh, 2005). This setup allowed the investigation of a serial robot's global stiffness. The external force was exerted on the end-point of the robot using a simple pulley system. The end-effector position and orientation deflection under load were measured by a laser tracker.

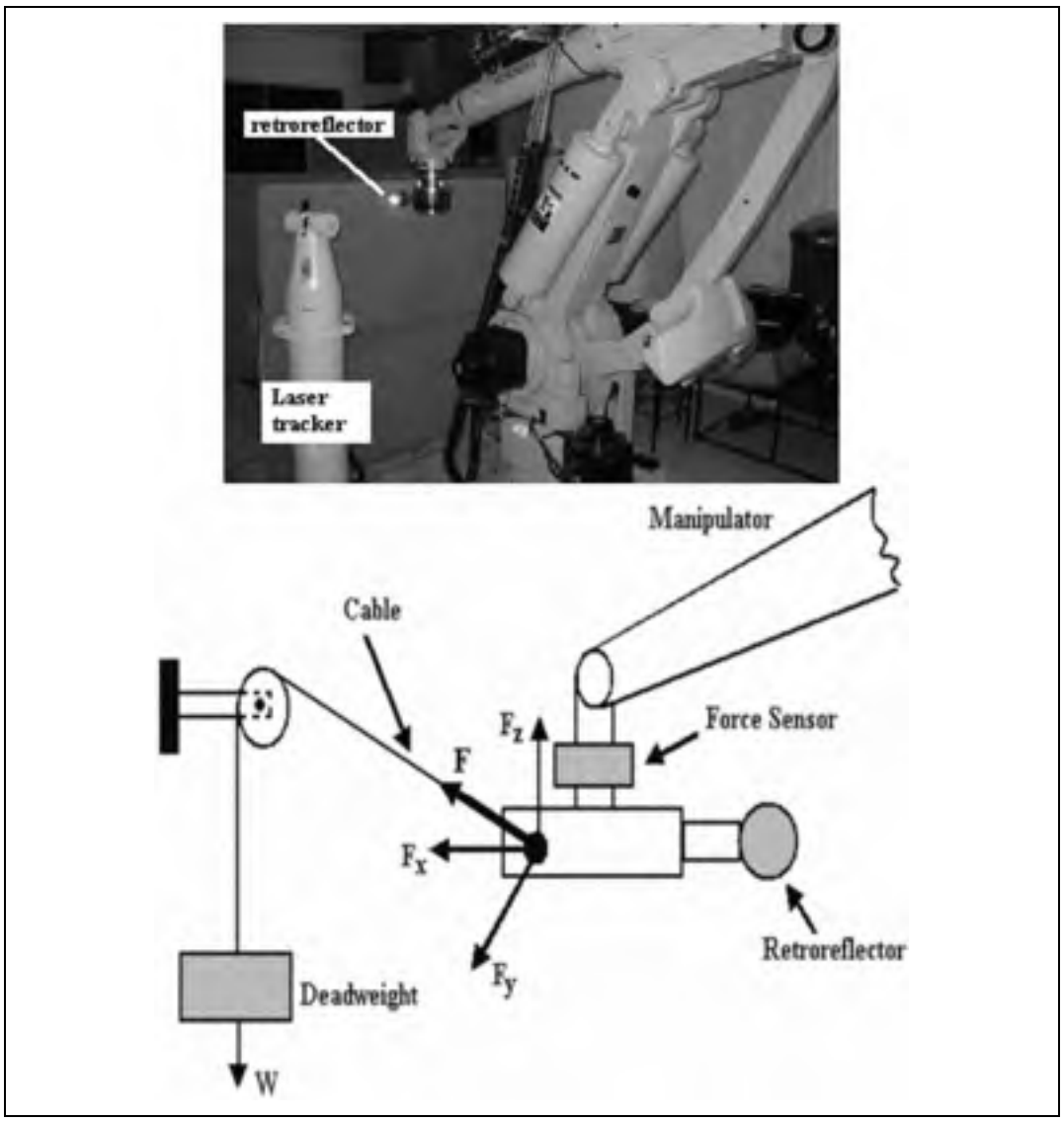

Figure 1.20 Experimental setup for global stiffness identification, and a schematic of the loading simulator (Alici et Shirinzadeh, 2005).

Figure 1.21 shows another experimental setup (Jianjun, Hui et Fuhlbrigge, 2009). In this setup the external force is imposed by an air cylinder through a pulley relayed steel cable. The amplitude of the external load can be adjusted by changing the air pressure. The direction of the load can be varied by changing the position of the pulley on the base column. In this manual setup, it is not possible to apply torque because of the point connection of the string to the robot's end-effector. In this setup, by using static equilibrium, the force vector at the force action coordinate is the same as the one at the force sensor coordinate. Three

calibrations are necessary before starting the load simulation: i) The calibration of the digitizer base coordinate relative to the robot base; ii) that of the position of the force action coordinate and iii) that of the position of the measurement coordinate.

Another example is the experiment by (Dumas et al., 2010) which is shown in figure 1.22. The setup is composed of the robot, a laser tracker, reflectors and a mass connected to the end-effector by a chain and a spring balance. In this setup the force is always in the direction of gravity. The same method is used by (Olabi et al., 2012a) except that the force is applied directly to the joints (see figure 1.23).

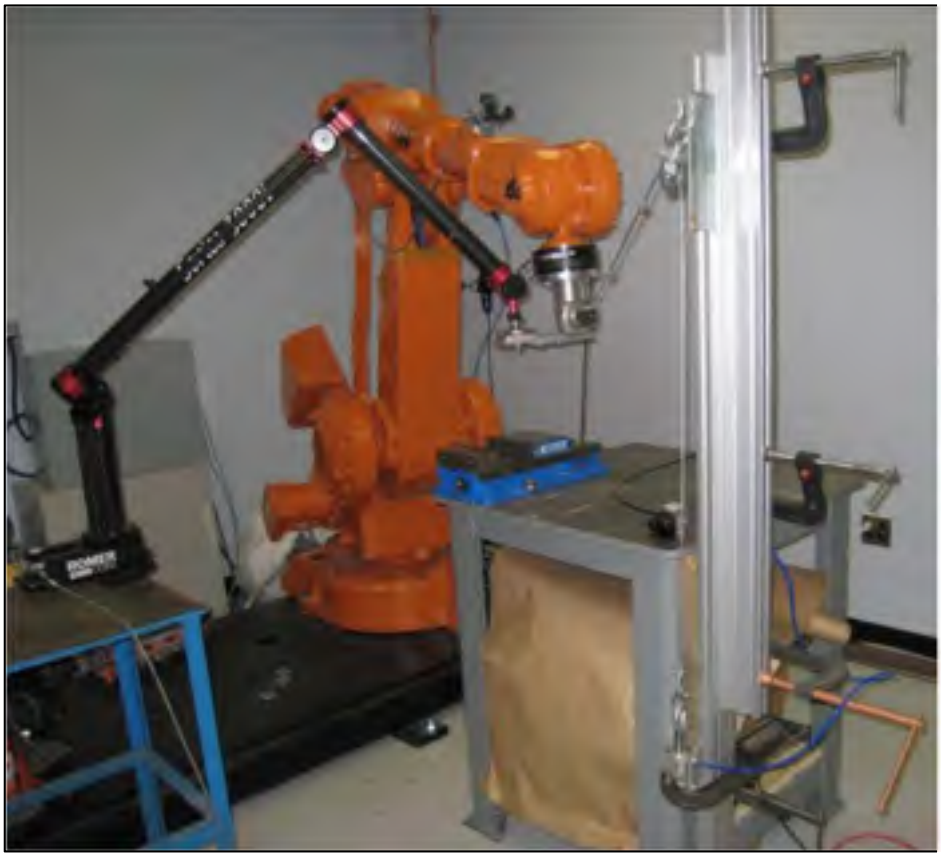

Figure 1.21 The experimental setup including air cylinder, pulley, steel cable, and digitizer (Jianjun, Hui et Fuhlbrigge, 2009).

Figure 1.22 Experimental setup and the robot end-effector showing the location of the laser tracker reflectors: P10, P11 and P12 (Dumas et al., 2010).

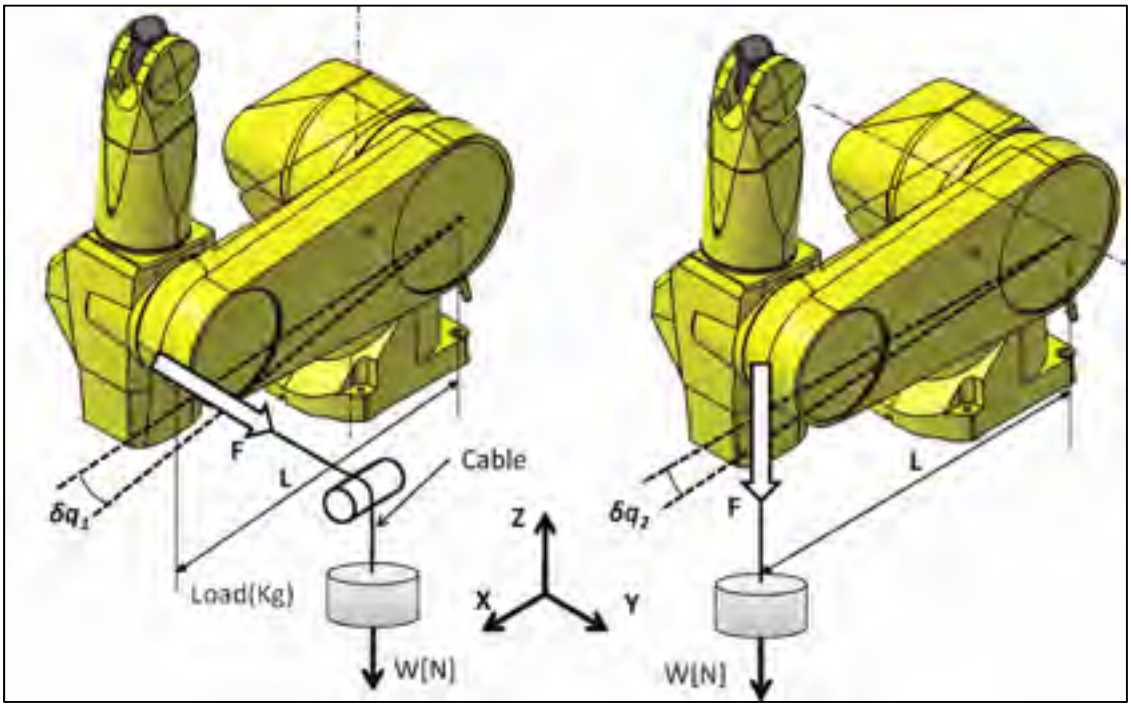

Figure 1.23 Individual joint stiffness identification. The load is applied directly to joints number 1 and 2 (Olabi et al., 2012a).

Experimentally, Cartesian space compliance is obtained through direct measurement of the absolute displacements (Figure 1.24). The displacement is caused by static force, which is induced along three Cartesian directions at the end point. It is also assumed that the joint flexibility has been identified. (Slavković et al., 2013) introduces an approach for obtaining the Cartesian compliance of a machining robot. The structure of the experimental setup is shown in figure 1.24. It includes a machining robot equipped with a sphere-tip tool, fixture, cable-pulley system and deadweight. The combination of pulley, fixture and deadweight exerts static force along three Cartesian directions at the end point of the sphere tip tool. The original and deformed positions of the tool's end point are measured by a FARO Portable CMM 3D digitizer. The process is entirely manual and, since it requires a large number of tests, it is time consuming.

Figure 1.24 Experimental setup for robot loading and displacement measurement in Cartesian space compliance identification (Slavković et al., 2013).

The stiffness of a parallel robot is examined by (Shin et al., 2013a). Their experimental setup is demonstrated in figure 1.25. They applied external forces along the different directions by excreting force through a steel cable. The resulting displacements are observed by a camera vertically fixed to the tool plate, which captures the pixel data of the end-effector. Each test and displacement measurement is repeated three times to obtain tow displacement deflections (Δx and Δy), and one rotational deflection ($\Delta \alpha$) in the x-y plan.

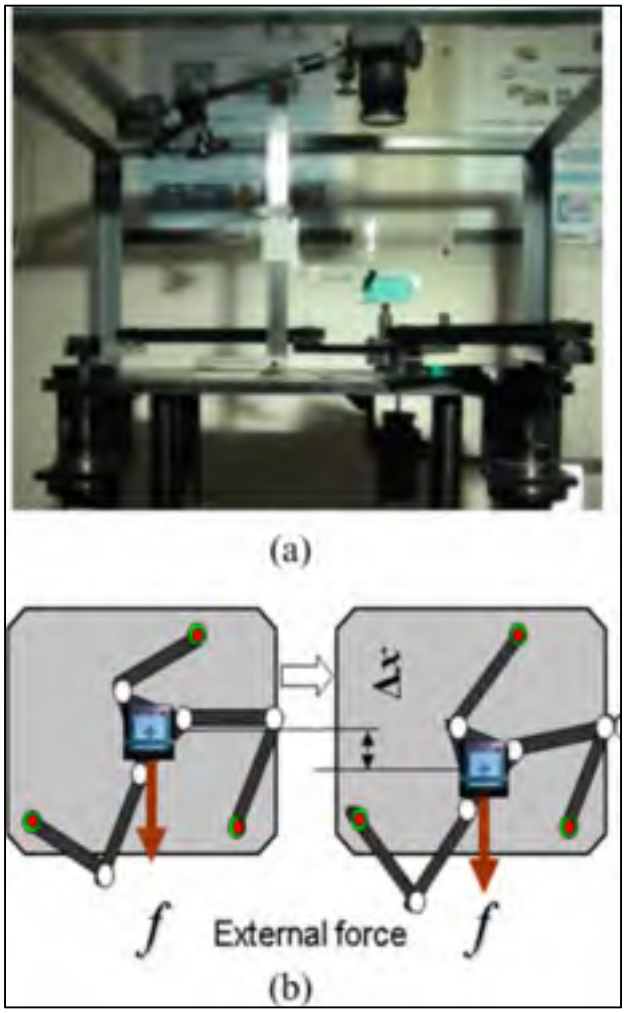

Figure 1.25 Experimental setup for measuring the displacement of a planar parallel robot. (a) Measurement setup. (b) External force and displacement (Shin et al., 2013a).

In summary, a load simulator for stiffness analysis could be a mass connected to the end-effector (Olabi et al., 2012a) (Dumas et al., 2010). In order to obtain force in different directions, the load simulator might be a cable-pulley system and a deadweight (Alici et Shirinzadeh, 2005). In (Shin et al., 2013a), the same setup is used for a parallel robot. In (Jianjun, Hui et Fuhlbrigge, 2009) the external load is applied by an air cylinder through a pulley-relayed string, and its amplitude can be adjusted by changing the air pressure whereas the direction of the load can be altered by the position of the pulley.

The above mentioned experimental setups apply maximum static force only in an arbitrary direction. The direction of the force can be changed manually. The process is always manual and time-consuming especially when Cartesian space compliance identification is required (Slavković et al., 2013). Moreover, depending on the configuration of the robot in its work space, the above-mentioned mechanisms does not ensure that all joints are adequately stressed during the test (Dumas et al., 2011) (Dumas et al., 2010) . Furthermore, the stiffness of the last joints is most sensitive to error, which means that the stiffness identification of the last joints is more difficult than that of its counter joints (Dumas et al., 2011). Moreover, since the process is not automated, a non-expert operator could not handle it. Therefore, it seems that developing an automated system to include a load simulator, deflection measurements and automated stiffness analysis is invaluable in the robotics industry. The development of such an automated setup is the objective of this work and is presented in the following chapter.

CHAPTER 2

LAGRANGIAN DYNAMICS OF CABLE-DRIVEN PARALLEL MANIPULATORS: A VARIABLE MASS FORMULATION

Yousef B. Bedoustani, Pascal Bigras and Ilian A. Bonev
Department of Automated Manufacturing Engineering, École de technologie supérieure,
1100 Rue Notre-Dame Ouest, Montréal, Québec H3C 1K3

This paper has been published as an article in
Transactions of the Canadian Society for Mechanical Engineering:
vol. 35, no. 4 (2011), pp 529-542

Abstract

In this paper, dynamic analysis of cable-driven parallel manipulators (CDPMs) is performed using the Lagrangian variable mass formulation. This formulation is used to treat the effect of a mass stream entering into the system caused by elongation of the cables. In this way, a complete dynamic model of the system is derived, while preserving the compact and tractable closed-form dynamics formulation. First, a general formulation for a CDPM is given, and the effect of change of mass in the cables is integrated into its dynamics. The significance of such a treatment is that a complete analysis of the dynamics of the system is achieved, including vibrations, stability, and any robust control synthesis of the manipulator. The formulation obtained is applied to a typical planar CDPM. Through numerical simulations, the validity and integrity of the formulations are verified, and the significance of the variable mass treatment in the analysis is examined. For this example, it is shown that the effect of introducing a mass stream into the system is not negligible. Moreover, it is

nonlinear and strongly dependent on the geometric and inertial parameters of the robot, as well as the maneuvering trajectory.

2.1 Introduction

The equations of motion of constant mass systems can be derived using various classical approaches, such as the Newton-Euler, Lagrangian, virtual, and Kane formulations. These basic principles of classical dynamics usually apply to systems comprising a definite number of objects with constant masses (Ardema, 2005), and they can be extended to cases where the masses of the system components change. Such a complete treatment of the dynamic analysis of systems with variable mass is a challenging problem. The difficulties arise from the fact that the mass, center of mass, and moments of inertia may vary in such mechanisms by a stream mass that is overtaken or expelled at a non-zero velocity, and that mass may change the linear and angular momentum of the overall system (Cveticanin, 1998a). The dynamics of variable mass systems have been studied for a very long time. Some of their first applications were in applied mechanics, in systems of continuously variable mass, such as rockets (Cornelisse, Schoyer et Wakker, 1979), and most of the first works reported in this area is related to these applications. Meshchersky was among the first scientists to understand the modern dynamics of a rigid body with variable mass (Cveticanin et Kovacic, 2007b). At the same time, in robotics applications, the motion of robots that pick up objects can be treated by varying mass dynamic analysis. Representative of this type of analysis is the work of McPhee in the dynamic analysis of multiple rigid bodies (McPhee et Dubey, 1991). Djerassi (Djerassi, 1998) reported similar work in such applications. The most recent work reported in the area of variable mass systems has been performed by Cveticanin (Cveticanin, 1998a), (Cveticanin et Kovacic, 2007a), (Cveticanin, 1993) and (Cveticanin, 2009). She studied the dynamics of body separation and developed an analytical procedure to determine the dynamic parameters of the remaining body after mass separation (Cveticanin, 2009). This method is based on the general principles of the momentum and angular momentum of a system of bodies. She also extended the Lagrangian formulation to systems of varying mass (Cveticanin, 1998b). The latest reported work of Cveticanin and Djukic explains the

extended kinematic and dynamic properties of a body in general motion (Cveticanin et Djukic, 2008), and presents their modification of the principle of linear and angular momentum conservation to obtain the linear and angular velocity of the body during mass separation.

Furthermore, the dynamic analysis of cable-driven parallel manipulators (CDPMs) shows their inherent complexity due to their closed-loop structure and kinematic constraints. Although the dynamic analysis of such manipulators is essential for stability analysis and closed loop control synthesis, little work has been reported on the dynamic analysis of CDPMs (Taghirad et Nahon, 2008), (Bedoustani, Taghirad et Aref, 2008), (Barrette et Gosselin, 2005b) and (Pham, Yang et Yeo, 2005). In these manipulators, a change in cable length causes the effective mass of their limbs to continuously vary in time. Moreover, the varying mass of the cables is a function of the position of the moving platform. In all the work reported in the dynamics of CDPMs, the effect of varying mass in cables has been neglected, because of the small changes of mass in the cables. However, in some applications, such as the large adaptive reflectors used in the next generation of giant telescopes (Bedoustani, Taghirad et Aref, 2008), the cables can be as long as 1,000 meters, and so the mass variation of cables plays a vital role in the dynamics of the manipulator.

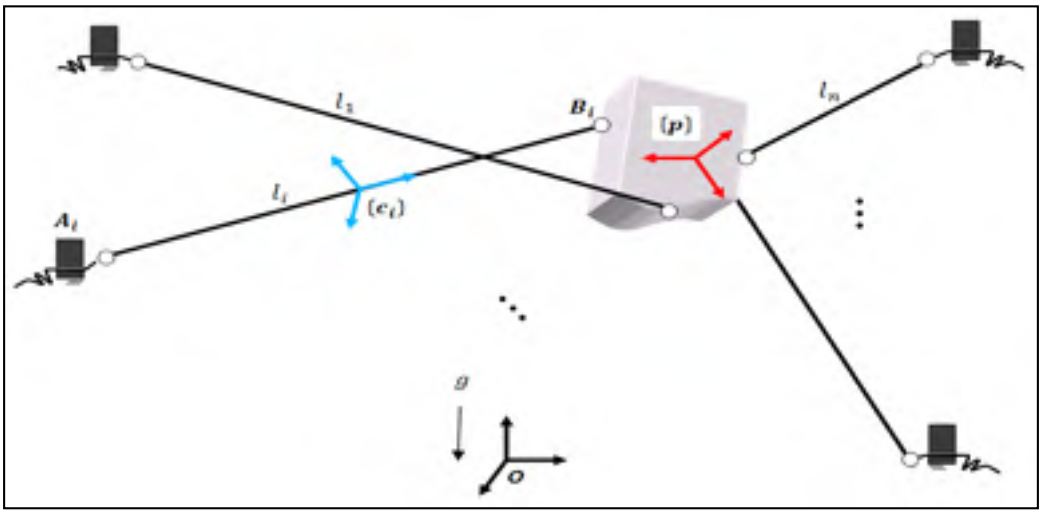

Figure 2.1 General structure of cable-driven parallel manipulators (CDPMs).

In this paper, the dynamic equations of CDPMs are discussed in detail in terms of the Lagrangian formulation, and a set of compact and closed-form formulations is obtained. Furthermore, the effect of varying the mass of the cables is carefully analyzed with respect to the dynamics of the manipulator. Finally, this general formulation is adopted for a typical planar CDPM, for which a simulation study is performed. It is shown that the effect of a mass stream entering into the system is not negligible: it is nonlinear and strongly dependent on the geometric and inertial parameters of the robot, and on the maneuvering trajectory.

2.2 Kinematics analysis of CDPMs

The general structure of CDPMs that is used in this paper is shown in figure 2.1. In this manipulator, the moving platform is supported by *n* limbs (cables) of identical kinematic structure, while the limbs are considered as rigid slender rods for the sake of dynamic analysis. The kinematic structure of the limb may be considered as spherical-prismatic-spherical (commonly denoted as SPS), in which only the prismatic joint is actuated. The kinematic structure of a prismatic joint is used to model the elongation of each link. As shown in figure 2.2, A_i denote the fixed base points of the cables, B_i denote the points of attachment of the cables to the moving platform, and $l = [l_1 \quad ... \quad l_n]$ denotes the vector of the cable lengths. Moreover, the position vector of the moving platform frame $\{p\}$, as well as the cable frame $\{c_i\}$, are defined as $\left[x_p^T \quad x_c^T\right]^T$, in which, x_p denotes the position of the moving platform according to the base frame $\{0\}$, and $x_c = [x_{c1}^T \quad ... \quad x_{cn}^T]^T$ denotes the vector of the cable coordinates where x_{ci}^T is the position of the cable's center c_i, according to the base frame (see figure 2.2).

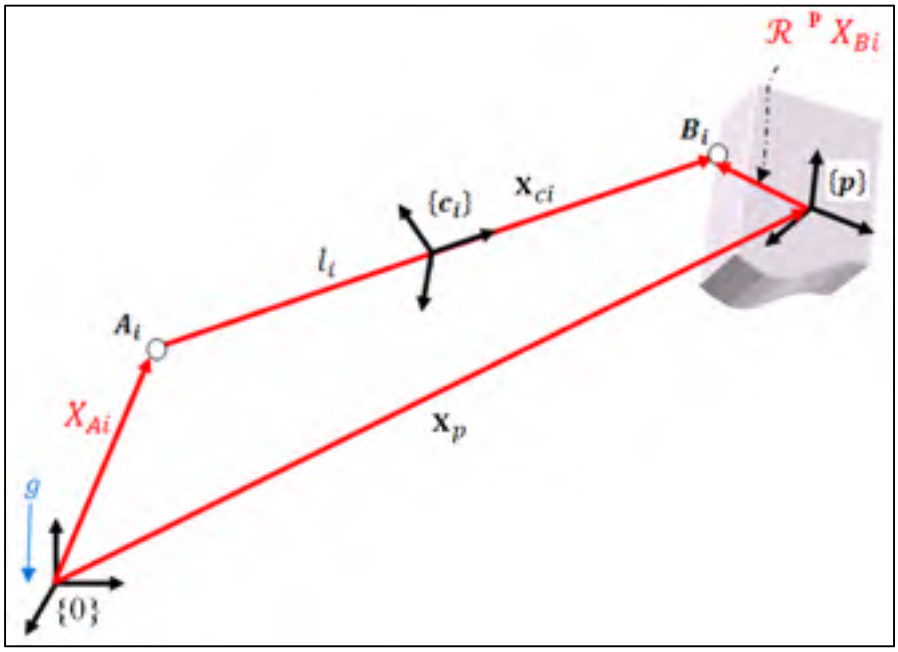

Figure 2.2 A single limb in a cable-driven parallel manipulator.

Similarly, the angular coordinates of the moving platform {p} and the cables $\{c_i\}$ relative to the base frame are defined as $\left[\varphi_p^T \quad \varphi_c^T\right]^T$, in which $\varphi_p = [\gamma \quad \beta \quad \alpha]^T$are any user-defined Euler angles of the moving platform, and $\varphi_c = [\varphi_1^T \quad ... \quad \varphi_n^T]^T$ are the angle vectors of the coordinates attached to the center of the cables. Subsequently, each angle vector is defined by its three Euler angles: $\varphi_i = [\gamma_i \quad \beta_i \quad \alpha_i]^T$. Accordantly, we consider the following rotational matrices:

$$\begin{aligned} R(\gamma, \beta, \alpha) &= {}^{O}R_p, \\ R(\gamma_i, \beta_i, \alpha_i) &= {}^{O}R_{c_i}. \end{aligned} \tag{2.1}$$

As explained in (Bedoustani, Taghirad et Aref, 2008), (Merlet, 2006), and (Aref et Taghirad, 2008), the inverse kinematics of CDPMs, like that of any other parallel manipulator, can be obtained by writing the loop closure equations. These equations allow all the coordinates of the system to be expressed as a function of the generalized coordinates. By choosing

$x = \begin{bmatrix} x_p^T & \varphi_p^T \end{bmatrix}^T \in R^m$ (position and orientation of the moving platform) as generalized coordinates, we obtain:

$$x_c = f_x(x), \varphi_c = f_\varphi(x), \; l = f_l(x), \tag{2.2}$$

where f_x, f_φ, and f_l are kinematic equations obtained from the loop closure. The time derivative of equation. (2.2) may lead to a relation that expresses the linear and angular velocities of the cables, as well as the time derivative of the cable lengths, as function of the linear and angular velocities of the moving platform:

$$\begin{bmatrix} \dot{x}_c \\ \omega_c \end{bmatrix} = \begin{bmatrix} J_{xx}(x) & J_{x\omega}(x) \\ J_{\omega x}(x) & J_{\omega\omega}(x) \end{bmatrix} \begin{bmatrix} \dot{x}_p \\ \omega_p \end{bmatrix}, \dot{l} = \begin{bmatrix} J_{lx}(x) & J_{l\omega}(x) \end{bmatrix} \begin{bmatrix} \dot{x}_p \\ \omega_p \end{bmatrix}, \tag{2.3}$$

whereJ_{xx}, $J_{x\omega}$, $J_{\omega x}$, and $J_{\omega\omega}$ are Jacobian matrices; $\dot{x}_c$ and $\dot{x}_p$ are the linear velocities of the cables and the moving platform respectively, and ω_c and ω_p are the angular velocities expressed in the cables and moving platform frame respectively. In order to eliminate the velocities of the cable in the Lagrangian formulation presented below, equation (2.3) is used to collect all the linear velocities of the cables and the moving platform as function of only the linear and angular velocities of the moving platform:

$$\begin{bmatrix} \dot{x}_p \\ \dot{x}_c \end{bmatrix} = \begin{bmatrix} I & 0 \\ J_{xx}(x) & J_{x\omega}(x) \end{bmatrix} \begin{bmatrix} \dot{x}_p \\ \omega_p \end{bmatrix}. \tag{2.4}$$

Similarly, the angular velocities of the cables and the moving platform are rewritten as:

$$\begin{bmatrix} \omega_p \\ \omega_c \end{bmatrix} = \begin{bmatrix} 0 & I \\ J_{\omega x}(x) & J_{\omega\omega}(x) \end{bmatrix} \begin{bmatrix} \dot{x}_p \\ \omega_p \end{bmatrix}. \tag{2.5}$$

Conveniently for the Lagrangian formulation, equations. (2.4) and (2.5) can be expressed as a function of the derivative of the generalized coordinates. In order to achieve this, the

following relation between the derivative of the Euler angles and the angular velocity can be established (Merlet, 2006):

$$\omega_p = J_{\omega\varphi}(x)\dot{\varphi}_p. \tag{2.6}$$

This equation can then be used to rewrite (2.4) and (2.5) as:

$$\begin{bmatrix}\dot{x}_p\\ \dot{x}_c\end{bmatrix} = \begin{bmatrix} I & 0 \\ J_{xx}(x) & J_{x\omega}(x)J_{\omega\varphi}(x)\end{bmatrix}\begin{bmatrix}\dot{x}_p\\ \dot{\varphi}_p\end{bmatrix} = J_x(x)\dot{x}\ , \tag{2.7}$$

$$\begin{bmatrix}\omega_p\\ \omega_c\end{bmatrix} = \begin{bmatrix} 0 & J_{\omega\varphi}(x) \\ J_{\omega x}(x) & J_{\omega\omega}(x)J_{\omega\varphi}(x)\end{bmatrix}\begin{bmatrix}\dot{x}_p\\ \dot{\varphi}_p\end{bmatrix} = J_{\varphi}(x)\dot{x}\,. \tag{2.8}$$

2.3 Kinetic energy of CDPMs

In order to derive the kinetic energy of the system, the kinetic energy of the robot components are derived and added. A CDPM consists of a moving platform and several limbs, in which the limbs are modeled as rigid slender rods. Therefore, the mass of all the objects in the mechanism can be expressed as:

$$M(l) = \begin{bmatrix} M_p & 0 \\ 0 & M_c(l)\end{bmatrix}, \tag{2.9}$$

in which $M_p$and M_c denote the mass matrices of the moving platform and all the cables respectively:

$$M_p = \begin{bmatrix} m_p & 0 & 0 \\ 0 & m_p & 0 \\ 0 & 0 & m_p\end{bmatrix},\ M_c(l) = \begin{bmatrix} m_{c1}I_3(l_1) & 0 & 0 \\ \vdots & \ddots & \vdots \\ 0 & 0 & m_{cn}I_3(l_n)\end{bmatrix}. \tag{2.10}$$

In this definition, m_p is the moving platform mass and m_{ci} is the mass of the cables expressed as a function of its density ρ_m and its lengths l_i, as follows:

$$m_i(l_i) = \rho_m l_i. \tag{2.11}$$

Similarly, the moment of inertia of all the components of a CDPM can be collected into:

$$I(l) = \begin{bmatrix} I_p & 0 \\ 0 & I_c(l) \end{bmatrix}, \tag{2.12}$$

where I_p and I_c are the inertial matrices of the moving platform and the cables respectively, given by:

$$I_p = \begin{bmatrix} I_{xx} & I_{xy} & I_{xz} \\ I_{xy} & I_{yy} & I_{yz} \\ I_{xz} & I_{yz} & I_{zz} \end{bmatrix}, I_c(l) = \begin{bmatrix} I_{c1}(l_1) & 0 & 0 \\ \vdots & \ddots & \vdots \\ 0 & 0 & I_{cn}(l_n) \end{bmatrix}. \tag{2.13}$$

Since the cables are modeled as slender rods, the moment of inertia of the cables I_{ci} is defined as:

$$I_{ci}(l_i) = \frac{\rho_m}{12} \begin{bmatrix} {l_i}^3 & 0 & 0 \\ 0 & {l_i}^3 & 0 \\ 0 & 0 & 0 \end{bmatrix}. \tag{2.14}$$

According to equation. (2.2), l_i can be expressed as a function of the generalized coordinates. Thus, the total kinetic energy for all the components of a CDPM can be expressed as:

$$T = \frac{1}{2} \left[\begin{bmatrix} \dot{x}_p \\ \dot{x}_c \end{bmatrix}^T M(x) \begin{bmatrix} \dot{x}_p \\ \dot{x}_c \end{bmatrix} + \begin{bmatrix} \omega_p \\ \omega_c \end{bmatrix}^T I(x) \begin{bmatrix} \omega_p \\ \omega_c \end{bmatrix} \right]. \tag{2.15}$$

The substitution of the Jacobian matrices defined by equations (2.7) and (2.8) leads to:

$$T = \frac{1}{2} \dot{x}^T D(x) \dot{x}\,, \tag{2.16}$$

where the mass matrix of the system is given by:

$$D(x) = J_x^T(x)M(x)J_x(x) + J_\varphi^T(x)I(x)J_\varphi(x). \tag{2.17}$$

2.4 Variable mass Lagrangian approach

In this section, the dynamics of a cable-driven parallel manipulator is obtained by the variable mass Lagrangian formulation. As the length of the cables in a CDPM is a function of the position of the moving platform, the cable mass changes in time. In fact, the mass that is added to or removed from the system will add momentum to the system or remove momentum from it. The dynamics of the mechanism with variable mass is discussed in detail in (Cveticanin, 1998b) by Cveticanin, who extends the Lagrangian formulation to:

$$\frac{d}{dt}\left(\frac{\partial T}{\partial \dot{x}}\right)^T - \left(\frac{\partial T}{\partial x}\right)^T = q + q^{Fi} + d + q^{R^*}. \tag{2.18}$$

In this formulation, q and q^{Fi} are the generalized forces caused by non conservative and conservative external forces acting on the system respectively. Furthermore, $d + q^{R^*}$ accounts for the effect of changing mass in the system. In other words, q^{R^*} is an impact force that is caused by the mass stream entering into the system or being expelled from it, and is a function of the mass variation and its relative velocity. Furthermore, d accounts for the direct energy that is added to or removed from the system by entry or departure of the stream mass.

2.4.1 Kinetic energy term

Let us examine the required terms of the Lagrangian formulation for a CDPM. As usual, the first two terms can be derived from the kinetic energy of the system given by (2.16):

$$\frac{d}{dt}\left(\frac{\partial T}{\partial \dot{x}}\right)^T - \left(\frac{\partial T}{\partial x}\right)^T = D(x)\ddot{x} + \left(\dot{D}(x) - \frac{1}{2}\frac{\partial}{\partial x}\left(\dot{x}^T D(x)\right)\right)\dot{x}, \tag{2.19}$$

where $\dot{D}(x)$ are the time derivatives of the terms given by (2.17).

2.4.2 Generalized forces

As explained for the extended Lagrangian formula, q^{Fi} and q are the generalized forces caused by non conservative and conservative external forces acting on the system respectively. The generalized force acting on the system caused by external non conservative forces is composed of the elements $w_x + q_{nc}$, such that:

$$q = w_x + q_{nc}, \tag{2.20}$$

where w_x is the wrench (forces and torques) corresponding to the projection of the actuator forces (cable force) on the platform, and q_{nc} represents the external forces and torques acting directly on the moving platform. According to the principle of virtual work and the Jacobians given by equations. (2.3) and (2.6), the vector w_x can be obtained by projecting the actuator forces into the Cartesian space, using the manipulator Jacobian matrices as follows:

$$w_x = [J_{lx}(x) \quad J_{l\omega}(x)J_{\omega\varphi}(x)]^T \ \tau = J_w^T(x)\tau, \tag{2.21}$$

where τ denotes the vector of the actuator (cable) forces. The contribution of the gravitational forces may be expressed as the following equation of potential energy:

$$V = g^T\left(M_1 x_p + \sum_{i=1}^{n} m_i(l_i)x_{ci}\right), \tag{2.22}$$

where g is the gravity vector represented in the base frame, and x_p is the position vector of the moving platform. According to (Cveticanin, 1998a), potential energy can be expressed as a function of the generalized coordinates. Therefore, q^{Fi} is obtained by the partial derivative of the potential energy with respect to the generalized coordinates:

$$G(x) = -\frac{dV}{dx}. \tag{2.23}$$

2.4.3 Variable mass term

The formulation proposed for the varying mass mechanism in (Cveticanin, 1998b) was defined for a particle mass system. The additional terms required to accommodate the variable mass mechanism are only a function of mass derivatives (a small variation in mass divided by a small variation in time). For this reason, and because these variations are continuous, the mass derivative acts as a particle, even for a body system. This interpretation has already been considered in (Cveticanin, 1998b; Pesce, 2003) for the analysis of the vibration of varying mass mechanisms (see also (Cveticanin et Kovacic, 2007a)). As discussed in (Cveticanin, 1998b), the effect of changing mass in the system is caused by a variable momentum. This effect can be divided into the impact forces denoted by q^{R^*} and the energy that was added or removed from the system by the variable mass, denoted by d. Since cables are the only source of variable mass and the variation is only function of the generalized coordinates, d_k can be determined by (Pesce, 2003):

$$d_k(x, \dot{x}) = -\frac{1}{2}\sum_{i=1}^{n} \frac{\partial m_i(l_i)}{\partial x_k} v_i^T v_i, \tag{2.24}$$

where $\mathbf{v}_i$ is the velocity of the variable mass i and k denote individual generalized coordinates. According to figure 2.1, this mass variation is located at the beginning of the cable *i* and its velocity is in only one direction when it is expressed in the frame of the cable. For this reason, $\mathbf{v}_i$ can be considered as a scalar given by $\dot{l}_i$. Then, using equations (2.2) and (2.11), equation (2.24) can be rewritten as:

$$d_k(x, \dot{x}) = -\frac{1}{2}\,\rho_m \sum_{i=1}^{m} \frac{\partial f_{li}}{\partial x_k}\left(\frac{\partial f_{li}}{\partial x}\dot{x}\right)^2. \tag{2.25}$$

Now, the effect of the impact forces $q_k^{R^*}$ can be obtained from (Pesce, 2003):

$$q_k^{R^*}(x,\dot{x}) = \sum_{i=1}^{m} \dot{m}_i(l_i) v_{oi}^T \frac{\partial p_i}{\partial x_k}, \tag{2.26}$$

where v_{oi} is the velocity of the expelled or gained mass, and **p** is the position of the mass variation. This variation is also located at the beginning of the cable *i* and its position variation, and its velocity is in only one direction when they are expressed in the frame of the cable. For this reason, $\mathbf{v}_{oi}$ and the variation of p_i can be interpreted as scalars, given by $\dot{l}_i$ and $\partial l_i/\partial x_k$ respectively. Then, using equations (2.2) and (2.11), equation (2.26) can be rewritten as:

$$q_k^{R^*}(x,\dot{x}) = \rho_m \sum_{i=1}^{m} \left(\frac{\partial f_{li}}{\partial x}\dot{x}\right)^2 \frac{\partial f_{li}}{\partial x_k}. \tag{2.27}$$

$d_k$and $q_k^{R^*}$ can be combined, as follows:

$$d_k(x,\dot{x}) + q_k^{R^*}(x,\dot{x}) = \frac{1}{2}\rho_m \sum_{i=1}^{m} \frac{\partial f_{li}}{\partial x_k}\left(\frac{\partial f_{li}}{\partial x}\dot{x}\right)^2. \tag{2.28}$$

2.4.4 Final dynamics equations

From equations (2.17), (2.18), (2.19), (2.21), (2.23), and (2.28), the general form of the dynamics of CDPM can be released in compact standard form, as:

$$D(x)\,\ddot{x} + c(x,\dot{x}) + G(x) = J_w(x)\tau + q_{nc}, \tag{2.29}$$

where D is given by equation (2.17), G is given by equation (2.23), J_w is defined by equation (2.21), and c is given by:

$$c(x,\dot{x}) = \left(\dot{D}(x) - \frac{1}{2}\frac{\partial}{\partial x}(\dot{x}^T D(x))\right)\dot{x} - \left(d(x,\dot{x}) + q^{R^*}(x,\dot{x})\right), \qquad (2.30)$$

where each element of $\mathbf{d} + q^{R^*}$ is given by equation (2.28). In equation (2.30), **D** is the mass matrix; c is the vector of the centrifugal, Coriolis, and mass variation terms; and **G** is the vector of the gravity terms. Finally, q_{nc} is the external wrench vector acting directly on the moving platform.

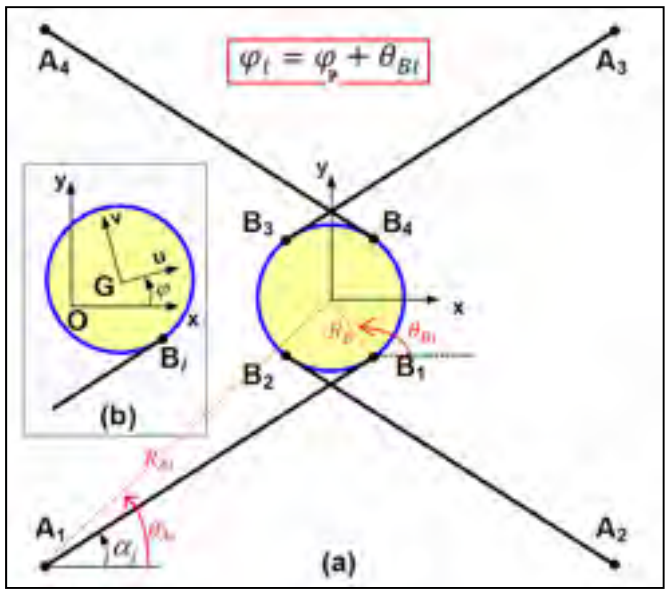

Figure 2.3 Simple schematic representation of the planar CDPM.

2.5 Case study

In this section, the dynamics of the planar CDPM discussed in (Bedoustani, Taghirad et Aref, 2008) (see figure 2.3) was considered. This CDPM is a simplified planar version adopted from the structure of the Large Adaptive Reflector (LAR). This structure consists of parallel redundant manipulators actuated by long cables. The control objective in the simplified mechanism is to track the position and orientation of the moving platform, as desired, in the

presence of disturbance forces, such as wind turbulence. The geometric and inertial parameters used in the simulations of the system have been adopted from the LAR design. In this way, the length of the cables is in the order of 900 meters and the mass density of the cables ρ_m is 0.215 kg/m. The main control purpose is the positioning of the moving platform $x = [x \quad y \quad \varphi_p]^T$, the mass of which is as follows: $M_p = 2500$ kg. First, the dynamics of the planar CDPM is obtained by the Lagrangian method. Then, the effect of the variable mass in the cables is studied in detail.

From the inverse kinematic analysis, the length of the cable l_i and the angle α_i can be obtained easily by writing the loop closure equations as follows:

$$\begin{gathered} l_i = [(x + R_B \cos\varphi_i - x_{Ai})^2 + (y + R_B \sin\varphi_i - y_{Ai})^2]^{\frac{1}{2}}, \\ \alpha_i = \operatorname{atan2}\big((y + R_B \sin\varphi_i - y_{Ai}), (x + R_B \cos\varphi_i - x_{Ai})\big). \end{gathered} \tag{2.31}$$

Also, by Jacobian analysis, we have:

$$\begin{gathered} J_{xx} = \begin{bmatrix} S_{1x} & S_{1y} \\ S_{2x} & S_{2y} \\ S_{3x} & S_{3y} \\ S_{4x} & S_{4y} \end{bmatrix}, J_{x\omega} = \begin{bmatrix} E_{1x}S_{1y} - E_{1y}S_{1x} \\ E_{2x}S_{2y} - E_{2y}S_{2x} \\ E_{3x}S_{3y} - E_{3y}S_{3x} \\ E_{4x}S_{4y} - E_{4y}S_{4x} \end{bmatrix}, \\ J_{\omega x} = \frac{1}{l_i}\begin{bmatrix} -S_{1y} & S_{1x} \\ -S_{2y} & S_{2x} \\ -S_{3y} & S_{3x} \\ -S_{4y} & S_{4x} \end{bmatrix}, J_{\omega\omega} = \frac{1}{l_i}\begin{bmatrix} E_{1x}S_{1y} + E_{1y}S_{1x} \\ E_{2x}S_{2y} + E_{2y}S_{2x} \\ E_{3x}S_{3y} + E_{3y}S_{3x} \\ E_{4x}S_{4y} + E_{4y}S_{4x} \end{bmatrix}. \end{gathered} \tag{2.32}$$

where vectors E and $\hat{S}$ are defined as follows:

$$\begin{gathered} [E_{ix} \quad E_{iy}]^T = [R_B \cos(\varphi + \theta_{Bi}) \;\; R_B \sin(\varphi + \theta_{Bi})]^T, \\ \hat{S}_i = [S_{ix} \quad S_{iy}]^T = [\cos\alpha_i \;\; \sin\alpha_i]^T. \end{gathered} \tag{2.33}$$

Moreover, for planar CDPMs, we have $J_{\omega\varphi} = I$, and the Jacobian matrices are therefore easily defined by equations (2.7) and (2.8). Finally, by deriving equations (2.17), (2.30), and (2.23), the mass matrix **D**, the centrifugal, Coriolis, and mass variation terms c, and the

gravity vector terms **G** are obtained. Thus, the dynamic modeling of planar CDPM is expressed as follows:

$$D(x)_{3\times3}\,\ddot{x}_{3\times1} + c(x,\dot{x})_{3\times1} + G(x) = [F_x \quad F_y \quad \tau_z]^T + q_{nc}, \tag{2.34}$$

where F_x, F_y, and τ_z form the wrench applied on the moving platform, defined by:

$$[F_x \quad F_y \quad \tau_z]^T = J_w(x)^T{}_{3\times4}\,\tau_{4\times1}. \tag{2.35}$$

In equation (2.35), $\tau_{4\times1}$ is the vector of the forces in links space or, in other words, the tensions in the cables that are generated by the actuators (motors). As the Jacobian matrix in a redundant manipulator is non square, tension in the cables can be obtained by the algorithms of Redundancy Resolution (optimal distribution of forces in cables) (Taghirad et Bedoustani, 2011), (Lawson et Hanson, 1974). This resolution ensures positive tension in all cables.

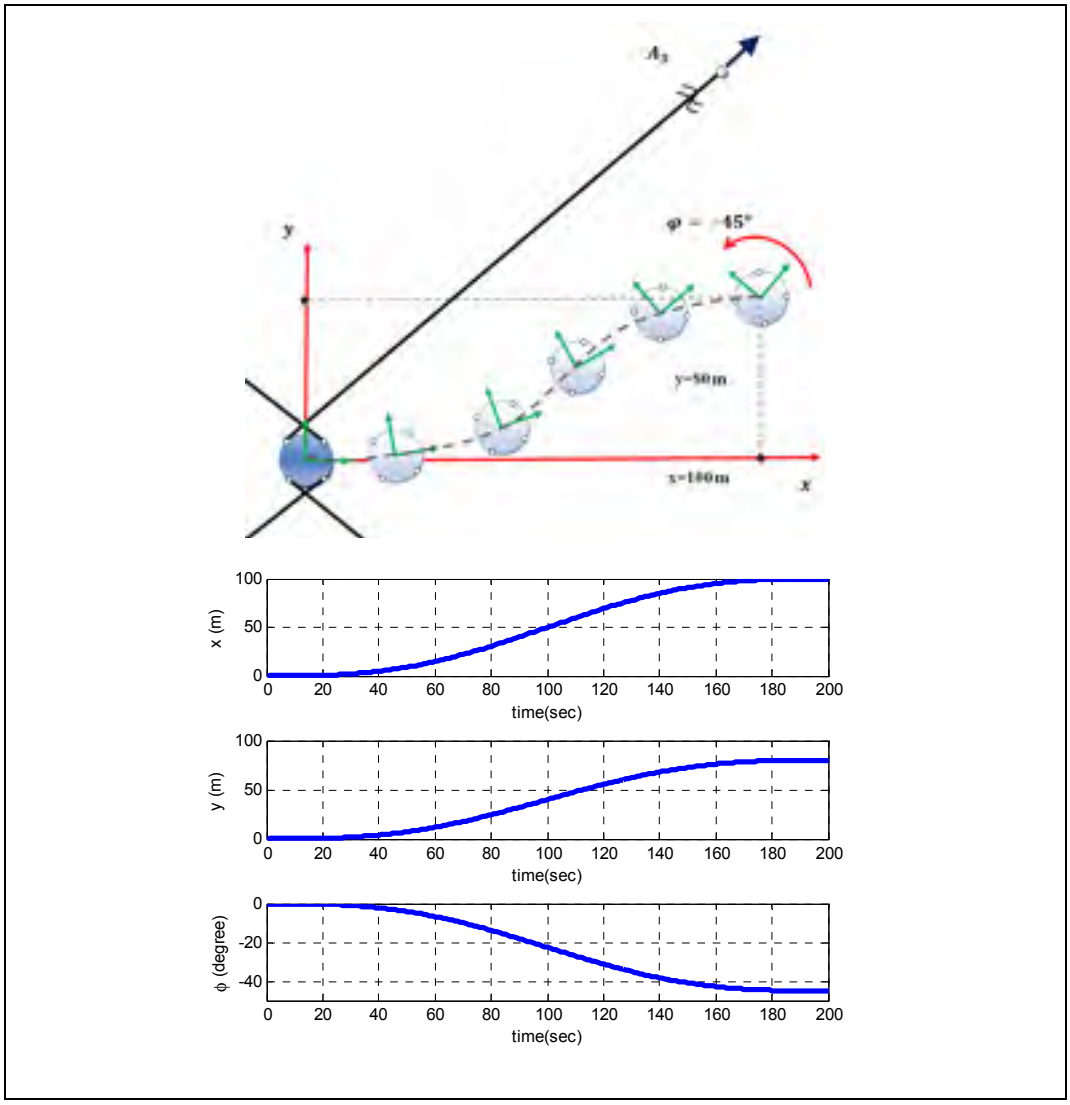

Figure 2.4 Desired trajectory.

For simulation, a specific displacement of the moving platform is chosen. This simple trajectory is shown in figure 2.4. Then, the forces in Cartesian space are obtained by the inverse dynamic model given by equation (2.34). These forces are compared with the forces obtained by the same simulation, in which the effect of variable masses in the cables is neglected. Figure 2.5 (a) shows the forces and torque in Cartesian space. Figure 2.5 (b) shows the projected forces in the links space. In other words, it shows the tensions in the cables that are defined by equation (2.35) as $\tau_{4\times1} = [\tau_1, \tau_2, \tau_3, \tau_4]^T$. These forces were obtained by driving the numerical algorithm used to solve the "non negative least-squares

constraints problem" described in (Lawson et Hanson, 1974) and implemented in the Matlab optimization toolbox. As we expect from the dynamics equation analysis, the variable mass has a significant effect on the dynamics of the manipulator. In applications such as the LAR project (Bedoustani, Taghirad et Aref, 2008), the length and mass density of the cables are important. In this context, the variable mass of the cables plays a vital role in the dynamics of the CDPM. Moreover, the effects of the variable mass in the cables are strongly dependent on the position and velocity trajectories. This effect is nonlinear, and dependent on parameters like the mass density of the cables, the mass of the moving platform, and the kinematic structure. In fact, the additional effect of the variable mass is completely described by equation (2.28). Therefore, this effect is directly proportional to the cable mass density ρ_m. This parameter could reduce the effect of the variable mass. However, such a reduction would increase the flexibility of the cables, which is not necessarily a better outcome. In addition, since $f_l(x)$ in equation (2.2) is a kinematic function of the position of the moving platform, the variable mass effect is strongly dependent on the size and topology of the CDPM.

2.6 Conclusion

This paper focused on the dynamic modeling of cable-driven parallel manipulators (CDPMs) using the Lagrangian formulation. In previous works, the effect of a mass stream entering into the system caused by elongation of the cables is neglected, whereas in this paper, this effect is treated using a Lagrangian variable mass formulation. In this way, a complete dynamics of the system is derived, while the compact and tractable closed form dynamics formulation is preserved. First, a general formulation for a general CDPM is given, where the effect of mass variation of the cables is integrated into its dynamics. The significance of such a treatment can be appreciated in a complete analysis of the dynamics, vibrations, and stability of such systems, and in any robust control synthesis of these manipulators. The general formulation is applied to a typical planar CDPM with cables 900 meters in length. Through simulation, the validity and integrity of the formulation obtained are verified, and the significance of variable mass treatment in such an analysis is examined. It is shown that

the effect of a mass stream entering into the system is not negligible: it is non-linear and strongly dependent on the geometric and mass parameters of the robot, and on the maneuvering trajectory.

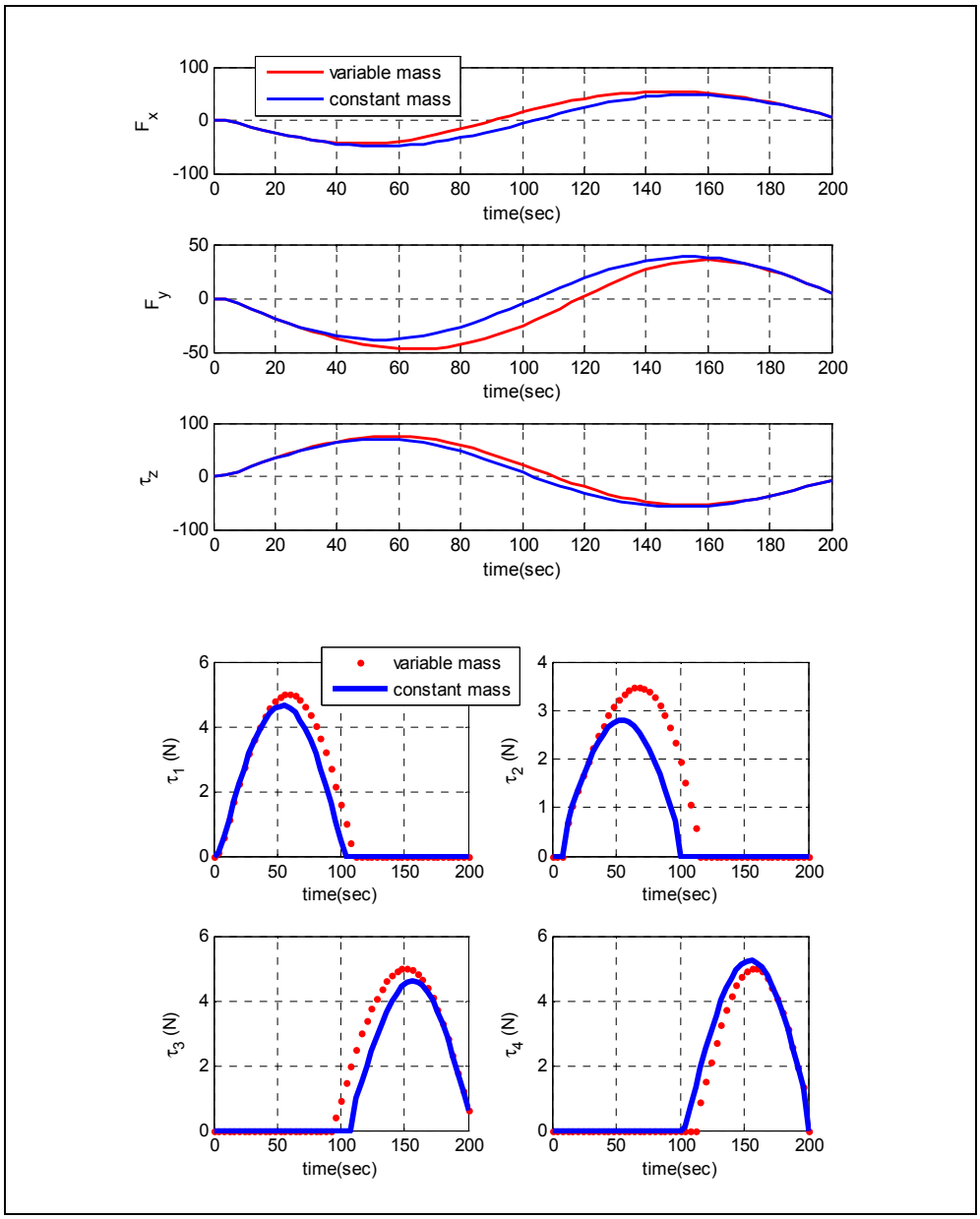

Figure 2.5 Forces and torque in Cartesian space (moving platform workspace); (b) tension in the cables (forces in the joint space).

CHAPTER 3

DESIGN AND CONTROL OF A 6-DOF CABLE-DRIVEN LOADING SIMULATOR

Yousef B. Bedoustani, Pascal Bigras and Ilian A. Bonev
Department of Automated Manufacturing Engineering, École de technologie supérieure,
1100 Rue Notre-Dame Ouest, Montréal, Québec H3C 1K3

This paper has been submitted as an article in
Journal of Dynamic Systems, Measurement, and Control.

Abstract

This paper introduces a new application of the cable-driven parallel manipulator (CDPM) as a force/torque simulator with 6 degrees of freedom (DOF). The CDPM presented is designed and controlled to precisely apply a 6-DOF force/torque on a target object fixed at a static but arbitrary position. The most significant advantages of the proposed device are the simplicity of the mechanical components and actuators, and the control topology that makes it cost efficient. The innovation consists of a precision extension spring added to each cable to help estimate the cable tension and reduce the effect of backlash. Two levels of control are considered for the control topology in order to achieve accurate force control on the target, one in the Cartesian space and the other in the joint space. For a fixed target object, it is shown that although the redundancy resolution algorithm is nonlinear, the combination of the redundancy resolution algorithm and the model of the CDPM can be formulated as a linear system. The pole placement method then is used to calculate the gains of the controller at the same time for both Cartesian and joints spaces. In addition, the real-time rapid algorithm of redundancy resolution is implemented in the closed-loop system. Finally, the experimental results of a 6-DOF force/torque trajectory are presented to illustrate the performance of the

innovative CDPM, the proposed controller and the real-time redundancy resolution. The results show that the proposed CDPM, its control topology and the real-time rapid redundancy resolution algorithm, perform well in force/torque simulator applications for fixed targets. The proposed device could be used for evaluating stiffness systems like spine segments and industrial robots.

3.1 Introduction

In several robotic applications, a desired wrench vector (force and torque) is applied on an object. These applications are mostly referred to as force/torque simulators or loading simulators. One example of this type of application is the spine test mechanism (Jirkova et al., 2007), in which forces or torques are applied on a spine segment and the deformation is measured so that their mechanical properties can be studied. Another example is a simple single-cable mechanism that applies a force/torque on an industrial robot to enable analysis of the stiffness and deflection of the latter (Jianjun, Hui et Fuhlbrigge, 2009). Loading simulators may be based on industrial robots (Schulze et al., 2012) and (Goertzen et Kawchuk, 2009); however, they often use custom robots, which can be serial (Schulze et al., 2012) or parallel (Goertzen et Kawchuk, 2009). It is also possible to use simple or complex cable-driven devices (Shin et al., 2013a) and (Eguizabal et al., 2010).

Using the cables as robot links has important advantages: (1) considerably reduced cost; and (2) the facility to change the topology of the CDPM in order to modify workspace and wrench feasibility. In other words, the geometry of CDPMs can be easily modified and optimized, depending on the required workspace or wrench vectors. For example, the workspace can be increased just by increasing the distances between actuators. In spite of these advantages, there are currently a few cable mechanisms being used as loading simulators (Eguizabal et al., 2010); moreover, they have not been developed to apply a 6-DOF wrench.

In this paper, the design and development of a cable-driven omnidirectional loading simulator (CabOLS) is presented (see figure 3.1). Even though there are several approaches available for controlling the platform position and orientation of 6-DOF cable robots (e.g. (Miermeister et Pott, 2010) and (Yao et al., 2010)), this is not the case for force/torque control. There exist some cable mechanisms for which forces or torques are controlled, but for very few DOFs. For instance in (Shin et al., 2013b) and (Eguizabal et al., 2010) a one-DOF cable-driven test set-up is used to produce pure moment (Eguizabal et al., 2010) and external force (Shin et al., 2013b) on the target object. However the operation is not fully automated.

As it is very common for robots not actuated by cables, the controller of CabOLS is based on a force control loop in the workspace combined with a force control loop in the joint-space. The first is implemented by using a force/torque sensor, however, in order to reduce the cost, no force sensors are used to implement the joint-space force control loop. Instead of using other solutions such as tendon force sensor (Palli et Pirozzi, 2012), a precision spring is used to estimate the force in each cable. This solution is simpler; however, it requires the knowledge of the end-effector position. Since this load simulator is often attached to another device (e.g. an industrial robot), knowing the pose of the end-effector is straightforward when it is assumed that the device is equipped with the necessary sensors. When it is not the case or when more accurate measurement is necessary or flexible coupling is used between the device and the simulator, it is also possible to add an external position sensor. In that case the load simulator could be used, for example, as a spine testing system or to estimate an experimental model of the stiffness of a robot.

The springs added to each cable of CabOLS have also the additional benefit of considerably reducing the backlash effects, which can be particularly important when low-cost gearboxes are used for the actuation. The combination of backlash and stiff cables cause the following problem: a very small motion of one motor in one direction can cause both zero tension and very high tension in the corresponding cable. The additional springs decrease this effect

because they increase the flexibility of the cables, and the small displacements caused by backlash generate much smaller force variations.

To validate CabOLS as a loading simulator, its platform is fixed to the end-effector of an ABB industrial robot equipped with a 6-DOF force/torque sensor (Figure 3.1). A C-track is also used to obtain an accurate measurement of the platform position, but it is not used with the CabOLS controller.

The rest of the paper is organized as follows: In the second section, the mechanical architecture and the actuator hardware of CabOLS is explained. Then, the kinematics of the system and Jacobian analysis is briefly discussed. The third section focuses on the control topology, as well as the redundancy resolution of CabOLS and the real-time implementation of the rapid algorithm that is generated. Finally, the performance of the closed-loop system is discussed in the last section.

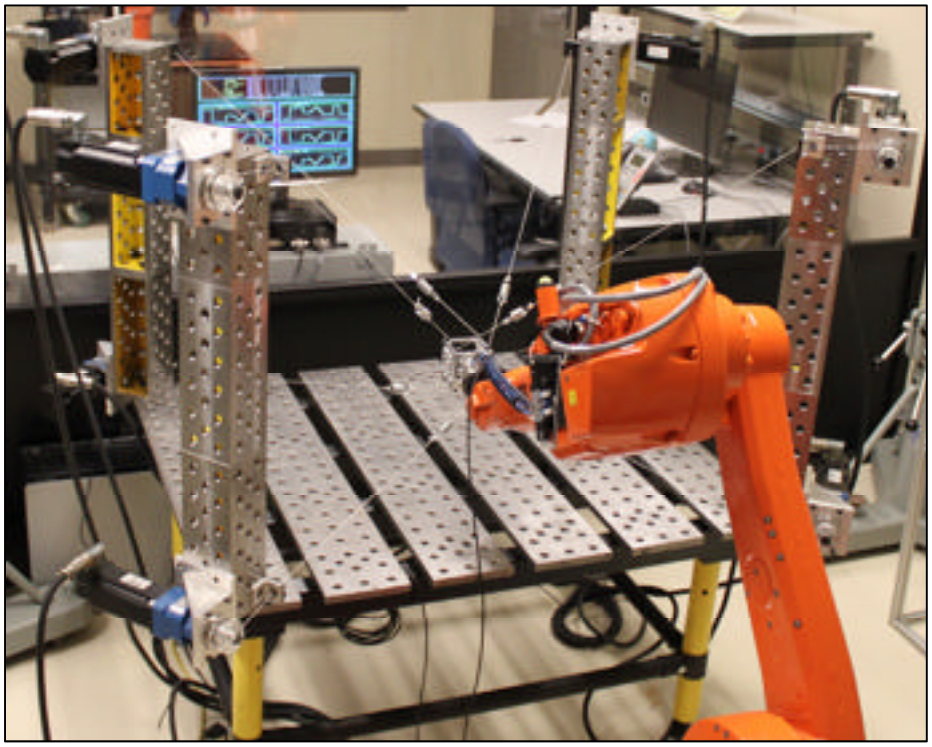

Figure 3.1 CabOLS fixed to an ABB industrial robot to simulate omnidirectional loading.

3.2 System architecture of CabOLS

The following section gives an overview of the design of CabOLS, including its mechanical components and hardware, as well as the real-time software used for controller implementation.

3.2.1 Mechanism description and geometry

The essential mechanical components of CDPMs are a mobile platform and limbs. Every limb of a CDPM includes a cable and a cable wrench mechanism, and every cable connects a fixed point on the base structure to the mobile platform. Figure 3.2(a) shows a simple schematic of a limb of CabOLS. One end of each cable is attached to the mobile platform at point B_i, and the other end is fixed at point A_i, where the cable is wound onto the wrench mechanism, which is a simple pulley. Each pulley is operated by a motor fixed at the base. CabOLS uses LaserPro™ Gold Spectra cables, which have a load capability of 890 N. These cables have the highest strength-to-diameter ratio commercially available, and low stretchability.

To reduce the backlash effect of the gearboxes and estimate the tension in each limb, a precision extension spring has been added to each cable. (The precision extension spring used in CabOLS is fabricated from zinc-plated steel music wire.) This makes it possible to estimate the tension on the cables directly from the elongation of the spring and cable combination. This elongation can be calculated from position of the platform (provided by the ABB robot used in the validation setup) combined with inverse kinematic equations and actuator displacement measured by encoders. Even if the stiffness of each cable is variable according to its length, the additional springs are chosen in order to obtain the equivalent stiffness of the combination approximately constant.

Figure 3.2(b) and figure 3.2(c) show a simple schematic of CabOLS geometry. In this structure, cables are connected to the mobile platform from the top and bottom in opposite

directions (counterclockwise and clockwise). This structure not only helps provide greater angles of rotation – up to about 90° without cable collision – but also pure moments around each axis, which are needed in some applications, such as the spine test mechanism (Eguizabal et al., 2010).

In CabOLS, eight cables provide the 6-DOF wrench capability. This gives the manipulator two degrees of redundancy, which are used to respect the physical constraint of positive forces in all the cables. Even with this redundancy, not every combination of wrench vector inside every point of the workspace, and in every orientation, is feasible. However the cable robot geometry (the position of the fixed points) and the configuration of the cable attachments could easily be changed, in order to achieve the combination of forces and torques required.

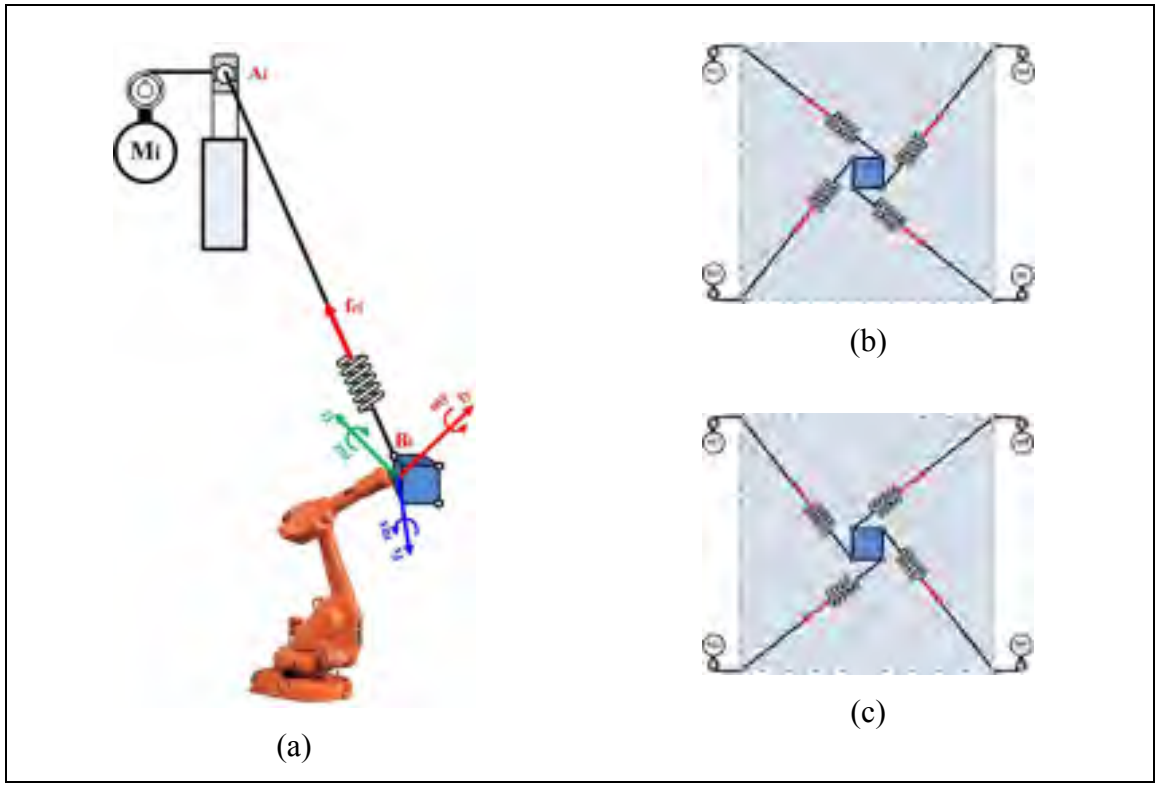

Figure 3.2 (a) Simple schematic of a limb of CabOLS; (b) cable attachments to the mobile platform from above; and (c) cable attachments from below.

3.2.2 Real-time system, software, and hardware environments

Figure 3.3 shows the electronic hardware of CabOLS. For the real-time implementation of the control topology and redundancy resolution algorithm, xPC Target from MathWorks is used. In the xPC Target environment, a real-time target computer, separate from a host computer, runs real-time codes. Simulink Coder and a C/C++ compiler create executable code that constitutes the control implementation. The generated executable code is downloaded from the host computer to the target via a TCP/IP port. A Quanser Q8 data acquisition card sends the control signals to the motors, reads the motors' encoders and the force/torque sensor signals. A Delta force/torque sensor from ATI performs wrench measurement. This sensor can measure forces up to 165 N in the x and y directions, and up to 495 N in the z direction, as well as torques up to 15 Nm. The sampling time selected for the real-time system is 1 ms. A pre-tightening limit-switch (Figure 3.3) is used in each limb to allow the cable to be preloaded with a negligible tension.

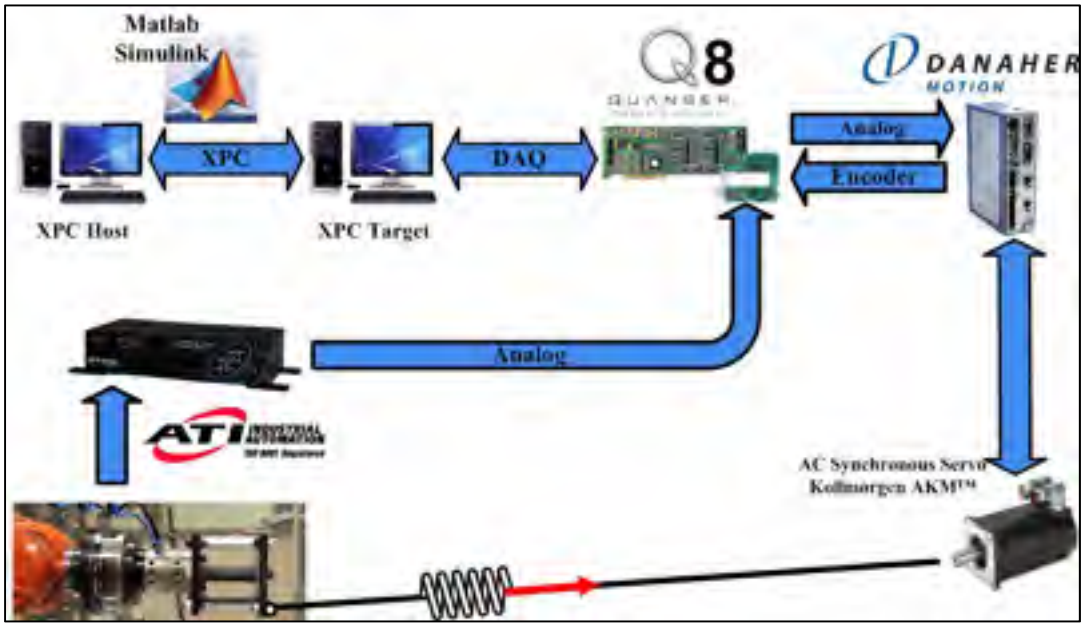

Figure 3.3 Real-time implementation of CabOLS.

3.3 Kinematics and Jacobian analysis

Following the analytical geometric method in (Merlet, 2006), the inverse kinematics of a parallel manipulator can be easily obtained by writing closed-loop vectors for each closed mechanical chain. Each chain consists of one active joint, links, and the mobile platform. Figure 3.4 shows a schematic of each limb of the CDPM. It is supposed that n limbs ($n = 8$ for our design) with an identical kinematic structure are attached to the mobile platform with m DOF ($m = 6$ for our design).

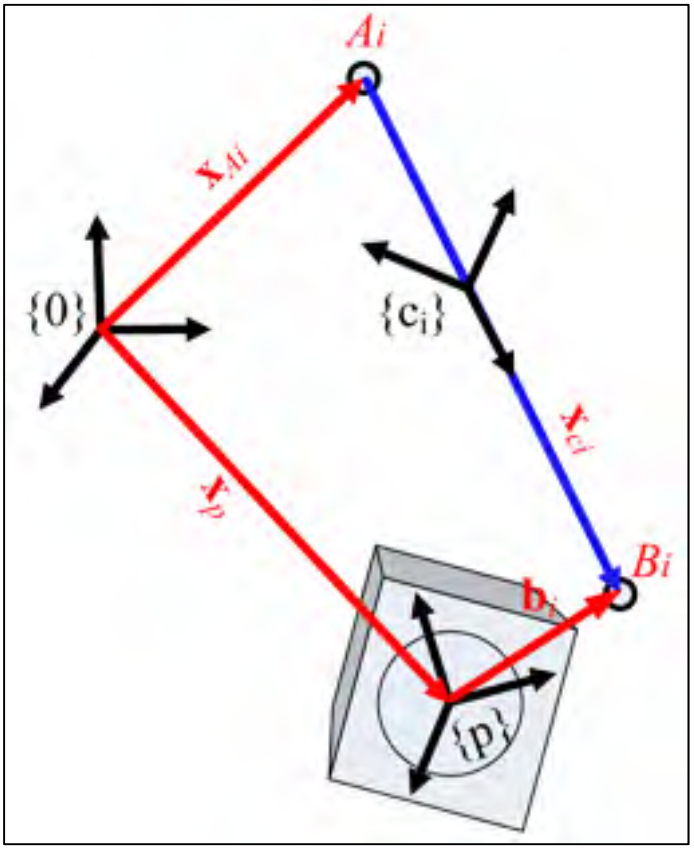

Figure 3.4 Loop closure vectors of each limb in a CDPM.

The kinematic structure of each limb consists of a series of spherical-prismatic-spherical (SPS) joints, where the prismatic joint is used to model the elongation of each link. In such

an SPS configuration, only the prismatic joint is active, while the other spherical joints are passive. In figure 3.4, A_i denotes the fixed base points of the cables, and B_i denotes the points of attachment to the mobile platform. The position and orientation vectors of the mobile platform, represented by the mobile frame $\{p\}$, relative to the base frame $\{0\}$, are defined as $\mathbf{x}_p$ and $\boldsymbol{\varphi}_p$ respectively, where $\boldsymbol{\varphi}_p=[\alpha \quad \beta \quad \gamma]^T$ is any user-defined set of Euler angles. Subsequently, the position and orientation vectors of each cable frame $\{c_i\}$, relative to the base frame $\{0\}$, are defined as $\mathbf{x}_{ci}$ and $\boldsymbol{\varphi}_{ci}$ respectively, where the angle vector of each limb is defined by its set of Euler angles: $\boldsymbol{\varphi}_{ci}=[\alpha_{ci} \ \beta_{ci} \ \gamma_{ci}]$. It is also assumed that the frame $\{c_i\}$ is located at the center of the cable *i*. According to figure 3.4, each closed-loop mechanical chain can be formulated as follows:

$$\mathbf{x}_{ci} + \mathbf{x}_{Ai} = \mathbf{x}_p + {}^0\mathbf{R}_p \mathbf{b}_i , \tag{3.1}$$

where ${}^0\mathbf{R}_p$ is the rotation matrix representing the orientation of the mobile frame $\{p\}$ with respect to the base frame $\{0\}$. This equation allows all the coordinates of the system to be expressed as a function of the generalized coordinates. As explained in detail in (Bedoustani et al., 2011) and (Taghirad, 2013), by choosing the position and orientation of the mobile platform $\mathbf{x} = \begin{bmatrix} \mathbf{x}_p^T & \boldsymbol{\varphi}_p^T \end{bmatrix}^T \in \mathrm{R}^m$ as generalized coordinates, the inverse kinematic equation can be formulated as follows:

$$\mathbf{x}_c = \mathbf{f}(\mathbf{x}), \tag{3.2}$$

where $\mathbf{f}$ is the kinematic equation obtained from the loop closure (3.1), and $\mathbf{x_c} = [\mathbf{x}_{c1} \quad ... \quad \mathbf{x}_{cn}] \in \mathrm{R}^n$ are the position vectors of all the limbs. Let the length of each cable be defined by $l_i = 2\left\|\mathbf{x}_{ci} - \mathbf{x}_{Ai}\right\|$ and use the time derivative of vector (3.1) as well as (3.2),

leads to a relation that expresses the linear velocities of the cable lengths as a function of the linear and angular velocities of the mobile platform:

$$\dot{\mathbf{l}} = \mathbf{J}\begin{bmatrix} \dot{\mathbf{x}}_p \\ \boldsymbol{\omega}_p \end{bmatrix}, \tag{3.3}$$

where $\mathbf{J}$ is a Jacobian matrix, $\dot{\mathbf{l}} = [\dot{l}_1 \quad ... \quad \dot{l}_n] \in \mathrm{R}^n$ is the derivative of the cable lengths, and $\dot{\mathbf{x}}_p$ and $\boldsymbol{\omega}_p$ are the linear and angular velocities of the mobile platform respectively. As is well known, analysis of the Jacobian matrix not only provides the relation between the joint variable velocities $\dot{\mathbf{l}}$ and the mobile platform velocities, but also exposes the transformation needed to find the wrench vector in the Cartesian space $\mathbf{W} \in \mathrm{R}^m$ relative to the forces in the cables $\boldsymbol{\tau} = [\tau_{c1} \quad ... \quad \tau_{cn}]^T \in \mathrm{R}^n$, as follows:

$$\mathbf{W} = \mathbf{J}^T\boldsymbol{\tau}, \tag{3.4}$$

where $\mathbf{J}^T \in \mathrm{R}^{m\times n}$ with $n > m$, such that CDPM has $n-m$ degrees of redundancy.

3.4 Force control strategy used in CabOLS

In order to control the force/torque **w** of CabOLS for a static position $\mathbf{x}_d$, the output of the 6-DOF force/torque sensor is used to close the main loop of the control system. As shown in figure 3.5, the desired force/torque $\mathbf{w}_d$ is tracked thanks to a combination of the outer loop with an inner loop adjusting the tensions $\boldsymbol{\tau}$ in the cables (via the courants $\mathbf{i}_m$ in the motors). The estimation of the tension $\hat{\boldsymbol{\tau}}$ is obtained by multiplying spring-cable stiffness by $\Delta\mathbf{l}$, the portion of the cables rolling around the actuators' pulley ($\mathbf{r\theta}$) added to the initial elongations of the springs combined with the cables ($\mathbf{l}_0 - \mathbf{l}$). According to figure 3.5, the initial elongation of the spring-cable is the difference between the initial length of the spring-cable and the initial length of the limb (i.e. the distance between A_i and B_i). Because of the redundancy in CDPMs, the non-square redundant Jacobian matrix **J** maps the tension in the eight cables to the 6-DOF tool wrench in the Cartesian space.

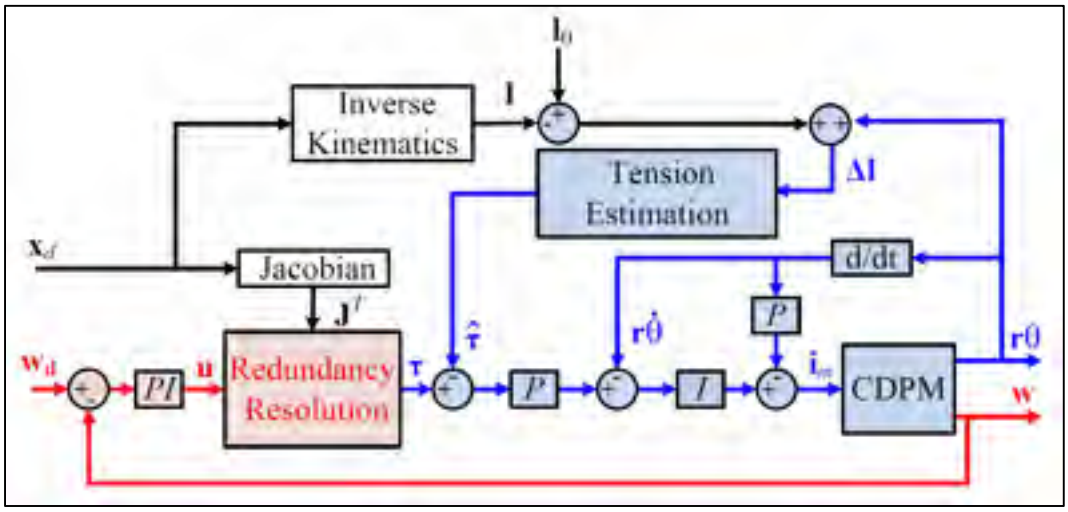

Figure 3.5 Force control topology of CabOLS: the blue lines indicate the inner loops in the joint space, and the red lines designate the outer loop in the Cartesian space.

3.4.1 Real-time implementation of redundancy resolution

Redundancy is a necessity in the CDPM, since each cable can only provide positive forces. Although it is possible to design a CDPM with only one degree of redundancy, in the symmetric design of CabOLS two degrees of redundancy are considered in order to achieve bigger dexterous wrench closure workspace (WCW) (Loloei, Aref et Taghirad, 2009) and bigger wrench feasible workspace (WFW).

Reference (Nakamura, 1991) provides a detailed discussion regarding redundancy resolution of redundant mechanisms based on linear and nonlinear programing approaches. Redundancy resolution is usually formulated as an optimization problem and solved numerically by using iterative algorithm (Nakamura, 1991). In this case, redundancy resolution must converge to a solution within the limits of the sampling time to allow real time implementation. In (Taghirad et Bedoustani, 2011), an efficient and rapid analytic/iterative algorithm is proposed for redundancy resolution which ensures that the number of iterations necessary to find the

solution is always bounded and known. Moreover, after this number of iterations, the algorithm determines whether or not the solution exists. Therefore, it can be used in real-time for the closed-loop control strategy shown in figure 3.5, which will be detailed further in next section. In the analytical/iterative method in (Taghirad et Bedoustani, 2011), redundancy resolution is formulated as the following convex optimization problem:

$$\begin{aligned} &\text{minimize } \|\boldsymbol{\tau}\| \\ &\text{subject to } \begin{cases} \mathbf{W} = \mathbf{J}^T\boldsymbol{\tau} \\ \boldsymbol{\tau} \geq \boldsymbol{\tau}_{min} \end{cases}. \end{aligned} \tag{3.5}$$

By choosing $\boldsymbol{\tau}_{min}$ to be a non-negative constant ($\boldsymbol{\tau}_{min} \geq 0$), the inequality constraints ensures that all the cables are always in tension. On the one hand, the linear equality constraint alone, which has *n-m* more unknown variables than the number of equations, can be solved by using generalized inverse when the rank of the Jacobian matrix is full, as follows (Nakamura, 1991):

$$\boldsymbol{\tau} = (\mathbf{J}^T)^{\dagger}\mathbf{W} + \mathbf{A}\mathbf{y}, \tag{3.6}$$

where the operator $(\square)^{\dagger}$ is the pseudo inverse, such as $\mathbf{J}^T(\mathbf{J}^T)^{\dagger} = \mathbf{I}$, $\mathbf{y} \in \mathrm{R}^n$ is a free variable, and $\mathbf{A}$ is a matrix where columns are composed of all the vectors of a base of the null space of $\mathbf{J}^T$. Thus $\mathbf{J}^T\mathbf{A}\mathbf{y} = \mathbf{0}$. On the other hand, the convex optimization problem (3.5) is solved using the Karush-Kuhn-Tucker (KKT) theorem (Taghirad et Bedoustani, 2011). However, since the objective function is quadratic and both the equality and the inequality constraints are linear, the solution can be simplified. In fact, in the KKT approach, the Lagrangian function is used to combine the objective function and the inequality constraint, but the equality constraint is eliminated at the same time using (3.6):

$$\boldsymbol{\varepsilon}(\mathbf{y},\boldsymbol{\mu}) = \mathbf{f}(\mathbf{y}) + \boldsymbol{\mu}^T \mathbf{r}(\mathbf{y}), \tag{3.7}$$

where $\boldsymbol{\mu} \in \mathrm{R}^n$ is the Lagrangian multiplier vector, $\mathbf{f}(\mathbf{y}) = \left\| (\mathbf{J}^T)^{\dagger}\mathbf{W} + \mathbf{A}\mathbf{y} \right\|^2$ is the quadratic objective function, and $\mathbf{r}(\mathbf{y}) = (\mathbf{J}^T)^{\dagger}\mathbf{W} + \mathbf{A}\mathbf{y} - \boldsymbol{\tau}_{min}$ is the linear inequality constraint. Using the KKT theorem allows a decomposition of the resolution into two parts: i) the stationary point of the Lagrangian with respect to **y** is obtained by differentiating the Lagrangian (3.7) and setting it equal to zero ($\frac{\delta}{\delta \mathbf{y}} \boldsymbol{\varepsilon}(\mathbf{y},\boldsymbol{\mu}) = 0$); and ii) the KKT necessary condition should be satisfied, $\boldsymbol{\mu}^T \mathbf{r}(\mathbf{y}) = 0$, where each Lagrangian multiplier $\mu_i \in \boldsymbol{\mu}$ must be positive or zero::

$$\begin{cases} 2\mathbf{A}^T (\mathbf{J}^T)^{\dagger}\mathbf{W} + 2\,\mathbf{A}^T\mathbf{A}\mathbf{y} - \mathbf{A}^T\boldsymbol{\mu} = \mathbf{0} \\ \boldsymbol{\mu}^T \left(\boldsymbol{\tau}_{min} - (\mathbf{J}^T)^{\dagger}\mathbf{W} - \mathbf{A}\mathbf{y} \right) = \mathbf{0} \end{cases}. \tag{3.8}$$

In this equation, only the second part is nonlinear. For this reason, the search algorithm proposed in (Taghirad et Bedoustani, 2011) takes into account the fact that the optimal solution is obtained when the vector of the Lagrangian multiplier is in a space composed by all the permutations of the two possibilities for each of its members: 1) the Lagrangian multiplier μ_i is zero when the corresponding constraint is at its limit, $\tau_i = \tau_{min}$; and ii) the Lagrangian multiplier μ_i is greater than zero when the corresponding constraint is inside its limit, $\tau_i > \tau_{min}$. For each possibility, equation (3.8) becomes linear and can be solved rapidly enough to implement the algorithm in real-time. Considering that a feasible suboptimal solution can be found before all the permutations have been tried, the maximum number of iterations is given by 2^n-1. For CabOLS, the maximum number of iterations is 255 (2^8-1).

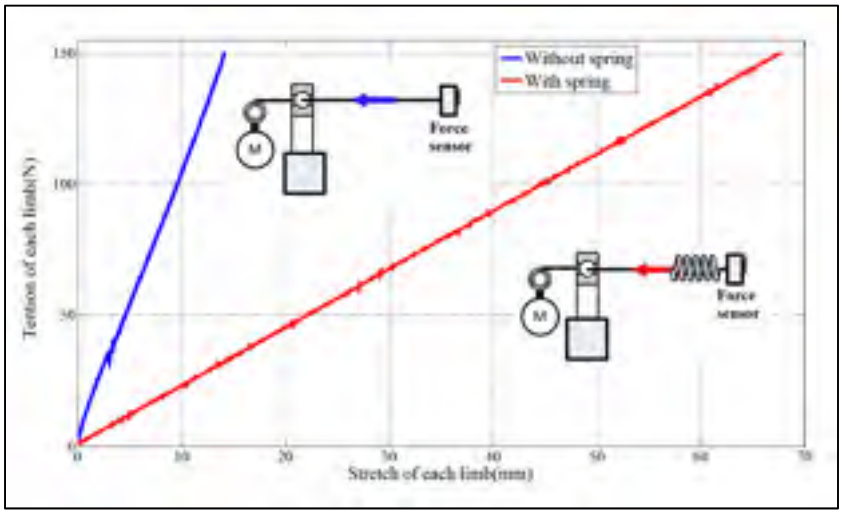

Figure 3.6 Force Elongation ratio in an individual limb of CabOLS with spring and without spring.

3.4.2 Control topology

Figure 3.5 shows the control topology of CabOLS. Here, it is assumed that the pose of the end-effector ($\mathbf{x}_d$) is known, since in the validation setup, the load simulator is attached to an ABB robot that provides the end-effector pose. However, as discussed in the introduction, in order to use CabOLS when it is connected to a device without position sensor or to have more accurate measurement, it is possible to used an external sensor. Moreover, the limit switches described in section 3.2.2 are used to ensure that the initial lengths of the springs are negligible. Thus, the disturbance ($\mathbf{l}_0 - \mathbf{l}$) introduced in figure 3.5 may be eliminated.

To obtain accurate force/torque control on the target object, two levels of control loops are considered: i) the outer loop controls the 6-DOF force/torque on the target object; and ii) the inner loops control the positive tension in the cables. Therefore, in the force/torque control of CabOLS, not only must the force/torque on the target be measured, but the tension in each cable as well.

As illustrated in figure 3.3, the 6-DOF force sensor is fixed on the target object to be used in the outer feedback loop. Also, the tension in each limb is estimated from its elongation which is the combination of the elongation of a precision spring and the cable. To be effective, this tension estimation requires that the stiffness of the spring and cable combination be identified. To achieve this, a motor and the force sensor are used in a closed-loop force control topology. The tension on the limb is increased slowly from zero to 150 N, and the elongation is measured with the motor's encoder. The stiffness of the limbs is thus measured to be ke ≈ 2.20 N/mm. Without springs, the stiffness is much greater, at ke ≈ 10.72 N/mm (Figure 3.6).

In the next subsection, it will be shown that the friction and backlash of the gearbox combined with the cable stiffness cause inaccurate force control, as well as poor estimation of the cable forces. To address this problem, the springs are used, and the tension/elongation ratio is approximated by the following linear function:

$$\hat{\boldsymbol{\tau}} \approx k_e \Delta \mathbf{l} . \tag{3.9}$$

3.4.3 Inner loops in the joint space

Figure 3.7 illustrates the inner loops for each individual limb of CabOLS in the joint space. The inner loops are composed of the force feedback and one additional inner PI velocity feedback, which is widely used in the decentralized position and velocity control of robotic manipulators. The inner loops control the linear velocity of the cables entering into the actuators in order to provide the required tension in the limb. The inner velocity feedback combined with the use of the spring improves the overall tension control in the limb in the

presence of nonlinear friction and backlash. The control signal for the inner loops in the joint space can be formulated as follows:

$$\mathbf{i_m} = -\mathbf{k}_{p1}\frac{\mathbf{d}}{\mathbf{dt}}\Delta\mathbf{l} + \mathbf{k}_I\int_0^t\left(\mathbf{k}_{P2}(\boldsymbol{\tau}-\hat{\boldsymbol{\tau}}) - \frac{\mathbf{d}}{\mathbf{dt}}\Delta\mathbf{l}\right)\mathbf{dt}, \tag{3.10}$$

where $\mathbf{k}_{P1} \in \mathrm{R}^n$ is the proportional gain in the cable force feedback, $\mathbf{k}_{P2} \in \mathrm{R}^n$ and $\mathbf{k}_I \in \mathrm{R}^n$ are the proportional and integral gain of the inner velocity feedback respectively, $\mathbf{i_m} \in \mathrm{R}^n$ is the current of the motors, and $\Delta\mathbf{l} \in \mathrm{R}^n$ is the elongation of the springs combined with the cables.

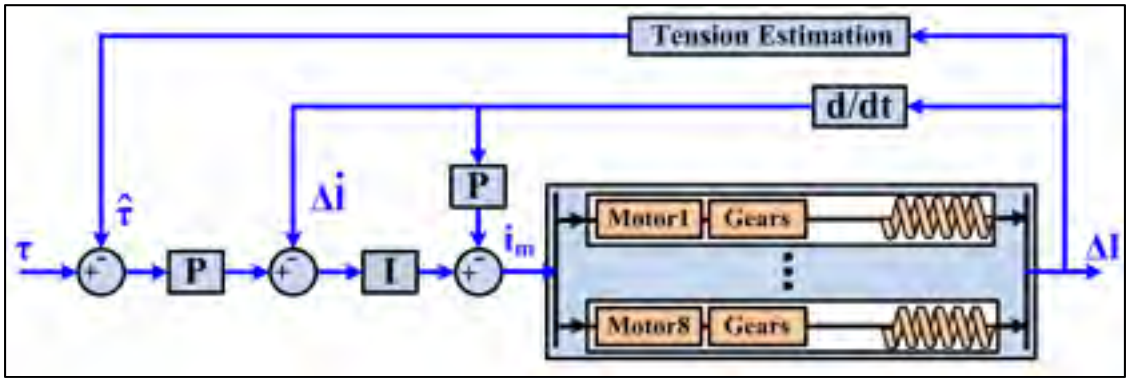

Figure 3.7 Inner loops of the CabOLS using position and velocity feedback.

To determine the gains of the controller in the inner loops, the linear model of each limb is first identified. As explained above, each limb includes a motor, a gearbox, a pulley, a cable, and a spring. Although the combination of backlash and friction in each limb is nonlinear, the low stiffness of the spring reduces the nonlinearity effects of limb actuation. For the identification of each limb, the transfer function of each motors and gears is first identified. For this purpose, the spring and cable are removed, and it is assumed that the input of the system is the input of the motor's driver (see figure 3.3), which it is proportional to the

motor's current, i_{mi} . It is also assumed that the output of the system is the radius of the pulley multiply by the actuator angle, $r\theta_i$. The experimental input-output data were obtained by considering a 0.5-ampere step as input, and the output, $r\theta_i$, was calculated using the motor's encoder measurement. The identification input-output data were used in combination with the Matlab identification toolbox to obtain the linear model, as follows:

$$G_i = \frac{r\theta_i}{i_{mi}} = \frac{k_i}{s(1+T_{pi}s)}. \tag{3.11}$$

The gain of the identified model k_i and the identified time constant T_{pi} are given in table 3.1. Then, the transfer function of each limb, including motor, gearbox, cable, and spring can be formulated as:

$$T_i = \frac{\hat{\tau}_i}{i_{mi}} = \frac{k_e k_i}{s(1+T_{pi}s)}. \tag{3.12}$$

In this linear modeling of the CDPM limbs, neither the spring disturbance force, nor the feedback of the nonlinear friction, nor the nonlinear backlash effect were taken into consideration. The step response of the model identified in (3.12), fits 96% to the identification data. While it was not the intention in this study to focus on the sensitivity of nonlinear actuator dynamics, it is clear, according to the results obtained from a practical test, that the effect of its nonlinearities can be reduced when the stiffness coefficient in the limb ke is decreased.

Table 3.1 Identification parameters of each limb in CabOLS

*i*th limb	k_i	T_{pi}
1	853	0.3564
2	2617	0.3146
3	1125	0.3497
4	2079	0.5640
5	1663	0.4660
6	1726	0.4494
7	2621	0.2499
8	1197	0.4180

Tuning the gains of the controller is based on the pole placement method. Therefore, the identified model for the limbs is used in the formulation of the controller closed-loop system. Figure 3.7 shows the control topology of the inner-loops system for an individual limb. From the block diagram of the inner loop control topology (Figure 3.7), the model and transfer function of the closed-loop system for the *i*th limb from desired input tension τ_{di} to the output estimated tension $\hat{\tau}_i$ could be formulated as:

$$T_{li} = \frac{\hat{\tau}_i}{\tau_{di}} = \frac{k_i k_e k_{Ii} k_{P2i}}{T_{pi} s^3 + (1 + k_i k_{P1i}) s^2 + k_i k_{Ii} s + k_i k_e k_{Ii} k_{P2i}}, \tag{3.13}$$

where the controller gains k_{Ii}, k_{P1i}, and k_{P2i} for each limb can be tuned in order to place the closed-loop poles for all limbs as follows:

$$(s - P_1)(s - P_2)(s - P_3) = s^3 + a's^2 + b's + c', \tag{3.14}$$

where P_1, P_2, and P_3 are the poles of the inner closed-loop system, and a', b' and c' are the coefficients of the desired characteristic polynomial. With this formulation the gains of inner-loops obtained by the pole placement are the following:

$$k_{Ii} = \frac{b' T_{Pi}}{k_i},\ k_{P1i} = \frac{a' T_{pi} - 1}{k_i},\ \text{and}\ k_{P2i} = \frac{c'}{k_e b'}. \tag{3.15}$$

In this formulation, the gains of the controller depend on the desired poles. Moreover, the gains k_{Ii} and k_{p1i} depend on the parameters of the identified model (k_i and T_{pi}), and the gain k_{p2i} depends on the elongation ratio k_e, which is assumed identical for all limbs.

Figure 3.8 shows the step response of the inner loops in which the gains are tuned, in order to locate all three poles of the closed-loop system at $P_1 = P_2 = P_3 = -10$. The test is repeated in two cases: i) with using an extension spring in the limb, in which, the elongation ratio $k_e = 2.20$ and related gains are obtained from (15); and ii) without using a spring in the limb, in which $k_e = 10.72$ and the related gains are obtained to locate the poles at the same places. Moreover, in this test the tension in the cable is measured with the force sensor, and compared with the response of the model (13) as well as the estimated tension obtained by the cable elongation combined with $\hat{\tau}_i \approx k_e \Delta l_i$. As shown in figure 3.8, when the extension spring is used, both the measured tension τ_i and the estimated tension $\hat{\tau}_i$ are fitted to the simulated model. However, when the spring is removed, the high stiffness of the cable in the presence of the motor's friction and backlash cause weak and unacceptable performance. In other words, this experimental test demonstrates the performance of the proposed simple strategy, in which a linear controller is combined with the use of springs.

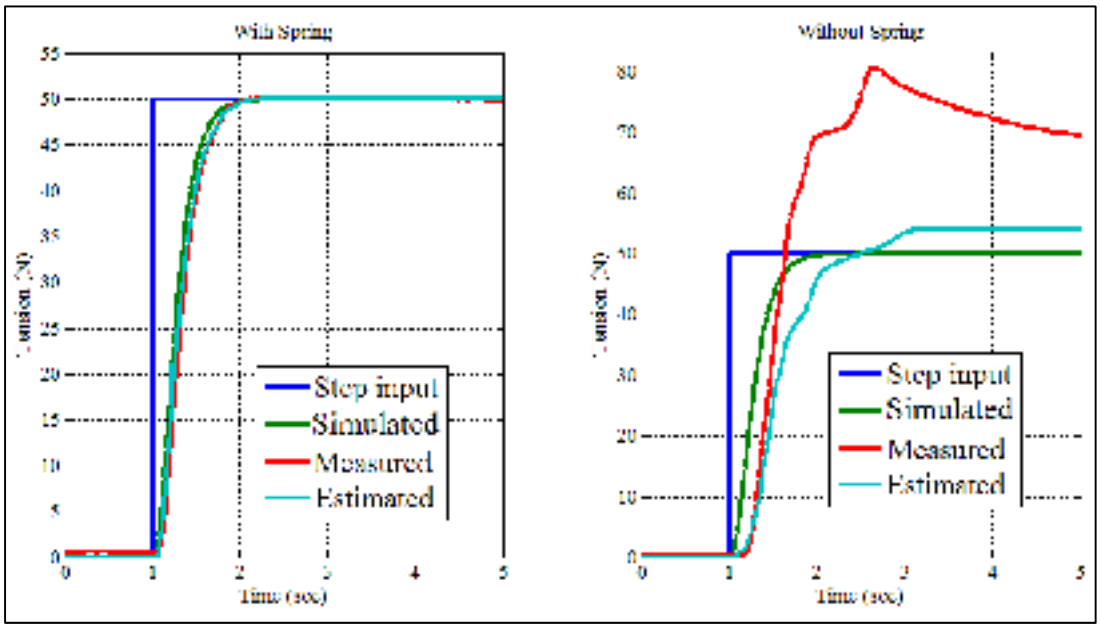

Figure 3.8 Step response of inner loops in which the gains are tuned to place the poles at *P1 = P2 = P3 = −10*. First, the spring is used in the limb (*ke = 2.20*), and then the spring is removed (*ke = 10.72*). The green line shows the simulated response of the ideal transfer function $10^3/(s+10)^3$.

3.4.4 Outer loop in the Cartesian space

As illustrated in figure 3.5, the outer loop of the control topology is in Cartesian space. This loop controls the 6-DOF force/torque **W** in the mobile platform coordinates or any virtual point relating to it. The tensions required in the inner loops of the control topology are obtained with the redundancy resolution algorithm, which is formulated as:

$$\boldsymbol{\tau}_d = \mathbf{RR}(\mathbf{u}) \tag{3.16}$$

where **u** is the proportional-integral control given by:

$$\mathbf{k}_{Po}(\mathbf{W_d}(t) - \mathbf{W}(t)) + \mathbf{k}_{Io}\int_0^t \mathbf{W_d}(\tau) - \mathbf{W}(\tau)d\tau \tag{3.17}$$

$\mathbf{k}_{Po} \in \mathrm{R}^m$ and $\mathbf{k}_{Io} \in \mathrm{R}^m$ are the proportional and integral gains of the outer loop, and $\mathbf{RR}(\cdot)$ is the redundancy resolution algorithm.

In order to formulate the dynamics of the complete closed loop system, the inner loops can be rewritten in the Laplace domain as:

$$\hat{\boldsymbol{\tau}}(s) = \mathrm{diag}\left(T_{I1}(s),...,T_{I\mathrm{n}}(s)\right)\boldsymbol{\tau}_d(s), \tag{3.18}$$

where T_{Ii} is given by (3.13). If the Jacobian matrix is assumed constant during wrench stabilization, the redundancy resolution (3.16), characterized by (3.6), can be expressed in the Laplace domain as:

$$\boldsymbol{\tau}_d(s) = (\mathbf{J}^T)^{\dagger}\mathbf{u}(s) + \mathbf{A}\mathbf{y}(s). \tag{3.19}$$

Thanks to this assumption, the combination of (3.4), (3.18), and (3.19) yields

$$\mathbf{W}(s) = \mathbf{J}^T \mathrm{diag}\left(T_{I1}(s),...,T_{I\mathrm{n}}(s)\right)\left((\mathbf{J}^T)^{\dagger}\mathbf{u}(s) + \mathbf{A}\mathbf{y}(s)\right). \tag{3.20}$$

If the Jacobian was not constant, it would be impossible to obtain (3.20). In fact, in that case, the linearity property of Laplace transform could not be applied and the result would be a Laplace transform of a product that cannot be separated.

Now, it is necessary to assume that $T_{I1}(s) = ... = T_{I\mathrm{n}}(s)$. Then, even though the identified parameters for each limb k_i and T_{pi} are different, the controller gains k_{P1i}, k_{P2i}, and k_{Ii} of the inner loops can be tuned for each limb, in order to ensure that this assumption is confirmed. Then, this assumption is combined with properties $\mathbf{J}^T(\mathbf{J}^T)^{\dagger} = \mathbf{I}$ and $\mathbf{J}^T\mathbf{A} = \mathbf{0}$ to rewrite (3.20) as:

$$\mathbf{W}(s) = T_{Ii}(s)\mathbf{J}^T\left((\mathbf{J}^T)^{\dagger}\mathbf{u}(s) + \mathbf{A}\mathbf{y}(s)\right) = T_{Ii}(s)\mathbf{u}(s). \tag{3.21}$$

Using (3.17) transformed in the Laplace domain,

$$\mathbf{W}(s) = T_{I1}(s)\left(\mathbf{K}_{po} + \mathbf{K}_{Io}\frac{1}{s}\right)\left(\mathbf{W}_d(s) - \mathbf{W}(s)\right). \tag{3.22}$$

Equation (3.22) demonstrates that, although the redundancy resolution algorithm itself is nonlinear, the overall model of the CDPM with inner loops and the redundancy resolution algorithm is linear. This can be explained as follows: Since the Jacobian is assumed constant, the redundancy resolution maps the tension from the Cartesian space to the joint space, and the inverse mapping is achieved by linear Jacobian transformation.

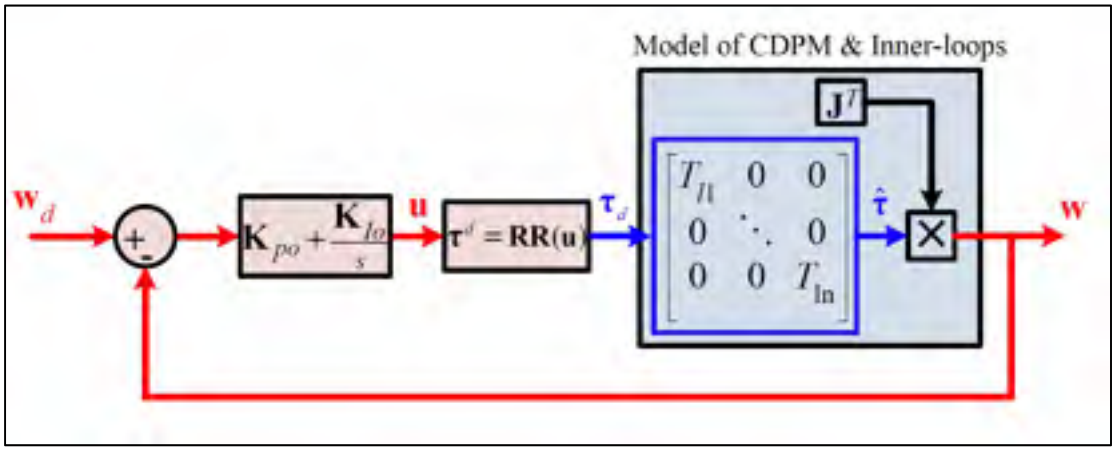

Figure 3.9 Main loop of CabOLS.

According to (3.22), figure 3.9 shows the equivalent block diagram of outer-loop, which is completely linear. Solving this block diagram, the closed-loop transfer function for the overall system in Cartesian space is obtained as (3.23), in which $\mathbf{I} \in \mathrm{R}^m$ is the identity matrix, and $\mathbf{k}_{Io} = k_{Io}\mathbf{I}$ and $\mathbf{k}_{Po} = k_{Po}\mathbf{I}$ are the gains of the outer loop controller. With this formulation, the controller gains of the inner loops for each limb (k_{Ii}, k_{P1i}, and k_{P2i}) and the outer loop (k_{Io} and k_{Po}) can be obtained at the same time considering the desired zero Z, and the desired poles P_1, P_2, P_3, and P_4, such that:

$$(s-P_1)(s-P_2)(s-P_3)(s-P_4) \equiv s^4+as^3+bs^2+cs+d\,, \tag{3.23}$$

where a, b, c, and d are the coefficients of the desired characteristic equation. Therefore, by imposing the same zero and the equality of the denominators of (3.23) identically for all limbs, the gains of the inner loops and the outer loop are formulated as follows:

$$k_{Ii}=\frac{bT_{Pi}}{k_i}, k_{P1i}=\frac{aT_{Pi}-1}{k_i}, k_{P2i}=\frac{cZ-d}{k_e bZ}, i=1...n\,, \tag{3.24}$$

$$\mathbf{k}_{Io}=\frac{dZ}{cZ-d}\mathbf{I}, \mathbf{k}_{Po}=\frac{d}{cZ-d}\mathbf{I}. \tag{3.25}$$

In this formulation, all the gains depend on the location of the poles and the zero, which are identical for all the limbs.

$$T=\frac{k_i k_e k_{Ii} k_{P2i}(k_{po}s+k_{Io})}{T_{pi}s^4+(1+k_i k_{P1i})s^3+k_i k_{Ii}s^2+(k_i k_e k_{Ii} k_{P2i}+k_i k_e k_{Ii} k_{P2i} k_{po})s+k_i k_e k_{Ii} k_{P2i} k_{Io}}\mathbf{I} \tag{3.26}$$

Moreover, based on the proposed control topology, the gains k_{P1i} and k_{Ii} also depend on the parameters T_{pi} and k_i, which are identified for each limb separately. The gain k_{P2i} also depends on the limb elongation ratio k_e, which is assumed identical for all the limbs. Now, by replacing the gains given by (3.24) into (3.13), the transfer function of inner loops can be rewritten as:

$$T_{li}=\frac{\frac{cZ-d}{Z}}{s^3+as^2+bs+\frac{cZ-d}{Z}}. \tag{3.27}$$

Equation (3.27) demonstrates that, as a result of choosing the same zero and poles for each element of the Cartesian space characteristic equation (3.23), all the transfer functions of the

inner loops are identical. This confirms our assumption concerning the identical inner loop transfer function.

Remark: *The assumption concerning the constant Jacobian can be confirmed only when the position of the platform is constant. This assumption implies that the motion caused by the wrench applied to the target must be sufficiently small to consider the Jacobian variations negligible. The target must thus be attached to a sufficiently rigid mechanism such as spine segment or rigid robot.*

To allow arbitrary motion of the platform during wrench tracking, the singular perturbation approach could be used. It would formally extend the proposed controller for time varying position trajectories. However, in that case, it should be assumed that the other loop is much slower than the inner loop. This assumption could increase considerably the time response of the other loop since the inner loop could not be very fast because of the flexibility caused by the additional springs. Consequently, the performance of the system would be reduced. For load simulator at static position, the proposed approach is thus more appropriate.

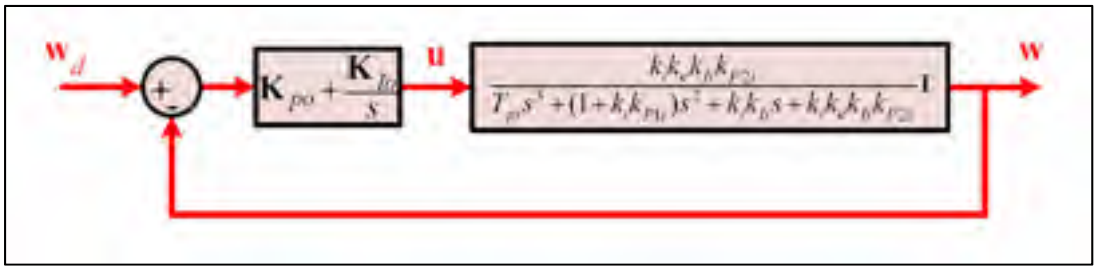

Figure 3.10 Linear model of overall CDPM with inner-loops and the redundancy resolution algorithm which is used in outer-loop.

3.5 Real-time implementation and results

To evaluate the performance of CabOLS in force/torque simulator applications, a feasible 6-DOF trajectory of wrench vector $\mathbf{W} = [f_x, f_y, f_z, m_x, m_y, m_z]$ was considered. However, studying

feasible conditions of wrench vectors in general was not a concern in this paper. For the validation, CabOLS applies the chosen wrench on the end-effector of the ABB robot, which keeps the position of the mobile platform at the desired fixed position $\mathbf{x}_d$ = [0, 1234.615, 792.718, 0, 0, 0] where the first 3 terms are x-y-z position in millimeter and the last 3 terms are the 3 angles associated to x-y-z Euler convention in degrees. The real-time codes are generated by the host computer and transferred to the Target computer by a TCP/IP link (see figure 3.3). To calculate the gains, the poles of the closed-loop system are located at $P_1 = -10$, $P_2 = -90$, $P_3 = -40$, and $P_4 = -40$, while the zero is chosen as $Z = -40$ to eliminate one of the poles. Subsequently, the related gains in the inner loops for each limb, and also the related gain in the outer loop, are obtained using (25) and (26). Table II shows the related gains in each limb (inner loops) and in the Cartesian space (outer loop). The linearity of the system is valid as long as the current of the motors is not saturated. The maximum current of the motors is 3.82 A. However, to provide protection from overloads, this current is limited to 3 A.

For the redundancy resolution algorithm, the minimum tension in each limb is chosen as 1 N ($\boldsymbol{\tau}_{min} = \begin{bmatrix} 1 & \cdots & 1 \end{bmatrix}^T$). Figure 3.11 shows the feasible desired wrench vector tracked by the CabOLS in the Cartesian space. This figure demonstrates how well CabOLS performs in tracking the desired wrench vector. Moreover, the rise time (10% to 90%) relative to the input step is less than 0.2 seconds. Therefore, CabOLS could easily track a 1 second step reference (for example between 7.5 and 8.5 sec). Figure 3.12 also shows the tracking of the reference tension in each limb, which is generated with the redundancy resolution algorithm. Figure 3.13 shows the error signal in tracking the desired tension in each limb, while Figure 3.14 shows the control signal **u** in the Cartesian space. This signal is the input of the redundancy resolution algorithm. Figure 3.15 shows the projected signal in the joint space, which is the result of the redundancy resolution algorithm. Finally, Figure 3.16 shows the current of each motor, which is less than overload protection current (3 A).

Table 3.2 Gains of the inner loops and the outer loop

Gains in the joint space				Gains in the Cartesian space		
Limb	k_{Ii}	k_{P1i}	k_{P2i}		k_{Io}	k_{Po}
1	4.3871	0.0740	9.0177			
2	1.0212	0.0213	9.0177	f_x	360/49	9/49
3	3.2639	0.0551	9.0177	f_y	360/49	9/49
4	2.8484	0.0483	9.0177	f_z	360/49	9/49
5	2.9423	0.0498	9.0177	m_x	360/49	9/49
6	2.7339	0.0463	9.0177	m_y	360/49	9/49
7	1.0011	0.0168	9.0177	m_z	360/49	9/49
8	3.6667	0.0620	9.0177			

3.6 Conclusion

This work presented a new application of the cable-driven parallel manipulator (CDPM) as a 6-DOF loading simulator. CabOLS is designed to apply a 6-DOF force/torque on a target object for a static but arbitrary position. The simplicity of the mechanical components, actuators, and control topology, and the cost efficiency of this device are considered its most important advantages. The innovative and cost-effective method of controlling cable tension using a precision spring has provided two valuable advantages: i) compensation for the nonlinear effect of backlash, which makes a simple control topology possible; and ii) estimation of the tension in the cable, instead of using an expensive force sensor in the limbs. For the control topology, two levels of control, one in the Cartesian space and the other in the joint space, are considered, in order to achieve accurate force control on the target object. The real-time rapid redundancy resolution algorithm was analyzed and used in closed-loop system. The pole placement method was applied to formulate the gains of the controller in the Cartesian space and the joint space at the same time. In addition, it is shown that, even

though the redundancy resolution algorithm is nonlinear, the combination of the redundancy resolution algorithm and the model of the CDPM can be obtained as a linear system. Finally, the authors presented an experimental 6- DOF force/torque trajectory, in order to demonstrate the performance of the innovative CDPM and proposed controller, and of the real-time redundancy resolution. In future works, we will use CabOLS combined with a laser tracker to estimate an experimental model of the stiffness of an industrial robot. In that case, a list of random constant positions and orientations in the workspace of the robot will be used to estimate the stiffness almost everywhere.

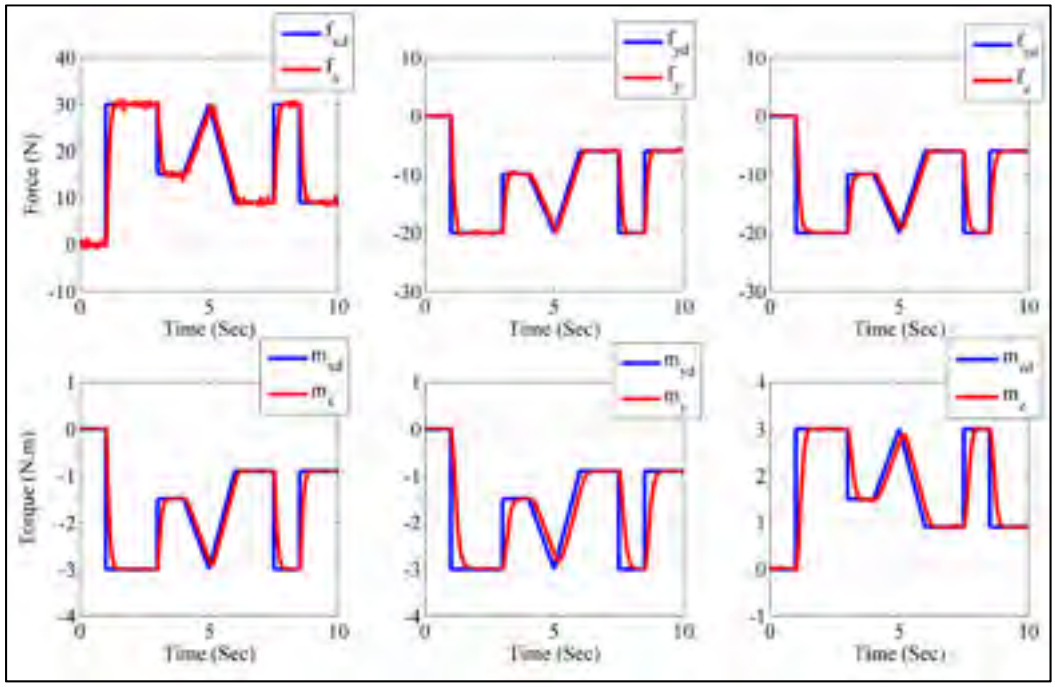

Figure 3.11 Tracking the desired 6-DOF force/torque in the Cartesian space.

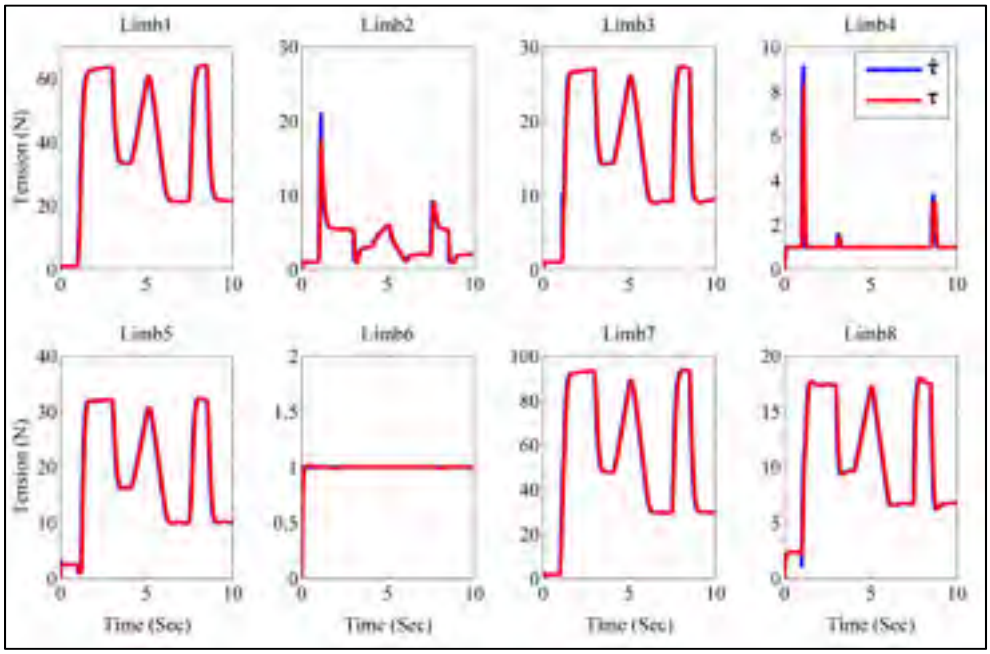

Figure 3.12 Tracking the desired tension in the joint space, which is generated with the redundancy resolution algorithm.

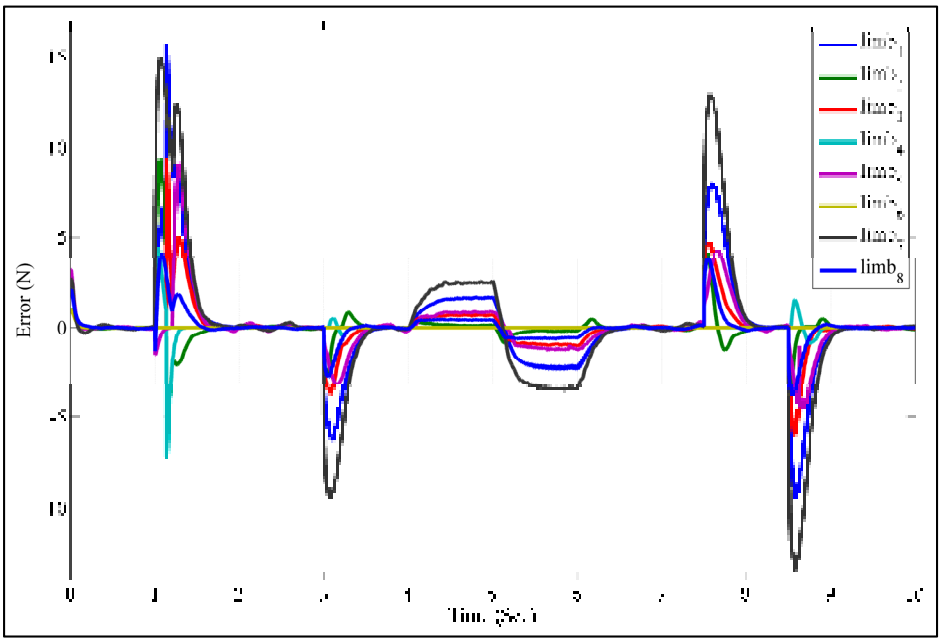

Figure 3.13 Tension error for each limb in the joint space.

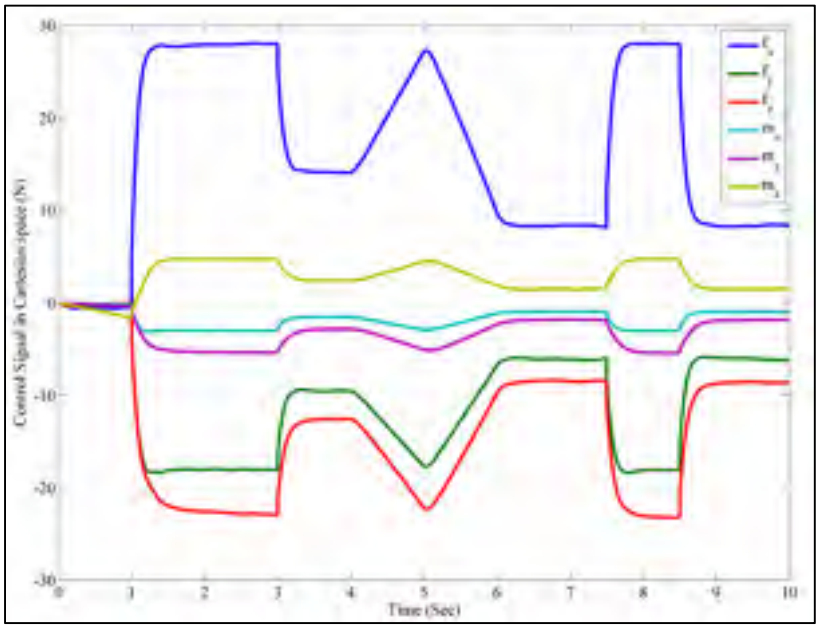

Figure 3.14 Control signal **u**, the input of the redundancy resolution algorithm, in the Cartesian space.

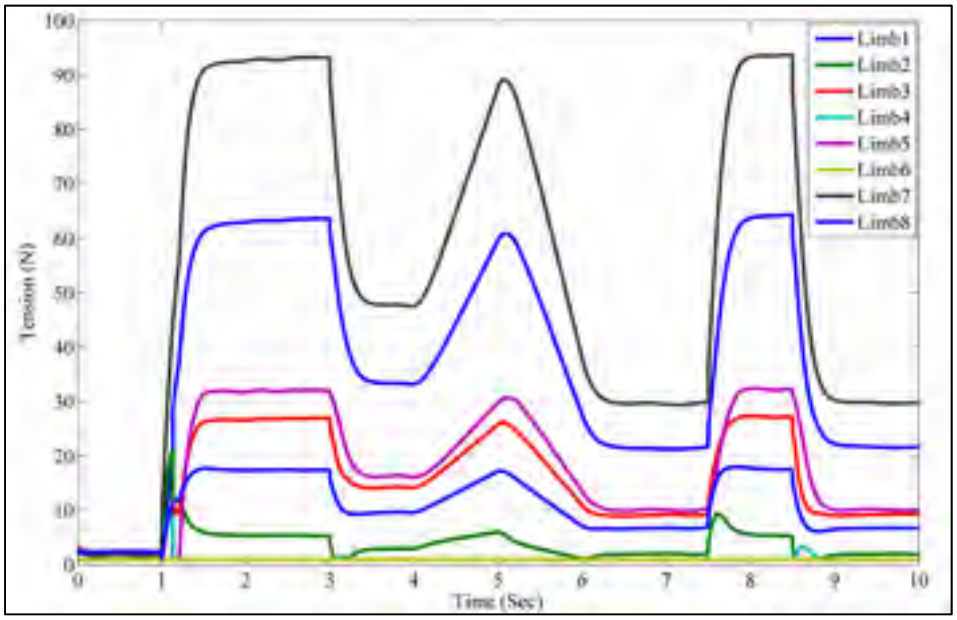

Figure 3.15 The positive tension generated with the redundancy resolution algorithm for each limb.

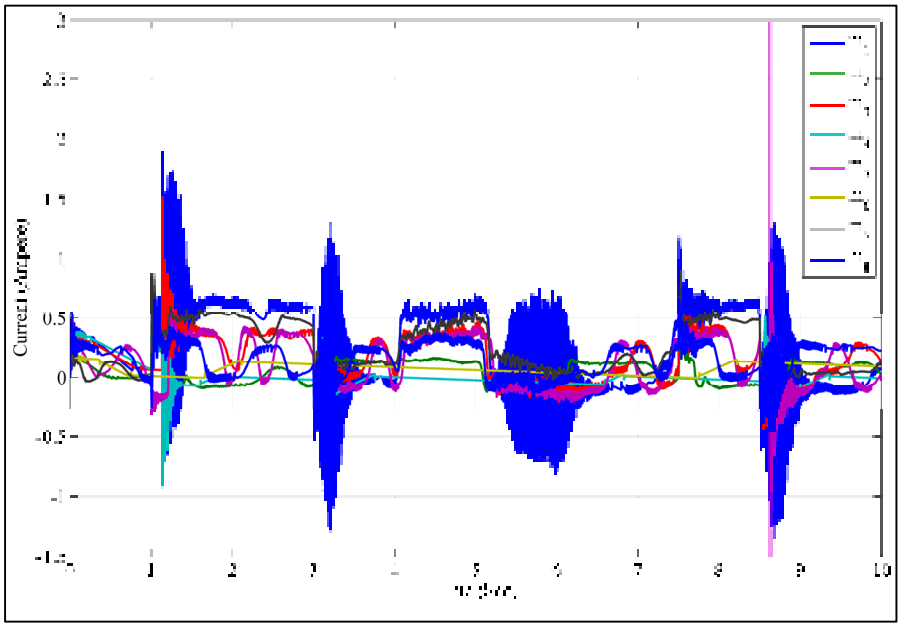

Figure 3.16 Motor current in each limb.

CHAPTER 4

THE APPLICATION OF CABLE-DRIVEN LOADING SIMULATOR IN STIFFNESS ANALYSIS OF ROBOTIC MANIPULATORS

Yousef B. Bedoustani, Pascal Bigras and Ilian A. Bonev
Department of Automated Manufacturing Engineering, École de technologie supérieure,
1100 Rue Notre-Dame Ouest, Montréal, Québec H3C 1K3

This paper has been submitted as an article in
Journal of Robotics and Computer-Integrated Manufacturing.

Abstract

The experimental stiffness analysis of robotic manipulators requires an automated omnidirectional load simulator and accurate deflection measurements, as well as proper modeling of the joints' stiffness. This paper demonstrates the application of a cable-driven omnidirectional loading simulator (CabOLS) for stiffness analysis of industrial robots. In this study the CabOLS is designed and controlled to apply desired 6-degree-of-freedom (DOF) wrench vectors to the end-effector of an industrial robot in different joint configurations and different end-effector poses along a desired trajectory. Furthermore, both a nonlinear and linear modeling of the joint stiffness are formulated. Nonlinear modeling is based on the nonlinearity of the Harmonic Drive used in each joint of recent industrial robots. A dynamic load simulator makes it possible to take advantage of nonlinear as well as linear modeling in identifying joint stiffness. Our work shows the performance of an automated loading simulator in an experimental stiffness analysis and the proposed experimental setup also makes it possible to validate the identified stiffness parameters.

4.1 Introduction

The flexibility of manipulator joints and transmission systems including motor, Harmonic Drive and bearing is producing significant errors in tool positioning. Moreover, robot manufacturers do not present any information about the flexibility of their robots to compensate for these errors. Furthermore, the flexibility of joints could change during the long term operation of the robot. Consequently, to improve and also maintain the accuracy of industrial manipulators, experimental stiffness analysis is essential. Two important parameters are among the elements which impact on the accuracy of experimental stiffness analysis: i) A sufficiently accurate modeling of the stiffness, i.e. linear and nonlinear modeling. ii) An automated experimental setup to apply proper wrench on the robot's end-effector, measure the deflection, and collect the data for stiffness identification.

The classical linear stiffness model introduced in several robotics textbooks (for example (Tsai, 1999)) is valid for the unloaded manipulator. The complete model, based on conservative congruence transformation (CCT), is discussed in (Chen, 2003) and (Chen et Kao, 2000). Alici and Shirinzadeh (Alici et Shirinzadeh, 2005) have devised a method for identifying the stiffness values of the first three joints of a six-revolute robot arm by measuring only the translational displacements of its end-effector. In these studies the links of the robot are assumed to be rigid, the damping is neglected and the stiffness of the joints is represented by linear torsional springs. In other words, it is usually assumed that joint stiffness is in the axial direction of the actuation torque, and it is lumped into a single constant linear stiffness value for each joint.

A further assumption is that the flexibility of industrial robots is principally located in their joints. However, the flexibility of the tool-changer, force/torque sensor, and robot base can also generate poor measurements during the identification process (Dumas et al., 2011). In addition, the robustness of the joint stiffness identification, with regard to measurement noise, is important (Dumas et al., 2011). Moreover, several commercial robots use flexible Harmonic Drives as actuator gear trains. This being the case, it is known that an appropriate

model must include nonlinear effects. Nonlinear models of the Harmonic Drive have been studied in several works for example (Kircanski et Goldenberg, 1997; Seyfferth et Angeles, 1995; Seyfferth, Maghzal et Angeles, 1995). In (Kim, Seki et Iwasaki, 2014) a parametric nonlinear modeling is used for two joints of a robot, for control purposes. In this work, based on the nonlinearity of the Harmonic Drive, a nonlinear model for the robot is considered.
Experimental stiffness analysis needs a setup that includes a load simulator and a device such as a laser tracker for accurate deflection measurements. The experimental setup could be a mass connected to the end-effector (Dumas et al., 2010; Dumas et al., 2012; Olabi et al., 2012b) or a cable-pulley system with a deadweight in order to exert maximum static forces (Alici et Shirinzadeh, 2005; Shin et al., 2013a). In (Jianjun, Hui et Fuhlbrigge, 2009) the external load is applied by an air cylinder through a pulley-relayed string. Its amplitude can be adjusted by changing the air pressure and the direction of the load can be modified by the position of the pulley. In this manual experimental setup no torque is applied at the force action point due to the use of a steel cable and its connection point to the robot's end-effector.

All the above-mentioned experimental setups apply maximum static force in one direction only. The process is always manual and time-consuming, especially when compliance identification in Cartesian space is required (Slavković et al., 2013). Moreover, depending on the configuration of the robot in its workspace, the described mechanisms fail to ensure that all robot joints be adequately stressed during the test (Dumas et al., 2010; Dumas et al., 2012). Furthermore, the stiffness of the last joints is most sensitive to errors and making it more difficult to identify than that of the counter joints (Dumas et al., 2012). Moreover, it is important to make the process automatic to be able to collect the data for identification in a short period of time.

This paper introduces the application of a cable-driven omnidirectional loading simulator (CabOLS) as a tool for automatically identifying the stiffness of a robot (Figure 4.1). This CabOLS is designed and controlled to simulate the trajectory of a dynamic wrench on fixed or moving objects like the end-effector of a robot. Thus, it could be used to simulate the

robot's external load and identify the stiffness of the robot joints. The proposed CabOLS aims to evaluate joint stiffness values, considering both translational and rotational displacements of the robot for a given applied force and torque. In this work also, nonlinear modeling of joint stiffness is introduced. The model is based on the nonlinearity of the Harmonic Drive and the rationale for this choice is that contemporary small and medium-size robots use Harmonic Drives. This general nonlinear modeling also can be used for other robots by eliminating nonlinear parameters. In this paper the CabOLS is used in the stiffness analysis of a medium-size industrial ABB robot (IRB 1600).

The rest of the paper is organized as follows: In the second section, we explain the mechanical architecture and hardware of the CabOLS following which its control topology is discussed. In the third section, the linear and nonlinear modeling of the joint stiffness is introduced. Finally, the last section demonstrates the performance of the CabOLS in identifying the joint stiffness of the ABB robot.

(a) (b)

Figure 4.1 (a) The CabOLS fixed to an ABB IRB 1600 industrial robot to simulate omnidirectional load and (b) a close-up of the robot's end-effector.

4.2 System architecture

This section provides an overview of the proposed system, including the CabOLS' mechanical structure, its mechanical components and real-time controller. This section also explains the flowchart of the CabOLS' software.

4.2.1 Mechanism and geometry description

The essential mechanical components of cable-driven parallel manipulators (CDPMs) are a mobile platform and limbs. Each limb of a CDPM includes a cable and a cable wrench mechanism, and every cable connects a fixed point on the base structure to the mobile platform. Figure 4.2(a) shows a simple schematic of a limb of the CabOLS: One end of each cable is attached to the mobile platform at point Bi, and the other end is fixed at point Ai, where the cable is wound onto the wrench mechanism, which is a simple pulley. Each pulley is operated by a motor fixed at the base. The CabOLS uses LaserPro™ Gold Spectra cables, which have a load capability of 890 N (200 lb). These cables have the highest strength-to-diameter ratio commercially available and very low stretchability.

Each limb of the CabOLS includes a cable, a precision extension spring, a motor, a gearbox, and a pulley. One end of each limb is attached to the moving platform at point Bi, and the other end is fixed at point Ai. In the CabOLS, eight cables provide the 6-degree-of-freedom (DOF) wrench. In other words the manipulator has two degrees of redundancy, which are used to respect the physical constraint of positive forces in all the cables. Even with this redundancy, not any wrench vector for a given pose in the workspace is feasible. However, the cable robot geometry (the position of the fixed points) and the configuration of the cable attachments could easily be changed, in order to achieve the combination of forces and torques required. Figure 4.3 shows three possible combinations of cable attachments to the moving-platform.

To reduce the backlash effect of the gearboxes and estimate the tension in each limb, a precision extension spring has been added to each cable, to give it a constant stiffness coefficient. (The precision extension spring used in this CabOLS is fabricated from zinc-plated steel music wire.) This makes it possible to estimate the tension on the cables directly from the elongation of the spring and cable combination. Since the exact position of the platform is known, thanks to accuracy of the ABB robot, which is calibrated, the elongation of the spring/cable system can be calculated by using the industrial robot's end-effector pose and the positions of the motors of the CDPM, which are measured by encoders.

Figure 4.2 (b-c) show a simple schematic of the CabOLS' geometry. In this structure, cables are connected to the mobile platform from the top and bottom in opposite directions (counterclockwise and clockwise), which not only helps provide greater angles of rotation — up to about 90° without cable collision — but also pure moments around each axis.

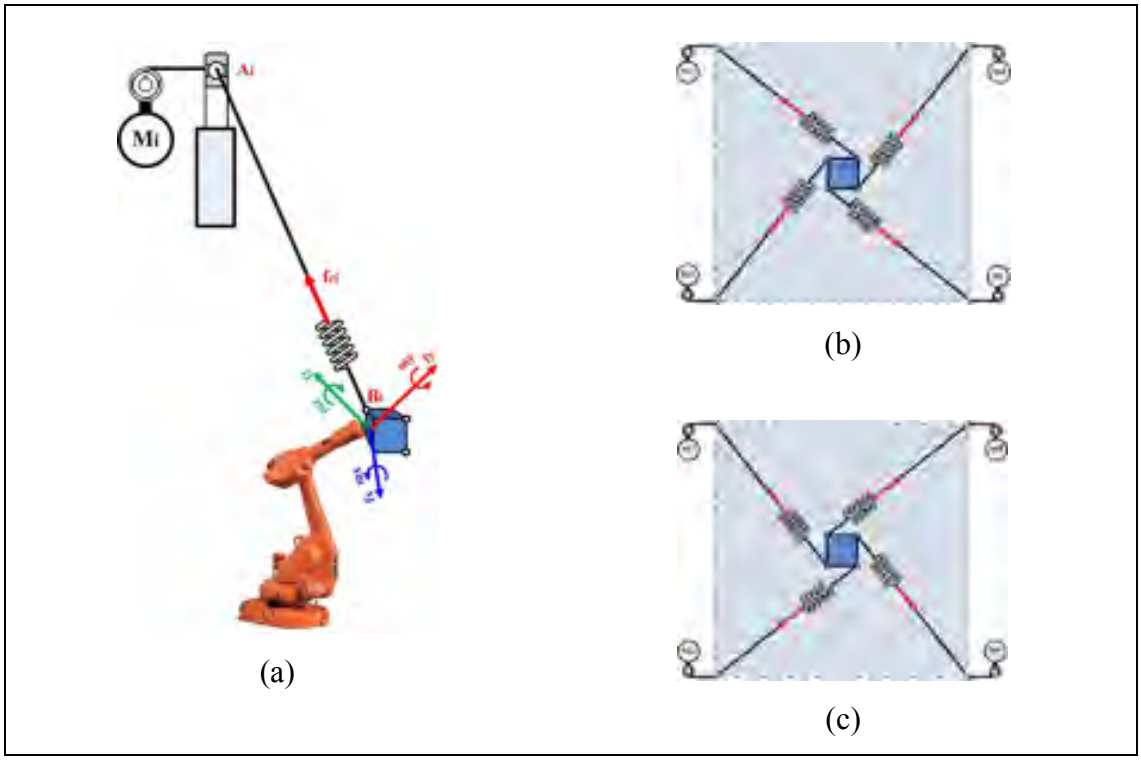

Figure 4.2 (a) Schematic of a limb of the CabOLS; (b) cable attachments to the mobile platform from above; and (c) cable attachments from below.

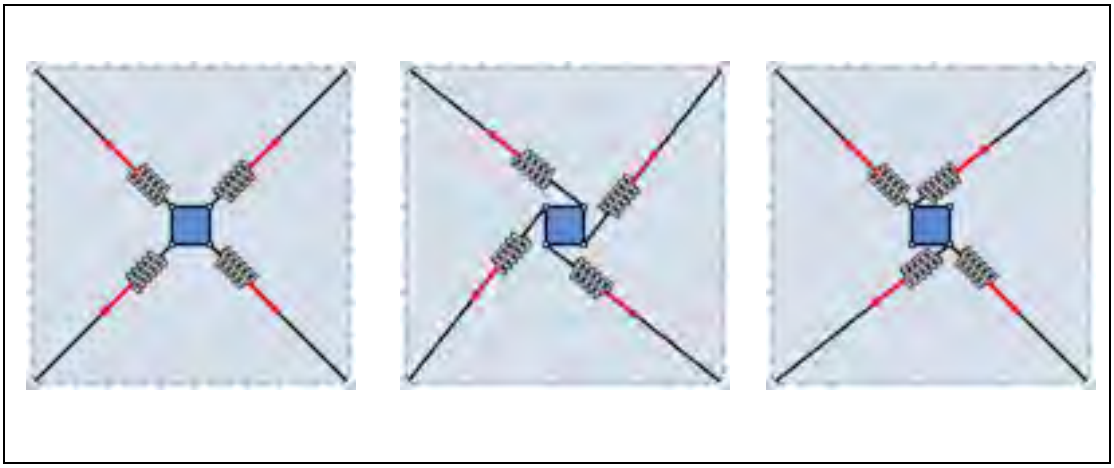

Figure 4.3 Three different combinations of the cable attachment to the moving-platform

4.2.2 Hardware and software environments

Figure 4.4 shows the electronic hardware of the CabOLS. The ABB robot and a FARO laser tracker are controlled by a host computer via an Ethernet connection. The designed graphical user interface (GUI) synchronizes the load simulator (CabOLS) and measurement tool (laser tracker) as well as the ABB robot.

A Matlab xPC-Target toolbox implements the real-time controller of the CabOLS. In the xPC Target environment, the real-time target computer, separate from the host computer, runs real-time codes. In the host computer a Simulink Coder and a C/C++ compiler create an executable code that constitutes the control implementation. This generated executable code is downloaded from the host computer to the target via a TCP/IP port. A Quanser Q8 data acquisition card sends the control signals to the motors, reads the motors' encoders and the force/torque sensor signals. Finally a Delta force/torque sensor from ATI performs the wrench measurement. This sensor can measure forces up to 165 N in the x and y directions, and up to 495 N in the z direction, as well as torques up to 15 Nm around x,y and z . The sampling time selected for the real-time system is 1 ms.

The CabOLS is designed to work in three different modes; (a) Free-moving mode; (b) Pre-tightening mode and (c) Loading Simulator mode. In Free-moving mode, the CabOLS follows the ABB robot which, in turn, carries the mobile platform. Pre-tightening mode pre-tightens the cable prior to entering the loading simulator mode. In Loading Simulator mode, the CabOLS simulates the desired wrench on the target object. A limit-switch is used in each limb of CabOLS. The limit-switches have a 4.7 N operating force which provides the minimum required tension on each spring and ensures that the springs are at the beginning of the linear area. When the CabOLS is in free-moving mode, the limit switches detect the movement of the ABB robot and allow the CabOLS to follow it. The next use of the limit switches is in the pre-tightening of the cables before starting Loading Simulator mode. To collect the experimental test data, we have designed an automated procedure for the CabOLS. The flowchart of the CabOLS' software is summarized in figure 4.5.

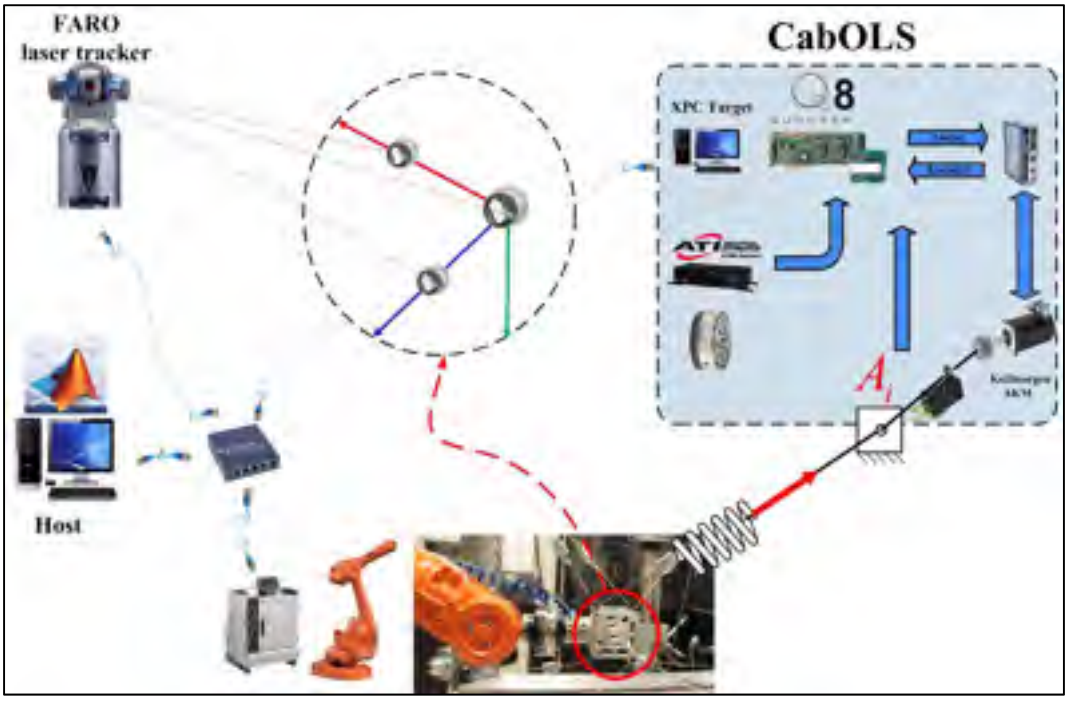

Figure 4.4 Real-time implementation of CabOLS.

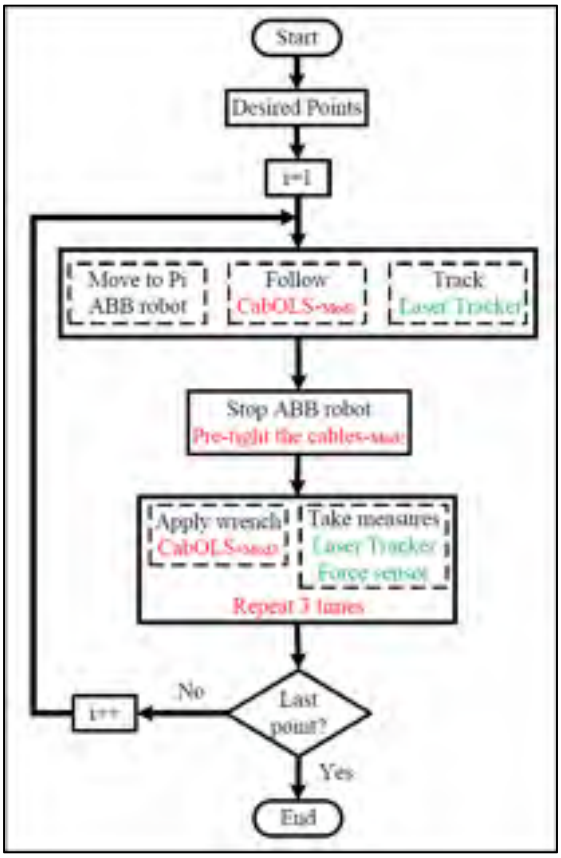

Figure 4.5 Flowchart of automatic operation of CabOLS to collect data for the joint stiffness identification.

4.3 The Force control algorithm

Cable robots have complex unfeasible wrench regions in Cartesian space. Notwithstanding, for stiffness identification, it is necessary to have a proper set of wrench and deflection data. Consequently, in order to avoid an unfeasible wrench vector in Cartesian space, the force control is applied in joint space, and the projected wrench in Cartesian space is measured with a 6-DOF force/torque sensor. In other words, the control loop provides positive tension within the cables which is always feasible. Therefore, the tension in each limb must be known for it to be used in control feedback. Measuring tension in a cable-driven mechanism is a challenge that increases the mechanical and electrical complexity as well as the cost.

In the CabOLS, the tension in each limb is not measured directly, but estimated from the limb's elongation, which is the combination of the elongation of the precision spring and the cable. For this purpose, the combination of the spring and cable stiffness must be identified and to achieve this, we used the specific setup illustrated in figure 4.6. In it, the motor and the force/torque sensor are used in a closed-loop force control topology. The tension on the limb is increased slowly from zero to the maximum allowed tension for the precision spring of 150 N, and the elongation is measured with the motor's encoder. With the spring, we measured the stiffness of the limbs at $ke \approx 2.20$ N/mm. Without the spring, the stiffness was much greater, *at* $ke \approx 10.72$ N/mm (see figure 4.6). It is obvious that the friction and backlash of the gearbox combined with the cable stiffness cause instability and inaccurate force control, as well as poor estimation of the cable force. To cover these issues, a spring is used, and the tension/elongation ratio is modeled approximately by the following linear function:

$$\hat{\boldsymbol{\tau}} \approx k_e \boldsymbol{\Delta l}\,. \tag{4.1}$$

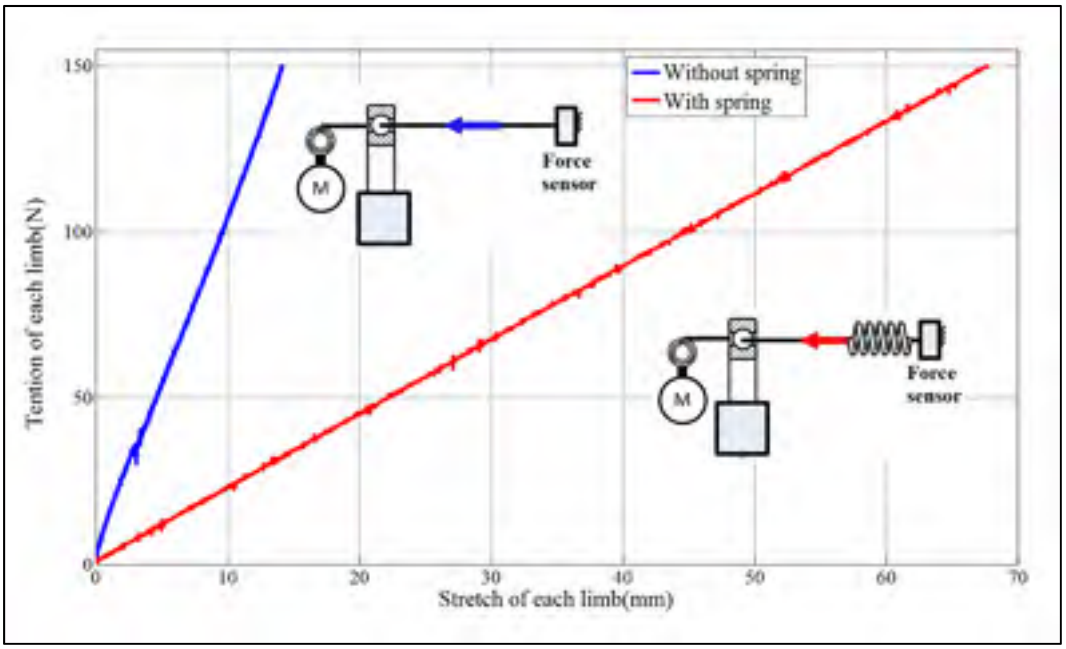

Figure 4.6 The elongation ratio in an individual limb of CabOLS with the spring and without the spring.

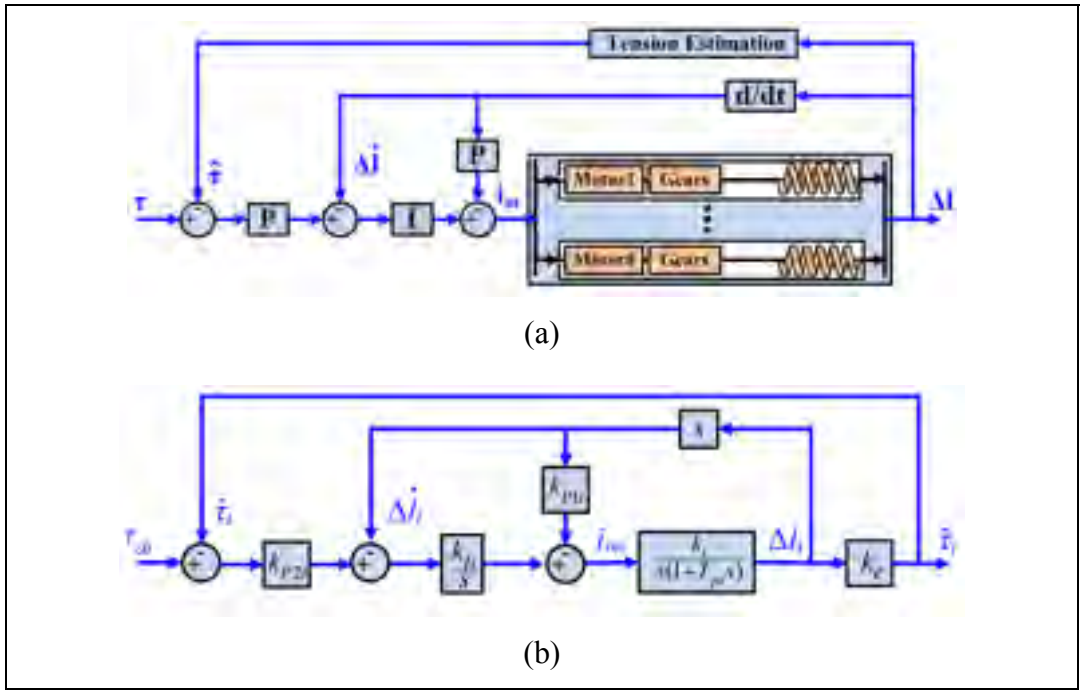

Figure 4.7 The control loops of the CabOLS using position and velocity feedback; and (b) control loops for each individual limb of the CabOLS with the linear model identified for that limb.

where $\mathbf{\Delta l} = [\Delta l_1, \Delta l_2, \ldots \Delta l_8,]^T$ is the vector of elongations for the eight limbs. Figure 4.7 illustrates the control loops of the CabOLS and those for each individual limb, in joint space. The control loops for each limb are composed of the force feedback and one additional inner PI velocity feedback, which is widely used in the decentralized position and velocity control of robotic manipulators. The internal loop controls the velocity of each limb's elongation in order to provide the required tension. The internal velocity feedback, combined with the use of the spring, improves the overall tension control in the limb when nonlinear friction and backlash are present. The control signal for the internal loop in the joint space can be formulated as follows:

$$\mathbf{i_m} = -\mathbf{k}_{p1}\frac{\mathbf{d}}{\mathbf{dt}}\mathbf{\Delta l} + \mathbf{k}_I \int_0^t \left(\mathbf{k}_{P2}(\boldsymbol{\tau} - \hat{\boldsymbol{\tau}}) - \frac{\mathbf{d}}{\mathbf{dt}}\mathbf{\Delta l} \right) \mathbf{dt} \cdot \tag{4.2}$$

where $\mathbf{k}_{P1}$ is the vector of proportional gains in the cable force feedback, $\mathbf{k}_{P2}$ and $\mathbf{k}_I$ are the vectors of proportional and integral gains of the internal velocity feedback respectively, and $\mathbf{i}_m$ is the vector of motor currents.

To define the gains of the controller in the control loops, the linear model of each limb is first identified. As explained above, each limb includes a motor, a gearbox, a pulley, a cable, and a spring. Although the combination of backlash and friction in each limb is nonlinear, the low stiffness of the spring reduces the nonlinearity effects of limb actuation. To separately identify each limb, the transfer function of each motor and gearbox is first identified. For this purpose, the spring and cable are removed, and it is assumed that the input of the system is the input of the motor's driver, which is proportional to the motor's current, i_{mi}. It is also assumed that the output of the system is a change in the length of the cable's output pulley, Δl_i. The experimental input-output data were obtained by considering a 0.5-ampere step as the input, and the output, Δl_i, was calculated by using the motor's encoder measurements. The resultant input-output data were used in combination with Matlab's identification toolbox to obtain the linear model, as follows:

$$G_i = \frac{\Delta l_i}{i_{mi}} = \frac{k_i}{s(1+T_{pi}s)}. \tag{4.3}$$

The gain of the identified model k_i and the identified pole of each limb $P_i = -1/T_{pi}$ are illustrated in table 4.1. Then, the transfer function of each limb, including motor, gearbox, cable, and spring can be formulated as:

$$T_i = \frac{\hat{\tau}_i}{i_{mi}} = \frac{k_e k_i}{s(1+T_{pi}s)}, \tag{4.4}$$

In this linear modeling of the CabOLS' limbs, neither the spring disturbance force, nor the feedback of the nonlinear friction, nor the nonlinear backlash effect was taken into consideration. The step response of the model identified in (4.4) has a 96% fit with the identification data. While it was not the intention in this study to focus on the sensitivity of nonlinear actuator dynamics, it is clear, according to the results obtained from a practical test, that the effect of its nonlinearities can be reduced when the stiffness coefficient in the limb k_e is decreased.

Table 4.1 Identification parameters of each limb in CabOLS

*i*th limb	k_i	T_{pi}
1	853	0.3564
2	2617	0.3146
3	1125	0.3497
4	2079	0.5640
5	1663	0.4660
6	1726	0.4494
7	2621	0.2499
8	1197	0.4180

The tuning of the controller gains is based on the pole placement method. Therefore, the identified model for the limbs is used to formulate the controller closed-loop system (Figure 4.7). From the block diagram of the control topology, the model and transfer function of the closed-loop system for the *i*th limb, from desired input tension τ_{di} to the estimated output tension $\hat{\tau}_i$, could be easily formulated as:

$$T_{li} = \frac{\hat{\tau}_i}{\tau_{di}} = \frac{k_i k_e k_{Ii} k_{P2i}}{T_{pi} s^3 + (1 + k_i k_{P1i}) s^2 + k_i k_{Ii} s + k_i k_e k_{Ii} k_{P2i}}, \tag{4.5}$$

where the controller gains k_{Ii}, k_{P1i}, and k_{P2i} for each limb can be tuned in order to place the closed-loop poles for all limbs as follows:

$$(s-P_1)(s-P_2)(s-P_3)=s^3+a's^2+b's+c', \tag{4.6}$$

where P_1, P_2, and P_3 are the poles of the inner closed-loop system, and a', b', and c' are the coefficients of the desired characteristic polynomial. Then, with this formulation the gains of controller are the following:

$$k_{Ii}=\frac{b'T_{Pi}}{k_i},\ k_{P1i}=\frac{a'T_{pi}-1}{k_i}, \text{ and } k_{P2i}=\frac{c'}{k_e b'}. \tag{4.7}$$

In this formulation, the controller gains depend on the desired poles. Moreover, the gains k_{Ii} and k_{P1i} depend on the parameters of the identified model (k and T_p), and the gain k_{P2i} depends on the elongation ratio k_e, which is assumed to be identical for all limbs.

Figure 4.8 shows the step response of the control loops in which the gains are tuned in order to locate all three poles of the closed-loop system at $P_1 = P_2 = P_3 = -10$. The test is repeated in two cases: i) with an extension spring on the limb, in which the elongation ratio $k_e = 2.20$ and related gains are obtained from (15); and ii) without a spring on the limb, in which $k_e = 10.72$ and the related gains are obtained by locating the poles in the same position. Moreover, in this test the tension in the cable is measured with the force sensor, and compared with the expected model: $10^3/(s+10)^3$ and the estimated tension: $\hat{\tau}_i \approx k_e \Delta l_i$. Figure 4.8 shows that, when the extension spring is used, both the measured tension τ_i and the estimated tension $\hat{\tau}_i$ fit the expected model. However, when the spring is removed, the high stiffness of the cable due to the motor's friction and backlash causes a weak and unacceptable performance. In other words, this experimental test demonstrates the desired

performance of our proposed simple strategy, in which a simple linear controller is combined with the use of springs.

To tune the gains, the poles of the closed-loop system for each limb are located at $P_1 = -40$, $P_2 = -70$ and $P_3 = -70$. Table II shows the related gains in each limb. The transfer function resulting from the poles and the zero of the closed-loop system is valid as long as the current of the motors is not saturated. The maximum current of the motors is 3.82 A. However, to provide protection from overloads, this current is limited to 3 A.

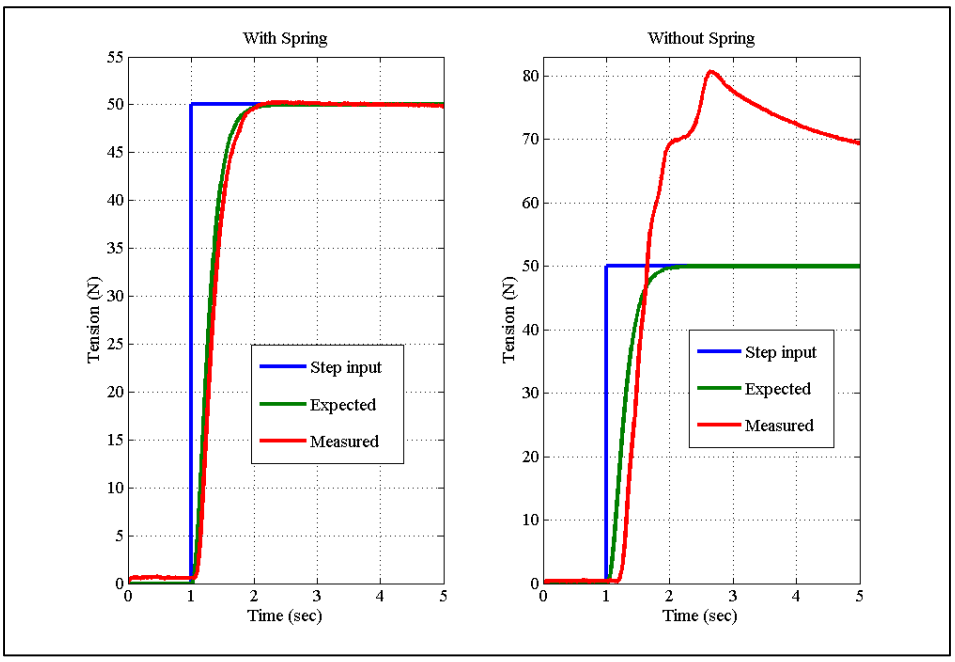

Figure 4.8 The step response of the control loops in which the gains are tuned to place the poles at $P_1 = P_2 = P_3 = -10$. First, the spring is used in the limb ($k_e = 2.20$), and then the spring is removed ($k_e = 10.72$). The green line shows the simulated response of the transfer function.

Table 4.2 Gains of the control loops.

Gains in the joint space			
Limb	k_{Ii}	k_{P1i}	k_{P2i}
1	4.3871	0.0740	9.0177
2	1.0212	0.0213	9.0177
3	3.2639	0.0551	9.0177
4	2.8484	0.0483	9.0177
5	2.9423	0.0498	9.0177
6	2.7339	0.0463	9.0177
7	1.0011	0.0168	9.0177
8	3.6667	0.0620	9.0177

4.4 Modeling and identification of joint stiffness

4.4.1 Nonlinear joint stiffness modeling and identification

Most small and medium-size robots use Harmonic Drive gearboxes in all their joints acting as a torque transmission system and speed reducer. The torsional stiffness of the Harmonic Drive gearbox is particularly low at low torques and is modeled as a nonlinear spring with hysteresis (Seyfferth, Maghzal et Angeles, 1995). The nonlinear spring has a hardening stiffness property. The hysteresis is explained by the friction in the gear teeth meshing (Seyfferth et Angeles, 1995). The torsional stiffness of the Harmonic Drive gearbox is modeled as the sum of the hardening spring, $\tau_b(\delta\theta)$, and the hysteresis function of the torsion angle, $\tau_h(\delta\theta)$. In order to avoid complexity without losing the insight of the analysis, the effect of the hysteresis has been ignored in the following modeling. Due to the nonlinear spring, $\tau_b(\delta\theta)$ can be approximated by a third order polynomial function of the torsion angle (Kircanski et Goldenberg, 1997; Seyfferth et Angeles, 1995; Seyfferth, Maghzal et Angeles, 1995):

$$\tau_b(\delta\theta) = a\delta\theta^3 + b\delta\theta. \tag{4.8}$$

Therefore for a serial manipulator with several revolute joints involving Harmonic Drive gearboxes, the nonlinear stiffness model of the joints can be formulated in vector form as:

$$\boldsymbol{\tau} = \mathbf{A}\,\delta\boldsymbol{\theta}^3 + \mathbf{B}\,\delta\boldsymbol{\theta}\,, \tag{4.9}$$

where $\boldsymbol{\tau} = [\tau_1, \tau_2, \ldots \tau_n]^T$ is the vector of torque in each joint of the manipulator, $\delta\boldsymbol{\theta}$ is the vector of the deflection of each joint, $\mathbf{A} = \mathrm{diag}(a_1, a_2, \ldots a_n)$ and $\mathbf{B} = \mathrm{diag}(b_1, b_2, \ldots b_n)$ are diagonal matrices of the stiffness parameters,. The relationship between the joint torques and the wrench vector in Cartesian space is established with the transpose of the manipulator Jacobian:

$$\boldsymbol{\tau} = \mathbf{J}^T\mathbf{w}\,. \tag{4.10}$$

The differentiation of eq. (4.10) with respect to $\boldsymbol{\theta}$ leads to the following relationship:

$$\frac{\partial\boldsymbol{\tau}}{\partial\boldsymbol{\theta}} = \frac{\partial\mathbf{J}^T}{\partial\boldsymbol{\theta}}\mathbf{w} + \mathbf{J}^T\frac{\partial\mathbf{w}}{\partial\mathbf{x}}\frac{\partial\mathbf{x}}{\partial\boldsymbol{\theta}}\,, \tag{4.11}$$

where $\partial\mathbf{x}$ is the 6-dimensional small displacement screw of the robot endpoint. Considering the concept of the stiffness matrix definition $\mathbf{K}_x = \frac{\partial\mathbf{w}}{\partial\mathbf{x}}$ and the Jacobian relationship $\mathbf{J} = \frac{\partial\mathbf{x}}{\partial\boldsymbol{\theta}}$, the following relationship can be established:

$$\delta\mathbf{w} = \mathbf{J}^{-T}(3\,\mathrm{diag}(\mathbf{A}(\mathbf{J}^{-1}\delta\mathbf{x})^2) + \mathbf{B} - \mathbf{K}_C)\mathbf{J}^{-1}\delta\mathbf{x}\,, \tag{4.12}$$

Such that:

$$\mathbf{K}_x = \mathbf{J}^{-T}(3\,\mathrm{diag}(\mathbf{A}(\boldsymbol{\delta\theta})^2)+\mathbf{B}-\mathbf{K}_C)\mathbf{J}^{-1}, \tag{4.13}$$

where $\mathbf{K}_C$ is the *complementary stiffness matrix*. For a given manipulator configuration $\mathbf{K}_C$ is formulated as:

$$\mathbf{K}_C = \left[\frac{\partial \mathbf{J}^T}{\partial \theta_1}\mathbf{w} \quad \dots \quad \frac{\partial \mathbf{J}^T}{\partial \theta_6}\mathbf{w} \right], \tag{4.14}$$

in which the Cartesian wrench vector $\mathbf{w} = \left[f_x, f_y, f_z, m_x, m_y, m_z \right]^T$ is the external load, and the related deflection in Cartesian space is $\boldsymbol{\delta}\mathbf{x} = \left[\delta x, \delta y, \delta z, \delta\alpha, \delta\beta, \delta\gamma\right]^T$.

Therefore, the nonlinear identification model could be formulated as:

$$\mathbf{f}(\mathbf{p}, \boldsymbol{\delta}\mathbf{x}, \mathbf{w}) = \mathbf{w} - \mathbf{J}^{-T}(3\,\mathrm{diag}(\mathbf{A}(\mathbf{J}^{-1}\boldsymbol{\delta}\mathbf{x})^2)+\mathbf{B}-\mathbf{K}_C)\mathbf{J}^{-1}\boldsymbol{\delta}\mathbf{x} = \mathbf{0}, \tag{4.15}$$

where $\mathbf{f}(\mathbf{p}, \boldsymbol{\delta}\mathbf{x}, \mathbf{w})$ is the nonlinear function of the deflection vector in Cartesian space $\boldsymbol{\delta}\mathbf{x}$, the wrench vector (external load) in Cartesian space $\mathbf{w}$, and the vector of the parameters $\mathbf{p} = \left[a_1, a_2, \dots a_6, b_1, b_2, \dots b_6\right]^T$, which must be identified through *n* samples.

4.4.2 Linear joint stiffness modeling and identification

Equation. (4.12) is a general formulation. In the case of robots with joints that do not involve a Harmonic Drive gearbox, linear modeling could be used. The linear model can be achieved by assuming that matrix A in eq. (4.12) equals zero. Therefore eq. (4.12) reduces to:

$$\mathbf{w} = \mathbf{J}^{-T}(\mathbf{B}-\mathbf{K}_C)\mathbf{J}^{-1}\boldsymbol{\delta}\mathbf{x}, \tag{4.16}$$

Matrix **B** is the joint stiffness matrix in the linear modeling and $\mathbf{B}=\mathbf{K}_\theta$ where $\mathbf{K}_\theta = \mathrm{diag}(k_{\theta 1}, k_{\theta 2}, \ldots k_{\theta 6})$ is the stiffness matrix in joint space. $\mathbf{K}_C$ is the *complementary stiffness matrix*. The same result could be achieved via linear modeling as explained in (Alici et Shirinzadeh, 2005).

Depending on the external load and configuration of the manipulator, $\mathbf{K}_x$ can be positive definite or not. If the joint stiffness $\mathbf{K}_\theta$ is accurately identified, by using some experimental deflection and wrench data, the stiffness $\mathbf{K}_x$ can be obtained from eq. (4.13). Equation (4.16) can be rewritten as follows:

$$\mathbf{b} = \mathbf{A}\,\mathbf{y}\ , \tag{4.17}$$

where $\mathbf{b} = \mathbf{J}^T\mathbf{w} + \mathbf{K}_C\mathbf{J}^{-1}\boldsymbol{\delta}\mathbf{x}$, $\mathbf{A} = \mathrm{diag}\left((\mathbf{J}^{-1}\boldsymbol{\delta}\mathbf{x})_1, (\mathbf{J}^{-1}\boldsymbol{\delta}\mathbf{x})_1, \ldots (\mathbf{J}^{-1}\boldsymbol{\delta}\mathbf{x})_6\right)$ and $\mathbf{y} = \left[k_{\theta 1}, k_{\theta 2}, \ldots k_{\theta 6}\right]^T$ is the vector of parameters which must be identified through finite numbers of samples. The 6×1 **b** vector and the 6×6 **A** matrix, are collected for each sample. The identification method, especially *linear least square*, can be used to identify the joint stiffness parameters $k_{\theta i}$. Joint stiffness identification is more simple when $\mathbf{K}_C$ is negligible with respect to the $\mathbf{K}_\theta$. In other words, from eq. (4.13) and eq. (4.14), the higher the wrench applied on the manipulator end-effector, the higher the effect of $\mathbf{K}_C$ on $\mathbf{K}_x$.

4.5 Experimental test and results

To produce a realistic test, it is supposed that a machining spindle is attached to the end-effector of an ABB IRB 1600 industrial robot. It is also supposed that the ABB robot is going to do machining within a desired trajectory. Next, ten arbitrary points of the trajectory are considered (see figure 4.9). At each point the robot has a different joint configuration. To

simulate a feasible external load on the endpoint of the spindle, a trajectory of the tension on each limb of the CabOLS is considered (see figure 4.10). Subsequently the transferred wrench in the Cartesian space is measured by the 6-DOF force/torque sensor which is shown in figure 4.11. In each joint configuration, the CabOLS exerts the desired wrench vector on the ABB robot three times. Each time, the laser tracker tracks one of the three reflectors located on the moving platform (see figure 4.4 and flowchart in figure 4.5). The collected data are used to obtain the 6-DOF deflection trajectory of the point, which is virtually fixed to the endpoint of the spindle (Figure 4.12). For the same point, the wrench vector is obtained by using measurements from the ATI 6-DOF force/torque sensor (Figure 4.13). To do this, the wrench vector is transformed from the force sensor coordinate frame to the coordinate frame attached to the endpoint of the spindle. The above mentioned procedures are summarized in the flowchart illustrated in figure 4.5.

The collected deflection and related wrench data are used for the linear identification of the joint stiffness. Figure 4.11 shows an example of the wrench trajectory $\mathbf{w} = \left[f_x, f_y, f_z, m_x, m_y, m_z \right]^T$ and figure 4.12 shows the corresponding deflection $\boldsymbol{\delta}\mathbf{x} = \left[\delta x, \delta y, \delta z, \delta\alpha, \delta\beta, \delta\gamma \right]^T$ in Cartesian space for one of the arbitrary points on the trajectory. For the linear identification, the Matlab function lscov is used. Table 3 shows the identified stiffness parameters $k_1, k_2, \cdots k_6$ for the ten arbitrary configurations on the desired trajectory. It also shows the mean value of the stiffness for each of the six joints.

To validate the identified parameters, the test is repeated with a different wrench at an arbitrary point in the trajectory. Figure 4.13 shows the measured deflection with the laser tracker (red line) as well as the estimated deflection, using the linear model from eq. (4.10) (blue line). It is clear that the linear modeling is fitted to the real deflection measured by the laser tracker.

4.6 Conclusion

This work introduces the application of a cable-driven omnidirectional loading simulator (CabOLS) in an experimental setup to automatically identify the joint stiffness of an industrial robot arm. The CabOLS is designed and controlled to simulate the trajectory of a wrench on fixed or moving objects like the end-effector of a robot. Thus, it could be used to simulate the external load of a robot in order to identify the robot's joint stiffness. The CabOLS aims to evaluate joint stiffness values by considering both the translational and rotational displacements of the robot for a given applied force and torque. Being automated and low cost, simplicity in mechanical structure as well as control topology are the advantages that CabOLS offers. This work also formulates the nonlinear modeling of robotic joints, based on the nonlinearity of the Harmonic Drive gearbox used in the joints of the robot arms. To perform the experimental test, an ABB IRB 1600 industrial robot and a linear model are used. In an automated process, the CabOLS and a laser tracker are employed to simulate the wrench vector and measure the related de-flection in different configurations of the ABB robot along a desired trajectory. The collected data are used to identify the joint stiffness parameters of the ABB robot within an application which runs automatically during the experimental tests. Further, another wrench vector and its related deflections are applied within the experimental setup to validate the identified parameters. The validation of identified parameters is a significant consideration that most works invariably overlook. The CabOLS and stiffness nonlinear modeling are promising candidates for future work on identifying the joint stiffness of industrial robots.

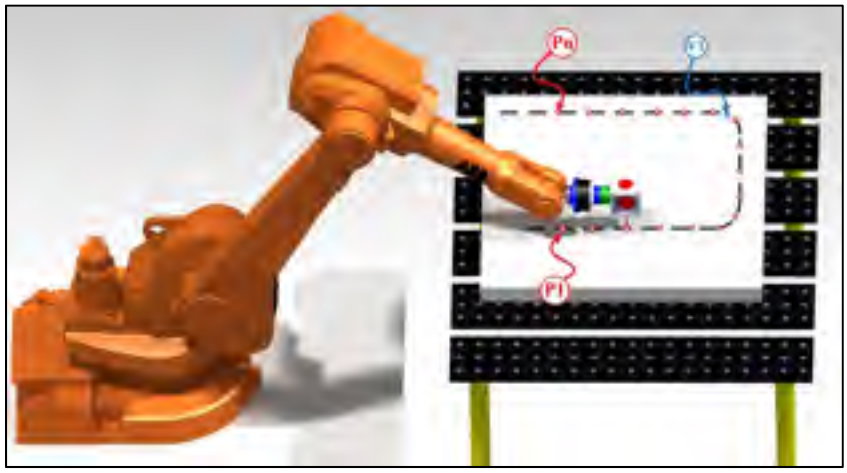

Figure 4.9 The joint stiffness of the ABB robot is identified in several configurations along the trajectory (*P1* to *Pn*). It is also validate in an arbitrary configuration *V1*.

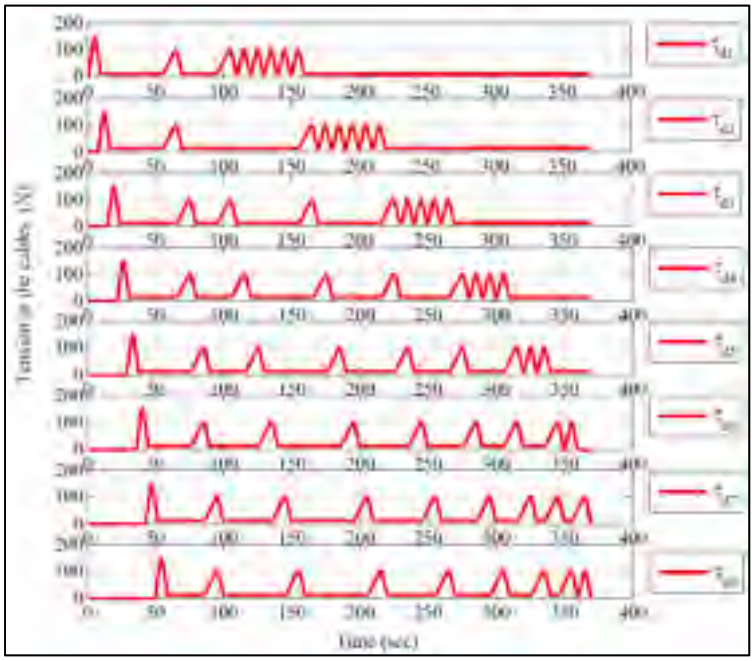

Figure 4.10 The trajectory of the desired tension in the joint space of the CabOLS.

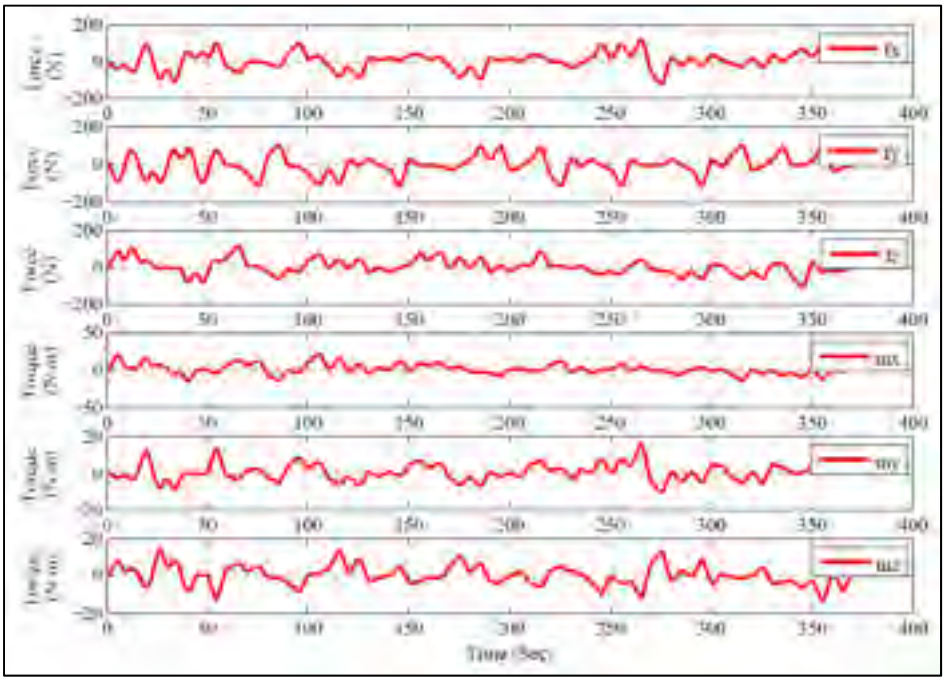

Figure 4.11 The wrench trajectory of the CabOLS in Cartesian space generated by the desired torque.

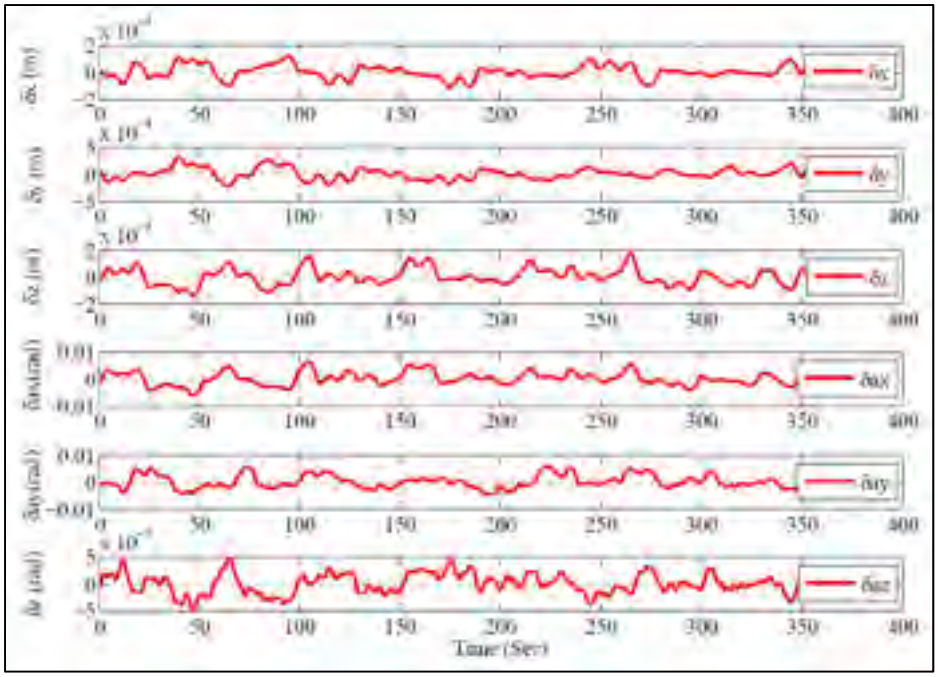

Figure 4.12 The deflection in Cartesian space caused by the external wrench trajectory.

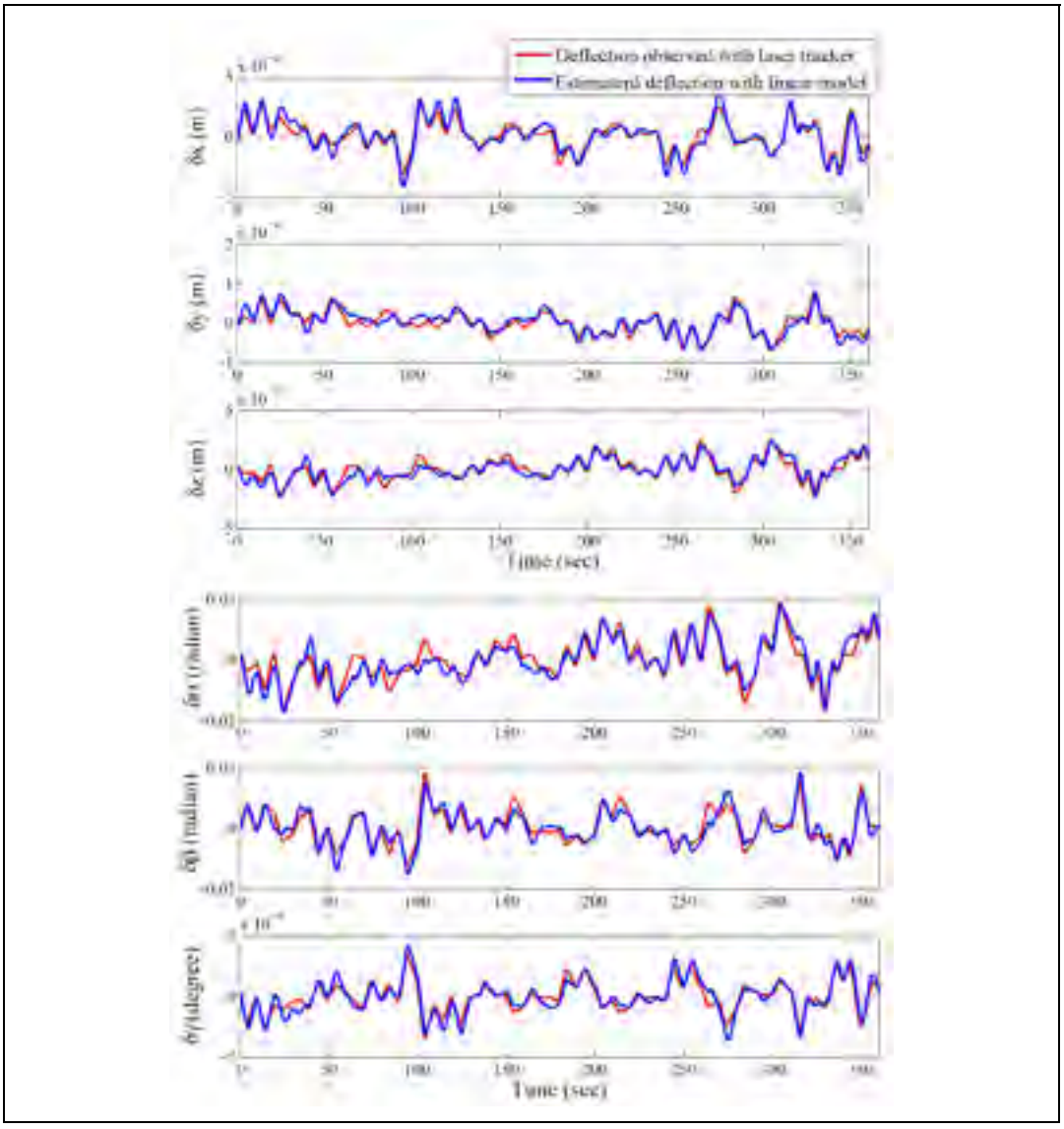

Figure 4.13 The measured deflection in Cartesian space (red line) for a different applied wrench trajectory vs. the estimated deflection with the linear model.

Table 4.3 Linear stiffness identification for n arbitrary configuration in a desired trajectory (Nm/rad).

	Conf.1	Conf.2	Conf. 3	Conf. 4	Conf. 5	Conf. 6	Conf. 7	Conf. 8	Conf. 9	Conf. 10	mean μ
k_1	1064205	905421	985424	942543	1085456	865842	915274	942413	954854	1002544	966398
k_2	725020	754235	741253	742546	687459	725687	785421	688745	763258	698455	731208
k_3	330272	305263	325242	305364	358964	339854	276428	291422	289654	356541	317900
k_4	15527	14541	12464	13534	13689	12542	13542	12156	12515	12256	13277
k_5	8005	7152	8569	7125	8525	7952	7042	8564	7024	7486	7744
k_6	1920	2514	2251	1809	2343	1900	2254	1945	2064	2410	2141

GENERAL CONCLUSION

The principal goal of this work was to design a cable-driven robot as a 6-DOF loading simulator. As a result, for application purposes, this work introduces a Cable-driven Omnidirectional Loading Simulator (CabOLS) as a fully-automatic setup for identifying the stiffness of robotic manipulators. Although existing approaches are capable of exerting a wrench vector on an industrial robot, they are not automated systems. Moreover they are not designed to apply a 6-DOF wrench vector.

This dissertation started with the dynamic analysis of Cable-driven Parallel Manipulators (CDPMs). A generalized compact and tractable closed-form dynamic modeling was obtained by using the Lagrangian variable mass formulation. A shortcoming of former works is that they have overlooked the effect of mass stream resulting from the elongation of the cables entering into or egressing from the CDPM. This is of paramount importance when a long cable is used in the CDPM. The present approach, is innovative in that the impact of the change of mass in the cables is integrated into the general dynamic formulation. The approach could be used for a complete analysis of the CDPM's dynamics, including stability, vibrations and any robust control analysis. The obtained dynamic model was applied to a planar CDPM in an astronomy application with long cables of around one kilometer. The validity and integrity of the formulations, as well as the significance of the variable mass treatment in the analysis, were established through numerical simulations. Moreover, besides being nonlinear, the mass streaming effect is heavily dependent on the kinematics, the inertial parameters of the CDPM, and the trajectory.

As stated above, this work also aimed to develop a CDPM as a 6-DOF loading simulator. To that end, a CabOLS has been designed to exert a 6-DOF static or low varying dynamic wrench vector over an object. The CabOLS offers several important advantages: From a mechanical design standpoint, the advantage is the simplicity of the mechanical structure compared with other serial or parallel robots. Simplicity of control topology and the cost efficiency of this mechanism are its added values.

The innovation of this design centers on the utilization of a precision spring to estimate the tension in the cable instead of using an expensive force sensor in the limbs. Besides being cost-effective, using the spring compensates for the nonlinear effect of the backlash from the gears, and thereby makes possible a control topology that has been managed to be as simple as possible while being highly efficient. To ensure precise force control on the target object, two levels of control, one in the Cartesian space and the other in the joint space, are implemented.

Also, in this work, a real-time rapid redundancy resolution algorithm, the optimal projection of the tension in the cables, has been successfully developed and utilized in the closed-loop control system. It is demonstrated that, even though the redundancy resolution algorithm is nonlinear, the combination of the redundancy resolution algorithm and the model of the CDPM in a closed-loop control system is linear. This proof is very important since it makes it possible to apply a simple pole placement method to simultaneously formulate the gains of the controller in Cartesian and joint spaces. The performance of the CabOLS, that of the proposed controller, and the real-time redundancy resolution were verified by simulating a desired feasible wrench vector in Cartesian space.

As the CabOLS has been designed and controlled to simulate the trajectory of a dynamic wrench on fixed or slow-moving objects like the end-effector of a robot, it could be used to simulate the external load of a robot in order to identify its joint stiffness. Consequently, this work has also illustrated the application of the CabOLS as part of an experimental setup to automatically identify the joint stiffness of an industrial robotic manipulator. The experimental setup involved the CabOLS as a loading simulator, a laser tracker as a measurement device, and a robot for which the joint stiffness needed to be identified. For the efficient operation of the experimental setup, the CabOLS, the laser tracker, and the robot were controlled, and the related data automatically collected. The setup aimed at obtaining joint stiffness values by considering both the translational and rotational displacements of the robot for a specific applied force and torque. Its advantages in joint stiffness identification

are being automated, low cost, and simple in mechanical structure as well as control topology.

The present work has also formulated the nonlinear modeling of the robot's joint stiffness. Nonlinear modeling is based on the nonlinearity of the Harmonic Drive gearbox used in the joints of midsize robotic manipulators. Using the CabOLS as a load simulator makes it possible to use nonlinear modeling in joint stiffness identification as well as linear modeling. An ABB IRB 1600 industrial robot was employed to conduct the experimental test. In an automated process, the experimental setup was used to simulate the wrench vector, and to measure the related deflections in different configurations of the ABB robot along a desired trajectory. The obtained data were used to identify the joint stiffness parameters of the ABB robot within an automatic application which runs at the same time as the experimental tests. Moreover, in order to validate the stiffness parameters, another wrench vector and its related deflections were used within the experimental setup. The examination of the identified parameters is an importance that has not been taken into consideration in most works. In sum, the CabOLS and the nonlinear modeling proposed in this work are promising candidates for the future direction of research into the identification of joint stiffness in industrial robots.

The following are some avenues for future research. A complete study of the cable collision-free workspace of the CabOLS must be performed. One idea could be to consider the location of the fixed points of the CabOLS as design parameters of the collision-free workspace and optimize the workspace volume. The wrench feasibility workspace of the CabOLS should also be analyzed in various configurations. It is also suggested to combine the collision-free workspace and the wrench feasibility workspace in an optimization problem and find the proper configuration for the CabOLS. Future research should also consider the dynamics of the springs in the general dynamics modelling of the CabOLS. For instance, future research needs to investigate procedures for analysis of the vibration caused by the springs. For this purpose, the dynamics of the CabOLS could be analyzed with singular perturbation approaches and the proper rapid controller could be designed based on

the fast dynamics of the CabOLS versus the slow dynamics of the springs. In summary, future research should concentrate on the following issues: cable collision-free workspace, wrench feasibility workspace, different controller topology, and dynamics analysis of the springs.

LIST OF REFRENCES

Alici, Gürsel, et Bijan Shirinzadeh. 2005. « Enhanced stiffness modeling, identification and characterization for robot manipulators ». *Robotics, IEEE Transactions on,* vol. 21, n^{o} 4, p. 554-564.

Ardema, Mark D. 2005. *Analytical dynamics: theory and applications*. Springer.

Aref, Mohammad M, et Hamid D Taghirad. 2008. « Geometrical workspace analysis of a cable-driven redundant parallel manipulator: KNTU CDRPM ». In *Intelligent Robots and Systems, 2008. IROS 2008. IEEE/RSJ International Conference on*. p. 1958-1963. IEEE.

Barrette, G., et C. M. Gosselin. 2005a. « Determination of the dynamic workspace of cable-driven planar parallel mechanisms ». *Journal of Mechanical Design,* vol. 127, n^{o} 2, p. 242-248.

Barrette, Guillaume, et Clément M Gosselin. 2005b. « Determination of the dynamic workspace of cable-driven planar parallel mechanisms ». *Journal of Mechanical Design,* vol. 127, p. 242.

Bedoustani, Y. B., P. Bigras, H. D. Taghirad et I. A. Bonev. 2011. « Lagrangian Dynamics of Cable-Driven Parallel Manipulators: A Variable Mass Formulation ». *Transactions of the Canadian Society for Mechanical Engineering,* vol. 35, n^{o} 4, p. 529-542.

Bedoustani, Yousef Babazadeh, Hamid D Taghirad et Mohammad M Aref. 2008. « Dynamics analysis of a redundant parallel manipulator driven by elastic cables ». In *Control, Automation, Robotics and Vision, 2008. ICARCV 2008. 10th International Conference on*. p. 536-542. IEEE.

Bostelman, Roger, Adam Jacoff et Robert Bunch. 1999. « Delivery of an Advanced Double-Hull Ship Welding System using RoboCrane ». In *IIA/SOCO*. Citeseer.

Bruckmann, Tobias, Lars Mikelsons, Manfred Hiller et Dieter Schramm. 2007. « A new force calculation algorithm for tendon-based parallel manipulators ». In *Advanced intelligent mechatronics, 2007 IEEE/ASME international conference on*. p. 1-6. IEEE.

Carlson, B., L. Bauwens, L. Belostotski, E. Cannon, Y. Y. Chang, X. H. Deng, P. Dewdney, J. Fitzsimmons, D. Halliday, K. Kurschner, G. Lachapelle, D. Lo, P. Mousavi, M. Nahon, L. Shafai, S. F. Stiemer, R. Taylor et B. Veidt. 2000. « The Large Adaptive Reflector: A 200-m diameter, wideband, cm-m wave radio telescope ». *Radio Telescopes,* vol. 4015, p. 33-44

Chen, J. 1996. « Development of a flexible biomechanical testing apparatus ». MS thesis. University of Tennessee, Memphis.

Chen, Shih-Feng. 2003. « The 6× 6 stiffness formulation and transformation of serial manipulators via the CCT theory ». In *Robotics and Automation, 2003. Proceedings. ICRA'03. IEEE International Conference on*. Vol. 3, p. 4042-4047. IEEE.

Chen, Shih-Feng, et Imin Kao. 2000. « Conservative congruence transformation for joint and Cartesian stiffness matrices of robotic hands and fingers ». *The International Journal of Robotics Research,* vol. 19, n° 9, p. 835-847.

Cornelisse, Jacobus W, HFR Schoyer et Karel F Wakker. 1979. « Rocket propulsion and spaceflight dynamics ». *London: Pitman, 1979,* vol. 1.

Cveticanin, L. 1998a. *Dynamics of machines with variable mass*, 7. CRC Press.

Cveticanin, L, et I Kovacic. 2007a. « On the dynamics of bodies with continual mass variation ». *Journal of applied mechanics,* vol. 74, n° 4, p. 810-815.

Cveticanin, L. 1993. « Conservation-Laws in Systems with Variable Mass ». *Journal of Applied Mechanics-Transactions of the Asme,* vol. 60, n° 4, p. 954-958.

Cveticanin, L. 1998b. *Dynamics of machines with variable mass*. Australia: Gordon and Breach Science Publishers, xv, 236 p. p.

Cveticanin, L. 2009. « Dynamics of body separation-analytical procedure ». *Nonlinear Dynamics,* vol. 55, n° 3, p. 269-278.

Cveticanin, L., et D. Djukic. 2008. « Dynamic properties of a body with discontinual mass variation ». *Nonlinear Dynamics,* vol. 52, n° 3, p. 249-261.

Cveticanin, L., et I. Kovacic. 2007b. « On the dynamics of bodies with continual mass variation ». *Journal of Applied Mechanics-Transactions of the Asme,* vol. 74, n° 4, p. 810-815.

DeSchutter, J., D. Torfs, H. Bruyninckx et S. Dutre. 1997. « Invariant hybrid force/position control of a velocity controlled robot with compliant end effector using modal decoupling ». *International Journal of Robotics Research,* vol. 16, n° 3, p. 340-356.

DiAngelo, Denis J, Kevin T Foley, Keith A Vossel, Y Raja Rampersaud et Thomas H Jansen. 2000. « Anterior cervical plating reverses load transfer through multilevel strut-grafts ». *Spine,* vol. 25, n° 7, p. 783-795.

Djerassi, Shlomo. 1998. « Algorithm for simulation of motions of variable-mass systems ». *Journal of guidance, control, and dynamics,* vol. 21, n° 3, p. 427-434.

Dumas, C., S. Caro, M. Cherif, S. Garnier et B. Furet. 2010. « A Methodology for Joint Stiffness Identification of Serial Robots ». *Ieee/Rsj 2010 International Conference on Intelligent Robots and Systems (Iros 2010)*, p. 464-469.

Dumas, Claire, Stéphane Caro, Mehdi Cherif, Sébastien Garnier et Benoît Furet. 2012. « Joint stiffness identification of industrial serial robots ». *Robotica,* vol. 30, n° 04, p. 649-659.

Dumas, Claire, Stéphane Caro, Sébastien Garnier et Benoît Furet. 2011. « Joint stiffness identification of six-revolute industrial serial robots ». *Robotics and Computer-Integrated Manufacturing,* vol. 27, n° 4, p. 881-888.

Oct.3, 2000. *Crane with Improved Reeving Arrangment*.

Eguizabal, Johnny, Michael Tufaga, Justin K Scheer, Christopher Ames, Jeffrey C Lotz et Jenni M Buckley. 2010. « Pure moment testing for spinal biomechanics applications: Fixed versus sliding ring cable-driven test designs ». *Journal of biomechanics,* vol. 43, n° 7, p. 1422-1425.

Faber, Henry B, Denis J DiAngelo et Kevin T Foley. 1997. « Development of an experimental testing protocol to study cervical spine mechanics ». In *Biomedical Engineering Conference, 1997., Proceedings of the 1997 Sixteenth Southern*. p. 323-326. IEEE.

Fang, S. Q., D. Franitza, M. Torlo, F. Bekes et M. Hiller. 2004. « Motion control of a tendon-based parallel manipulator using optimal tension distribution ». *Ieee-Asme Transactions on Mechatronics,* vol. 9, n° 3, p. 561-568.

Goertzen, D. J., et G. N. Kawchuk. 2009. « A novel application of velocity-based force control for use in robotic biomechanical testing ». *Journal of Biomechanics,* vol. 42, n° 3, p. 366-369.

Healy, Andrew T, Daniel Lubelski, Prasath Mageswaran, Deb A Bhowmick, Adam J Bartsch, Edward C Benzel et Thomas E Mroz. 2014. « Biomechanical analysis of the upper thoracic spine after decompressive procedures ». *The Spine Journal,* vol. 14, n° 6, p. 1010-1016.

Hiller, M., S. Q. Fang, S. Mielczarek, R. Verhoeven et D. Franitza. 2005. « Design, analysis and realization of tendon-based parallel manipulators ». *Mechanism and Machine Theory,* vol. 40, n° 4, p. 429-445.

2004. *Cable Array Robot for Material Handling*.

J.P. Dickey , G.A. Dumas and D.A. Bednar August 14-18, 1998 «Design and evaluation of an in vitro pure moment spinal testing machine ». In *North American Congress on Biomechanics, NACOB 98*. (Ontario, Canada). University of Waterloo.

Jianjun, Wang, Zhang Hui et T. Fuhlbrigge. 2009. « Improving machining accuracy with robot deformation compensation ». In *Intelligent Robots and Systems, 2009. IROS 2009. IEEE/RSJ International Conference on*. (10-15 Oct. 2009), p. 3826-3831.

Jirkova, L, Z Horak, R Sedlacek, P Tichy, J Michalec, D Weichert et M Stoffel. 2007. « Preliminary measurements of lumbar spine kinematics and stiffness ». In *Proceedings of the 5th Australasian Congress on Applied Mechanics*. p. 770. Engineers Australia.

Jirková, L., Z. Horák, R. Sedlácek, P. Tichý, J. Michalec, D. Weichert et M. Stoffel. 10-12 December 2007. « Preliminary measurements of lumbar spine kinematics and stiffness ». In *5th Australasian Congress on Applied Mechanics, ACAM 2007*. (Brisbane, Australia).

Kawchuk, Gregory N, Alejandro Carrasco, Grayson Beecher, Darrell Goertzen et Narasimha Prasad. 2010. « Identification of spinal tissues loaded by manual therapy: a robot-based serial dissection technique applied in porcine motion segments ». *Spine,* vol. 35, n^{o} 22, p. 1983.

Kim, Daniel H., Frank P. Cammisa et Richard G. Fessler. 2006. *Dynamic reconstruction of the spine*. New York: Thieme, xix, 402 p. p.

Kim, Eui-Jin, Kenta Seki et Makoto Iwasaki. 2014. « Motion control of industrial robots by considering serial two-link robot arm model with joint nonlinearities ». *Journal of Mechanical Science and Technology,* vol. 28, n^{o} 4, p. 1519-1527.

Kircanski, Nenad M, et Andrew A Goldenberg. 1997. « An experimental study of nonlinear stiffness, hysteresis, and friction effects in robot joints with harmonic drives and torque sensors ». *The International Journal of Robotics Research,* vol. 16, n^{o} 2, p. 214-239.

Landsberger, S.E., et T.B. Sheridan. 1985. « A new design for parallel link manipulator ». In *Proc. Systems, Man and Cybernetics Conf.* (Tucson), p. 812-814.

Lawson, Charles L, et Richard J Hanson. 1974. *Solving least squares problems*, 161. SIAM.

Loloei, Azadeh Zarif, Mohamad M Aref et Hamid D Taghirad. 2009. « Wrench feasible workspace analysis of cable-driven parallel manipulators using LMI approach ». In *Advanced Intelligent Mechatronics, 2009. AIM 2009. IEEE/ASME International Conference on*. p. 1034-1039. IEEE.

Lysack, J. T., J. P. Dickey, G. A. Dumas et D. Yen. 2000. « A continuous pure moment loading apparatus for biomechanical testing of multi-segment spine specimens ». *Journal of Biomechanics,* vol. 33, n° 6, p. 765-770.

McPhee, JJ, et RN Dubey. 1991. « Dynamic analysis and computer simulation of variable-mass multi-rigid-body systems ». *International journal for numerical methods in engineering,* vol. 32, n° 8, p. 1711-1725.

Merlet, J. P. 2006. *Parallel robots*, 2nd. Coll. « Solid mechanics and its applications », 74. Dordrecht ; Boston, MA: Kluwer Academic Publishers, xiv, 355 p. p.

Miermeister, Philipp, et Andreas Pott. 2010. « Modelling and Real-Time Dynamic Simulation of the Cable-Driven Parallel Robot IPAnema ». In *New Trends in Mechanism Science*, sous la dir. de Pisla, Doina, Marco Ceccarelli, Manfred Husty et Burkhard Corves. Vol. 5, p. 353-360. Coll. « Mechanisms and Machine Science »: Springer Netherlands. < http://dx.doi.org/10.1007/978-90-481-9689-0_41 >.

Nakamura, Yoshihiko. 1991. *Advanced robotics : redundancy and optimization*. Coll. « Addison-Wesley series in electrical and computer engineering Control engineering ». Reading, Mass.: Addison-Wesley Pub. Co., xi, 337 p. p.

Olabi, A., M. Damak, R. Bearee, O. Gibaru et S. Leleu. 2012a. « Improving the Accuracy of Industrial Robots by Offline Compensation of Joints Errors ». *2012 Ieee International Conference on Industrial Technology (Icit)*, p. 492-497.

Olabi, Adel, Mohamed Damak, Richard Bearee, Olivier Gibaru et Stephane Leleu. 2012b. « Improving the accuracy of industrial robots by offline compensation of joints errors ». In *Industrial Technology (ICIT), 2012 IEEE International Conference on*. p. 492-497. IEEE.

Palli, G, et S Pirozzi. 2012. « A miniaturized optical force sensor for tendon-driven mechatronic systems: Design and experimental evaluation ». *Mechatronics,* vol. 22, n° 8, p. 1097-1111.

Pesce, C. P. 2003. « The application of lagrange equations to mechanical systems with mass explicity dependent on position ». *Journal of Applied Mechanics-Transactions of the Asme,* vol. 70, n° 5, p. 751-756.

Pham, Cong Bang, Guilin Yang et Song Huat Yeo. 2005. « Dynamic analysis of cable-driven parallel mechanisms ». In *Advanced Intelligent Mechatronics. Proceedings, 2005 IEEE/ASME International Conference on*. p. 612-617. IEEE.

Schulze, M., R. Hartensuer, D. Gehweiler, U. Holscher, M. J. Raschke et T. Vordemvenne. 2012. « Evaluation of a robot-assisted testing system for multisegmental spine specimens ». *Journal of Biomechanics,* vol. 45, n° 8, p. 1457-1462.

Seyfferth, Wolfgang, et Jorge Angeles. 1995. « A Mechanical Model for Robotic Joints with Harmonic Drives ».

Seyfferth, Wolfgang, AJ Maghzal et Jorge Angeles. 1995. « Nonlinear modeling and parameter identification of harmonic drive robotic transmissions ». In *Robotics and Automation, 1995. Proceedings., 1995 IEEE International Conference on*. Vol. 3, p. 3027-3032. IEEE.

Shin, Hyunpyo, Sungcheul Lee, Jay I Jeong et Jongwon Kim. 2013a. « Antagonistic Stiffness Optimization of Redundantly Actuated Parallel Manipulators in a Predefined Workspace ».

Shin, Hyunpyo, Sungcheul Lee, Jay I Jeong et Jongwon Kim. 2013b. « Antagonistic Stiffness Optimization of Redundantly Actuated Parallel Manipulators in a Predefined Workspace ». *Mechatronics, IEEE/ASME Transactions on,* vol. 18, n^{o} 3, p. 1161-1169.

Slavković, Nikola R, Dragan S Milutinović, Branko M Kokotović, Miloš M Glavonjić, Saša T Živanović et Kornel F Ehmann. 2013. « Cartesian compliance identification and analysis of an articulated machining robot ». *FME Transactions,* vol. 41, n^{o} 2, p. 83-95.

Tadokoro, S., T. Matsushima, Y. Murao, H. Kohkawa et M. Hiller. 2001a. « A parallel cable-driven motion base for virtual acceleration ». *Iros 2001: Proceedings of the 2001 Ieee/Rjs International Conference on Intelligent Robots and Systems, Vols 1-4*, p. 1700-1705

Tadokoro, S., R. Murata, T. Matsushima, Y. Murao, H. Kohkawa et M. Hiller. 2001b. « A motion base with 6 degrees of freedom by parallel cable drive architecture ». *2001 Ieee/Asme International Conference on Advanced Intelligent Mechatronics Proceedings, Vols I and Ii*, p. 1193-1198

Taghirad, H. D., et Y. B. Bedoustani. 2011. « An Analytic-Iterative Redundancy Resolution Scheme for Cable-Driven Redundant Parallel Manipulators ». *Ieee Transactions on Robotics,* vol. 27, n^{o} 6, p. 1137-1143.

Taghirad, Hamid D. 2013. *Parallel Robots: Mechanics and Control*. CRC Press.

Taghirad, Hamid D, et Meyer A Nahon. 2008. « Dynamic analysis of a macro–micro redundantly actuated parallel manipulator ». *Advanced Robotics,* vol. 22, n^{o} 9, p. 949-981.

1996. *Tendon Suspended Platform Robot*.

Tsai, Lung-Wen. 1999. *Robot analysis: the mechanics of serial and parallel manipulators*. John Wiley & Sons.

Voor, Michael J, Sanjiv Mehta, Mei Wang, Yong-Ming Zhang, John Mahan et John R Johnson. 1998. « Biomechanical evaluation of posterior and anterior lumbar interbody fusion techniques ». *Journal of Spinal Disorders & Techniques,* vol. 11, n^{o} 4, p. 328-334.

Yao, Rui, Xiaoqiang Tang, Jinsong Wang et Peng Huang. 2010. « Dimensional optimization design of the four-cable-driven parallel manipulator in FAST ». *Mechatronics, IEEE/ASME Transactions on,* vol. 15, n^{o} 6, p. 932-941.